Scattering based Scheme for Generation of Photonic Tree-Cluster States

by

Hemant Sharma

to obtain the degree of Master of Science
at the Delft University of Technology

Student number:	5379113	
Project duration:	August 1, 2021 – March 30, 2022	
Thesis committee:	Prof. J. Borregaard,	Qutech, supervisor
	Prof. C. Andersen,	Qutech
	Prof. dr. Y. Blanter,	Kavli Institute of Nanoscience

TU Delft

Abstract

Quantum repeaters are critical in the development of the quantum internet because they enable quantum communication over long distances. Third-generation quantum repeaters or one-way quantum repeaters are the most advanced quantum repeaters that do not require two-way communication between nodes. Borregaard et al. (2019) proposed an architecture of one-way quantum repeaters based on photonic tree-cluster states. Tree-cluster states are highly entangled multi-qubit states that can protect quantum information from transmission losses. Creating these highly entangled multi-qubit states is a challenging and error-prone process. Conventional tree-cluster generation methods use an emitter that emits and entangles with photons. These methods, however, suffer from multiple photon emissions, which leads to errors. This paper presents a system for generating tree-cluster states that employ two different spin-cavity systems. The first spin-cavity system generates single photons using a cavity-assisted Raman scheme that prevents multiple photons from being emitted. The generated photons are scattered with a phase dependent on the spin state by the other spin-cavity system. The analytical model of the two spin-cavity systems for producing and scattering single-photons is presented. Furthermore, we model the errors that may occur during these processes.

We introduce a protocol for implementing a CZ gate between photons and spin. After that, this protocol is used to generate tree-cluster states. Furthermore, we optimize the entanglement between spin and photons by using the detuning between the two spin-cavity systems. Finally, we generate tree-cluster states using the spin-cavity system model and the photon-spin entanglement protocol. Following that, the effect of imperfect entanglement on the fidelity of the generated tree-cluster states is investigated. The fidelity of tree-cluster states with imperfect entanglement is then compared to the fidelity of tree-cluster states with single-qubit depolarising errors on photons. Unfortunately, we could not determine the relation between imperfect entanglement and the fidelity of the generated tree clusters in this study. Furthermore, we did not investigate the effects of imperfect entanglement on the encoding and decoding of information in tree-cluster states.

Acknowledgement

First and foremost, I would like to express my gratitude to Prof. Johannes Borregaard for giving me the opportunity to join his research group and work on this project. He provided me with encouragement and independence, which allowed me to develop my interests. When I was lost, and out of my depth, he was there to guide me through. Thank you for your patience and trust throughout this project.

I would also like to thank the Borregaard group for their inputs and suggestions during this project. The exciting discussions that we had in group meetings were inspiring and remarkable. Fenglei and Bernard have been of great help throughout the project. I would also like to thank Prof. Andersen and Prof. Blanter for joining my thesis committee.

Thanks to my parents and my sister for their unwavering support and encouragement during my search for knowledge and development. I am grateful to my friends in India and Delft for their help so that I was always filled with determination. Finally, I would like to dedicate this thesis to my grandmother, Indira Sharma. Nothing would have been possible without her.

This thesis is the result of eight months of hard work and struggle. Countless days were lost to lockdowns and COVID restrictions, but I am grateful I could reach this point.

Finally, I would like to thank the natural view outside my window just for being there always.

If we're just information, just noise in the system,
we might as well be a symphony.
-Root,
Person of Interest

Contents

List of Figures

1 Motivation

In the past decades, there have been massive developments in experimental quantum computing [1]. Recently, scientists from Google claimed to have achieved the much-sought quantum supremacy [2]. Quantum computing utilizes the properties of quantum systems to gain an advantage over classical systems. Moreover, the principles of quantum mechanics can be used to implement secure quantum communication [3, 4]. A quantum network capable of communicating between two different points on the earth could be used to build the quantum internet [5, 6]. The underlying idea for quantum communication is efficiently distributing quantum information over long distances. Due to the presence of noise and losses in channels, the idea of quantum repeaters has been proposed for quantum communication over long distances [7].

Quantum repeaters function by segmenting the network into smaller pieces and sending information over those pieces [8]. The idea behind quantum communication is the distribution of entanglement between two parties on the network. Quantum repeaters have been classified into generations based on how well they distribute entanglement and deal with errors during the transmission process [9]. The traditional (first generation) quantum repeater design is based on the heralded quantum entanglement distribution, which necessitates long-lived quantum memory and two-way communication between sender and receiver. On the other hand, third-generation quantum repeaters rely on quantum error correction codes to deal with loss and operation errors and only require one-way communication. All-photonic quantum repeater architectures which utilize highly entangled states for quantum communication have been proposed [10, 11, 12]. Varnava et al. [13] proposed the use of photonic tree-cluster states for quantum communication. Other than quantum communication, cluster states have found their application in photonic quantum computing [14, 15] and quantum simulations [16]. Therefore, it is imperative to develop effective methods for generating photonic clusters due to their various uses.

Generating an entangled multiphoton state is a highly challenging task because photons do not interact with each other. Therefore, entangling photons with each other requires a non-linear interaction or a measurement [10]. Non-linear interactions are weak [17] and measurements are probabilistic. Earlier approaches for generating multiphoton states employed pair-wise "fusion" of Bell pairs to grow multiphoton cluster states [18, 10]. This process requires the generation of many Bell states and measurement of photons to merge different Bell pairs. Implementing these schemes for one-way quantum communication would require many two-qubit operations at each repeater and a significant number of qubits. Moreover, due to measurements being involved in the cluster generation, these methods are probabilistic, thus its not practical to use them in quantum repeaters. Buterakos et al. proposed a method to deterministically generate arbitrary large cluster states using only one emitter and an auxiliary qubit [19]. Their scheme requires an emitter that can be repeatedly entangled to a memory/auxiliary qubit and single-qubit gates on photons and emitter. The

details of their protocol can be found in the reference [19].

Recently, Tiurev et al. [20] proposed architecture for deterministic generation of entangled multiphoton states using solid-state emitters. Their approach can be used to generate the Greenberger–Horne–Zeilinger (GHZ) state or a one-dimensional cluster state. Borregaard et al. [21] proposed a design of a one-way quantum repeater based on tree-cluster states. In the paper, they also discussed the process for the generation of tree-cluster states. They require an emitter and two memory qubits for generating the tree cluster. Yuan Zhan et al. [22] proposed a protocol for generating arbitrary sized tree-cluster states using just one emitter. These schemes involve exciting the spin to an excited state and emitting a photon by decaying to the ground state or other stable state. They also require a protocol-specific set of single-qubit operations between different excitations. The main issue with generating photons by spontaneous decay is that it is possible to have multiple excitations while driving the spin to the excited state. To reduce the chance of multiple excitations, one could make the driving pulse short, but short driving pulses have a wide distribution in the frequency domain, leading to the driving of other transitions, therefore, errors. One could also increase the coupling between the spin and the waveguide but it could lead to higher decay rate, thus requiring shorter driving pulse widths.

To overcome the problems of emission-based schemes, we propose a scattering-based scheme for entangling photons with spin. Our system consists of two spins, each of them coupled to their respective cavity. The first spin-cavity system emits single-photons as time-bin qubits by undergoing cavity-assisted Raman transitions, we call that system the Emitter. Time-bin qubits are a type of encoding in which the presence of the single-photon is limited to one of two non-overlapping spatiotemporal modes, early $|E\rangle$ and late $|L\rangle$ [23]. The second spin-cavity system, which we refer to as the Gate, reflects the time-bin photons with state-dependent reflection coefficients. Applying a set of single-qubit gates on this spin could entangle it with the incoming photons. We will begin by describing the entanglement protocol for entangling photons with the spin. Then, we will model the photon generation process in the first spin-cavity system and the photon reflection process in the second cavity system. In what follows, it can be observed that improving the coupling of the spin to the cavity decreases the probability of having multiple excitations. The procedure for generating tree-cluster states will next be introduced. Furthermore, we optimize the Gate's parameters to maximize the photon-spin entanglement fidelity. Finally, we will simulate the generation of tree-cluster states and estimate the fidelity of the generated states. The structure of the remainder of the thesis is as follows:

- In chapter 2 we introduce all the basics essential to comprehend the remainder of the report. We introduce the Hamiltonian of a spin-cavity system necessary for modeling photon-spin interaction. Then we introduce the methods for solving the dynamics of the spin-cavity system. The last parts of this chapter introduce the basics of tree-cluster states and motivate Silicon vacancy centers for realizing our system for generating tree-cluster states.

- Chapter 3 starts by introducing the protocol for entangling photons with a spin coupled to a cavity. The modeling of the Emitter and the Gate is introduced in this chapter. Furthermore, the model for errors in Emitter and Gate is also described in this chapter.

- Chapter 4 presents the results of the thesis. We present the results of the optimization of Gate parameters. The protocol for tree-cluster generation is explained after that. We introduce the method for the estimation of tree-cluster fidelity. Finally, we estimate the fidelity of the tree-cluster states generated by our system and discuss the results.

- The conclusions and outlook are provided in chapter 5.

2

Background

This chapter introduces the fundamental principles necessary for understanding the remainder of the report. We begin by introducing the Jaynes-Cummings Hamiltonian in sec. 2.1. Following that, we shall introduce the equations governing the dynamic behavior of the system which are the master equation (sec. 2.2) and the Heisenberg-Langevin equation (sec. 2.2.1). In section 2.3 we introduce the method for solving the dynamics of the system. Finally, we discuss the tree-cluster state and their properties in sec. 2.4.

2.1. Jaynes-Cummings model

We present the Jaynes-Cummings model in this section, which is used to describe the interaction of an atom with the optical modes of a cavity [24]. The Jaynes-Cummings model can be used to describe the interaction between a two-level atom and the cavity modes. The Jaynes-Cummings model can be extended to more than two levels [25] and we use the extended models because our system have more that two levels.

2.1.1. Three-level Λ-system inside a cavity

The system consists a spin with three levels coupled to a cavity, shown in fig. 2.1. It has two ground states, $|g\rangle$ and $|f\rangle$, and one excited state $|e\rangle$. We can write the Hamiltonian of the system as a sum of contributions from Hamiltonian of spin, field and their interaction.

$$\hat{H} = \hat{H}_s + \hat{H}_{field} + \hat{H}_{int} \tag{2.1}$$

The electromagnetic fields are quantized inside the cavities, however we do not talk about the quantization of the field in this report, it can be found in [26, 27]. Omitting the vacuum term ($\hbar\omega_c/2$) of the field, we can write $\hat{H}_a$ and $\hat{H}_{field}$ as ($\hbar = 1$),

$$\hat{H}_s = \omega_g |g\rangle\langle g| + \omega_f |f\rangle\langle f| + \omega_e |e\rangle\langle e| \tag{2.2}$$

$$\hat{H}_{field} = \omega_c \hat{c}^\dagger \hat{c} \tag{2.3}$$

where, ω_g, ω_f and ω_e are the frequencies of the levels of the spin, and ω_c is the cavity resonance frequency. Considering the interaction between the spin and photon field and making the rotating wave approximation by ignoring the fast oscillating terms in the interaction Hamiltonian [27]. The interaction Hamiltonian is given by

$$\hat{H}_{int} = \left(g |e\rangle\langle f| \hat{c} + H.C.\right) + \left(\Omega(t) |e\rangle\langle g| e^{-i\omega_L t} + H.C.\right) \tag{2.4}$$

Here Ω is the amplitude of the driving laser and ω_L is its frequency. g is the coupling between the spin and the cavity field. The Jaynes-Cummings Hamiltonian for the system is thus given by

$$\begin{aligned}\hat{H} =&\omega_f |f\rangle\langle f| + \omega_g |g\rangle\langle g| + \omega_e |e\rangle\langle e| + \omega_c \hat{c}^\dagger \hat{c} \\ &+ \left(g |e\rangle\langle f| \hat{c} + H.C.\right) + \left(\Omega(t) |e\rangle\langle g| e^{-i\omega_L t} + H.C.\right)\end{aligned} \tag{2.5}$$

To simplify our analysis of dynamics of the system, we move to the rotating frame of the ground states and the cavity. In the rotating frame, the Hamiltonian is

$$\hat{H} = \Delta |e\rangle\langle e| + \delta \hat{c}^\dagger \hat{c} + (g |e\rangle\langle f| \hat{c} + H.C.) + (\Omega |e\rangle\langle g| + H.C.) \tag{2.6}$$

where Δ is the detuning between the levels and the cavity frequency and δ is the two photon detuning (as shown in fig. 2.1). These two detunings are described as,

$$\begin{aligned}\Delta &= \omega_e - \omega_g - \omega_L \\ \delta &= \omega_f + \omega_c - \omega_g - \omega_L\end{aligned}$$

In our analysis, we will assume that δ is zero. Thus, $\omega_f + \omega_c = \omega_g + \omega_L$.

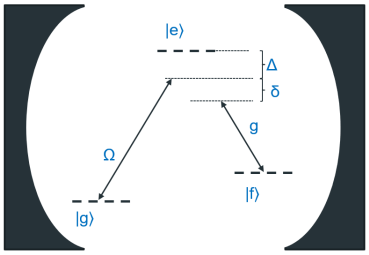

Figure 2.1: A three-level Λ-system coupled to a cavity

2.1.2. Four-level system inside a cavity

The Hamiltonian of a spin with four levels (shown in fig. 2.2), two ground states ($|0\rangle$ and $|1\rangle$) and their respective excited states ($|e_0\rangle$ and $|e_1\rangle$) can be written in a way similar to a three-level system. In our system, we do not drive this system using a laser, therefore, only spin cavity interaction come into the Jaynes-Cummings Hamiltonian. The coupling of the two levels with the cavity are g_1 and g_2. Again, to write the interaction part of the Hamiltonian, we have applied the rotating wave approximation and neglected the fast oscillating terms in the interaction Hamiltonian.

$$\begin{aligned}\hat{H} =&\omega_0 |0\rangle\langle 0| + \omega_1 |1\rangle\langle 1| + \omega_{e_0} |e_0\rangle\langle e_0| + \omega_{e_1} |e_1\rangle\langle e_1| + \omega_c \hat{c}^\dagger \hat{c} \\ &+ \left(g_0 |e_0\rangle\langle 0| \hat{c} + H.C.\right) + \left(g_1 |e_1\rangle\langle 1| \hat{c} + H.C.\right)\end{aligned} \tag{2.7}$$

We move into a rotating frame rotating with the cavity frequency to simplify the Hamiltonian of the system [28].

$$\hat{H} = \Delta_0 |e_0\rangle\langle e_0| + \Delta_1 |e_1\rangle\langle e_1| + \left(g_0 |e_0\rangle\langle 0| \hat{c} + H.C.\right) + \left(g_1 |e_1\rangle\langle 1| \hat{c} + H.C.\right) \tag{2.8}$$

where Δ_0 and Δ_1 are the detuning between levels and cavity frequency.

$$\begin{aligned}\Delta_0 =&\omega_{e_0} - \omega_0 - \omega_c \\ \Delta_1 =&\omega_{e_1} - \omega_1 - \omega_c\end{aligned} \tag{2.9}$$

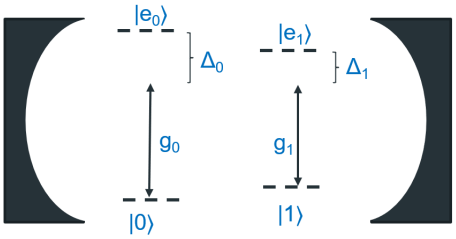

Figure 2.2: The level structure of a four-level spin required for photon-spin entanglement

To realize the level structures as shown in fig. 2.1 and 2.2, one could use a quantum dot coupled to a photonic waveguide [20]. One other exciting system that could be used is a Silicon vacancy center (SiV) coupled to a nanocavity. SiV centers exhibit a four-level structure when a magnetic field is applied [29]. Orthogonal magnetic fields allow the spin to undergo spin-flipping transitions resulting in fast spin initialization and photon generation [30, 31]. Moreover, SiV centers can be efficiently coupled to diamond nanocavities [32] and a recent study demonstrated systems with a single-photon Rabi frequency $g = 2\pi \times 6.81$ GHz, cavity decay rate $\kappa = 2\pi \times 328$ GHz, atomic decay rate $\gamma = 2\pi \times 0.1$ GHz and a cooperativity of $\frac{4|g|^2}{\kappa\gamma} \approx 6$ [33]. The level structure of SiV centers along with their ability efficiently couple to cavities make them an attractive choice for experimental implementation our system.

So far, we have introduced the Hamiltonian of the systems. In the next section, we will introduce the equations that govern the time evolution of the system.

2.2. Master equation

The master equation is a valuable equation for determining the dynamics of a system which is interacting with the environment, such systems are called open quantum systems. Our system is a spin coupled to a cavity interacting with the environment or reservoir. The derivation of this equation is not a part of this report. The derivations could be found in [34, 27]. The master equation in the Schrödinger picture may be represented as ($\hbar = 1$)

$$\dot{\rho} = -i[\hat{H}, \rho] + \sum_x \left(L_x \rho L_x^\dagger - \frac{1}{2}\{L_x^\dagger L_x, \rho\} \right) \tag{2.10}$$

where $\dot{\rho}$ represents the time derivative of ρ and $\hat{H}$ is the Hamiltonian of the system. The first term describes the evolution of the system according to this Hamiltonian. The L_x are called the Lindblad operators or quantum jump operators for different system-environment interactions. The sum over x in the equation describes the transitions in the system due to interactions with the environment. Each $L_x \rho L_x^\dagger$ term is responsible for introducing the jump in the evolution of the system, whereas, the term $\frac{1}{2}\{L_x^\dagger L_x, \rho\}$ is needed to normalize the density matrix of the system.

For a spin-cavity system, we assume that spontaneous emissions are caused by the interaction between the spin and the vacuum state of the environment. We treat the decay as jumps from the excited state to the ground state. For a three-level system with excited state $|e\rangle$ and ground states $|g\rangle$ and $|f\rangle$ the jump operators are

$$\begin{aligned} \hat{L}_{\gamma_g} &= \sqrt{\gamma_g}\,|g\rangle\langle e| \\ \hat{L}_{\gamma_f} &= \sqrt{\gamma_f}\,|f\rangle\langle e| \end{aligned} \tag{2.11}$$

Here, γ_g and γ_f are the respective rates of the decay. The master equation governs the evolution of the density matrix of the system. Therefore, it is capable of dealing with mixed states. However, it comes with the cost of dealing with a large number of differential equations for the entries of the density matrix. The computational power required for solving dynamics of a system with n degrees

of freedom scales up with $\mathcal{O}(n^2)$. The method of Stochastic Hamiltonian has been introduced [35] to reduce the required computational power. We will introduce the Stochastic Hamiltonian in the coming sections in this chapter, sec. 2.3.

Extending the master equation to the Heisenberg picture might seem trivial. However, it is not correct to write the master equation in the Heisenberg picture in general. We discuss the evolution of the system in the Heisenberg picture in the next section.

2.2.1. Heisenberg-Langevin equation

The Heisenberg equations of motion describe the time evolution of operators according to the Hamiltonian of the system. These equations look similar to the equations in the Schrödinger picture. However, we cannot write the equation for operators describing the dynamics of an open quantum system similar to the master equation [27]. If we describe the dissipation by introducing terms similar to Lindblad operators, it could lead to unphysical results (sec. 8.4 of [27]). Therefore, to ensure that the results obtained from the equation are true to the physics, we have to introduce the Langevin noise operator $\hat{f}$ to account for dissipation in the system. This noise operator has zero mean, so its average effect is zero ($\langle \hat{f} \rangle = 0$), but its second moment is non-zero ($\langle \hat{f}^2 \rangle \neq 0$).

However, if we start with an environment in the vacuum state (so that $\hat{f}\,|vac\rangle = 0$), it is possible to ignore the noise operator in the equation. In this case, the Heisenberg-Langevin equation matches with the master equation [27]. Under this assumption, for an operator $\hat{A}$, the Heisenberg-Langevin equation is of the form ($\hbar = 1$)

$$\dot{\hat{A}} = i[\hat{H}, \hat{A}] + \sum_x \left(L_x^\dagger \hat{A} L_x - \frac{1}{2}\{L_x^\dagger L_x, \hat{A}\} \right) \tag{2.12}$$

where $\dot{\hat{A}}$ represents the time derivative of $\hat{A}$. We use this equation to find the dynamics of operators of our spin-cavity systems. We also assume that these conditions hold so that we can ignore contribution from the Langevin noise operator.

Solving the master equation involves dealing with a number of differential equation because we solve for the density matrix of the system. Stochastic Hamiltonian is a method solve the master equation without having to deal with density matrices. In the next section, we introduce the method of stochastic Hamiltonian and discuss the consequences of using such a method.

2.3. Stochastic Wavefunction

To model our system, we need to solve the master equation. We have to model a spin coupled to a cavity undergoing spontaneous emissions. The spin has three levels, and the cavity also has two photonic degrees of freedom. There are a total of six degrees for freedom in the spin-cavity system. To solve the master equation to study the dynamics of the system, we would have to solve a differential equation for each element of the density matrix. In order to avoid solving a large number of differential equations, the method of stochastic Hamiltonian was developed [35, 36]. The stochastic Hamiltonian allows us to solve the Schrödinger equation of the wavefunction, with some caveats. In the remaining part of this section we will derive the stochastic Hamiltonian and study the consequences of using it to model our system.

The master equation takes the following form ($\hbar = 1$)

$$\dot{\rho} = -i[\hat{H}, \rho] + \sum_x \left(L_x \rho L_x^\dagger - \frac{1}{2}\{L_x^\dagger L_x, \rho\} \right) \tag{2.13}$$

expanding the commutation relation between H and ρ.

$$\dot{\rho} = -i\hat{H}\rho + i\rho\hat{H} - \sum_x \frac{1}{2} L_x^\dagger L_x \rho - \sum_x \frac{1}{2} \rho L_x^\dagger L_x + \sum_x L_x \rho L_x^\dagger \tag{2.14}$$

We expand the density matrix to write it as a sum of pure-states and rearrange the terms

$$\begin{aligned}\dot{\rho} = \sum_m p_m \Bigg[-i \Bigg\{ \Bigg(\hat{H} - i \sum_x \frac{1}{2} L_x^\dagger L_x \Bigg) |\psi_m\rangle \langle\psi_m| \\ - |\psi_m\rangle \langle\psi_m| \Bigg(\hat{H} + i \sum_x \frac{1}{2} L_x^\dagger L_x \Bigg) \Bigg\} \\ + \sum_x L_x |\psi_m\rangle \langle\psi_m| L_x^\dagger \Bigg]\end{aligned} \tag{2.15}$$

The first two terms in the sum can be written in terms of $\hat{H}_{eff}$ given by

$$\hat{H}_{eff} = \hat{H} - \frac{i}{2} \sum_x L_x^\dagger L_x \tag{2.16}$$

In terms of the H_{eff} the master equation can be written as,

$$\dot{\rho} = \sum_m p_m \left[-i \left(\hat{H}_{eff} |\psi_m\rangle \langle\psi_m| - |\psi_m\rangle \langle\psi_m| \hat{H}_{eff}^\dagger \right) + \sum_x L_x |\psi_m\rangle \langle\psi_m| L_x^\dagger \right] \tag{2.17}$$

The first term in the preceding equation is analogous to the master equation of a pure state evolving in accordance with a Hamiltonian $\hat{H}_{eff}$. The second term makes the density matrix transform due to the jump operators. The Schrödinger equation for the wavefunctions evolving according to the stochastic Hamiltonian is

$$\frac{d}{dt} |\psi_m\rangle = -i \hat{H}_{eff} |\psi_m\rangle \tag{2.18}$$

The stochastic Hamiltonian is not Hermitian. Hence the wavefunction at the end is not normalized. The method of stochastic Hamiltonian can be used to simulate systems using the Monte Carlo method. We will not simulate systems numerically. Instead, we will use the stochastic Hamiltonian to analytically find the time evolution of a system that does not undergo any spontaneous emissions. Therefore, we analyze a system that could interact with the environment without having to deal with density matrices.

The last term in eq. 2.17 is the term that adds the population to the target state of the jump operators (the ground states of the three-level system, eq. 2.11). If we assume that jump operators take the population from the excited state to a dump state (which is not a part of the system and has no affect on its dynamics), then we may ignore the contribution of the last term in eq. 2.17.

$$\begin{aligned}\hat{L}_{\gamma_g} &= \sqrt{\gamma_g} |\tilde{o}\rangle \langle e| \\ \hat{L}_{\gamma_f} &= \sqrt{\gamma_f} |\tilde{o}\rangle \langle e|\end{aligned} \tag{2.19}$$

In other words, we account for the population loss from the excited state, but we do not add that population to the ground states. The population goes into a dump state, and we do not care about the lost population. When we solve the system dynamics by using the Schrödinger equation and the stochastic Hamiltonian we only find the solution in which no decay occurs. We can find the probability of not "jumping" or decaying by using the square modulus of the wavefunction at the end of the analysis.

2.4. Tree-cluster states

The tree-cluster state is part of a larger class of multi-partite states called the graph state [37, 38]. A tree-cluster state can be represented by the branching parameters b_is. For a tree with l levels one can define branching vector $\vec{B} = [b_0, b_1, ..., b_{l-1}]$ to indicate the connectivity of the tree, with b_i being the branching parameter of the ith level of the tree, as show in fig. 2.3.

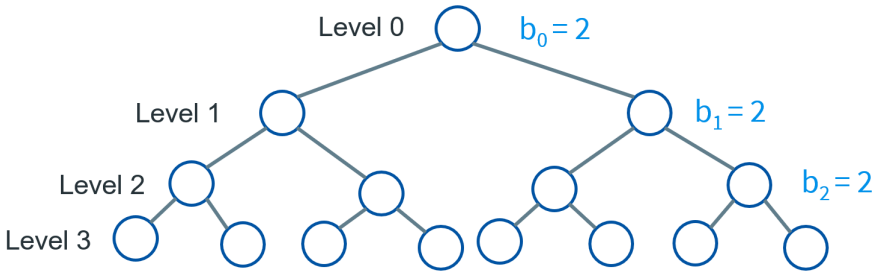

Figure 2.3: A tree with $\bar{B} = [2,2,2]$

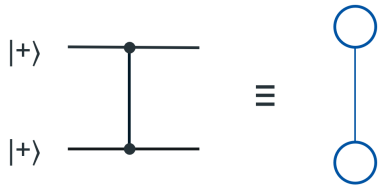

Figure 2.4: CZ operation in quantum circuit is equivalent to an edge between vertices on graph state

A tree-cluster state (also a graph state) $|\Psi\rangle$ can be described as an eigenstate of a set of operators, called the stabilizers. We can associate each vertex i of the state to a stabilizer operator s_i, defined as

$$s_i = \sigma_i^x \bigotimes_{j \in N(i)} \sigma_j^z \tag{2.20}$$

where $N(i)$ is the set of vertices which are neighbors to the vertex i. Thus a stabilizer applies Pauli-X operator to the vertex i and Pauli-Z operators to all its neighbors. The stabilizer acting on a cluster state should not change the state,

$$s_i |\Psi\rangle = |\Psi\rangle \tag{2.21}$$

This is the stabilizer definition of tree-cluster states. Other than this definition, they can also be defined as an interaction between different vertices/qubits of the state. Each vertex in a tree state is a qubit and each edge represents an entanglement operation between the two vertices/qubits it connects. More specifically, the CZ gate is the entangling operation that is applied to the two qubits in order to connect them with an edge. For two qubits, we have to prepare the qubits in $|+\rangle$ state and apply a CZ gate to entangle them, as shown in fig. 2.4. The final state is described as,

$$\begin{aligned} |\psi_{01}\rangle &= \frac{1}{2}(|0_0\rangle|0_1\rangle + |0_0\rangle|1_1\rangle + |1_0\rangle|0_1\rangle - |1_0\rangle|1_1\rangle) \\ &= \frac{1}{\sqrt{2}}(|0_0\rangle|+_1\rangle + |1_0\rangle|-_1\rangle) \\ &= \frac{1}{\sqrt{2}}(|+_0\rangle|0_1\rangle + |-_0\rangle|1_1\rangle) \end{aligned} \tag{2.22}$$

To validate the equivalence between this picture and the stabilizer picture, we can verify that the state $|\psi_{01}\rangle$ is indeed and eigenstate of the stabilizer operator s_i. For a two qubit state the stabilizers are given by

$$\begin{aligned} s_0 &= \sigma_0^x \sigma_1^z \\ s_1 &= \sigma_0^z \sigma_1^x \end{aligned} \tag{2.23}$$

To check if $|\psi_{01}\rangle$ is an eigenstate, we can apply the stabilizers to the two-qubit state

$$\begin{aligned} s_0 |\psi_{01}\rangle &= \frac{1}{\sqrt{2}} \sigma_0^x \sigma_1^z (|0_0\rangle |+_1\rangle + |1_0\rangle |-_1\rangle) \\ &= \frac{1}{\sqrt{2}} (|1_0\rangle |-_1\rangle + |0_0\rangle |+_1\rangle) = |\psi_{01}\rangle \end{aligned} \tag{2.24}$$

similarly it can be shown for the other stabilizer.

To characterize the quality of generated tree-cluster states, we make measurements on the generated tree-cluster state. Therefore, it is important to know what effects does a measurement has on the state. To study the effects, we first introduce the concept of local complementation. A more detailed description can be found in [38, 39, 40]. Local complementation τ_v is an operation that acts on a vertex v of the graph by inverting the edges connecting the neighbors of v. If any two neighbors were connected before local complementation, then after the operation the edge connecting them is removed. Similarly, if two neighbors were not connected before, then after the local complementation, they are connected by an edge. Using the local complementation, the measurement on vertex v in different bases can be summarized as follows,

- **Measuring in Z basis:** Z measurement removes the vertex from the graph/tree up to local Z rotation
- **Measuring in Y basis:** Applies a local complementation on the vertex v and removes the vertex, up to local single-qubit operations
- **Measuring in X basis:** It applies a local complementation τ_u to one of the neighbors $u \in N(v)$ of vertex v. Then it does a Y measurement on v and then does τ_u again (up to single-qubit operations on the state). An X measurement can also be represented as a series of local complementations $(\tau_u \circ \tau_v \circ \tau_u)$ followed by Z measurement. It is also equivalent to $(\tau_v \circ \tau_u \circ \tau_v)$ followed by a Z measurement.

3

Generating photon-spin entanglement

This chapter will explain the implementation of the entangling protocol in detail. Our methodology utilizes the scattering of a photon off a cavity to entangle the photon with a spin coupled to the cavity. We present a system that utilizes two spin-cavity systems. The first spin-cavity system generates a single-photon encoded in a time-bin qubit, and the second spin-cavity system interacts with the generated time-bin photon to give out an entangled photon-spin state.

We will first introduce the protocol for entangling photon and spin in section 3.1. In section 3.2, we shall discuss the dynamics of the Emitter system. The errors in the Emitter are discussed in sec. 3.3. We will then describe the dynamics of the Gate system responsible for photon-spin interaction, discussed in section 3.4. Lastly, the errors in the Gate system are explained in sec. 3.5.

3.1. Photon-spin entangling protocol

This section introduces the protocol for entangling time-bin photons with the Gate spin. The time-bin encoded photons are generated in the first spin-cavity system, the Emitter system. The Gate, which is the second spin-cavity system, reflects the time-bin photons with a reflection coefficient depending on the state of the spin. The state-dependent reflection coefficients coupled with single-qubit gates on the spin could therefore help us entangle photons with the spin. The design of our system is shown in fig. 3.1.

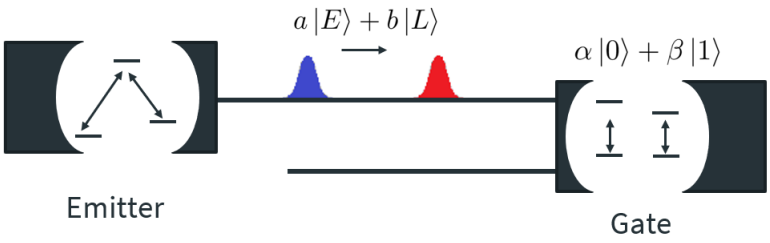

Figure 3.1: System of two spins for generating cluster states

The Gate is a spin coupled to a single-sided. A single-sided cavity can only reflect the incoming time-bin photons. The reflection coefficients of time-bin reflection depend on the state of the spin. In the case of state $|0\rangle$ of the spin, the reflection coefficient is written as r_0, and for the state $|1\rangle$, it is written as r_1. The ideal values of these coefficients are -1 for r_0 and 1 for r_1.

The two bases of a time-bin photon are early and late states, denoted by $|E\rangle$ and $|L\rangle$ respectively [23]. When the early time-bin comes and scatters off the Gate, we call it Early scattering, and when the late time-bin comes in, we call it Late scattering. An arbitrary superposition of the two time-bins

is can be represented as $a|E\rangle + b|L\rangle$, where a and b are chosen such that the state is normalized. An arbitrary state of spin is $\alpha|0\rangle + \beta|1\rangle$, α and β also follow the normalization condition. Therefore the arbitrary photon-spin state ($|\Psi_{ps}\rangle$) is given by:

$$\begin{aligned} |\Psi_{ps}\rangle &= (a|E\rangle + b|L\rangle) \otimes (\alpha|0\rangle + \beta|1\rangle) \\ &= a\alpha|E\rangle|0\rangle + a\beta|E\rangle|1\rangle + b\alpha|L\rangle|0\rangle + b\beta|L\rangle|1\rangle \end{aligned} \tag{3.1}$$

In the next section, we will introduce the protocol to implement CZ operation between time-bin photons and the spin. To get a CZ gate between the photon and the spin, we apply single-qubit gates on the Gate spin between the early and late scattering. The protocol is discussed in the next section.

3.1.1. Entangling photons with spin using single-sided cavity

We combine the state-dependent reflection coefficients with single-qubit gates on the spin between early and late scattering to entangle the photon and the spin. After the early time-bin scatters off the cavity, we change the state of the spin so that the late time-bin interacts with a different state of the spin. The reflection coefficients bunch differently for early and late states giving us an entangled state between the photon and the spin. We represent the photon-spin interaction and the single-qubit operations in the form of a quantum circuit, as shown in fig. 3.2.

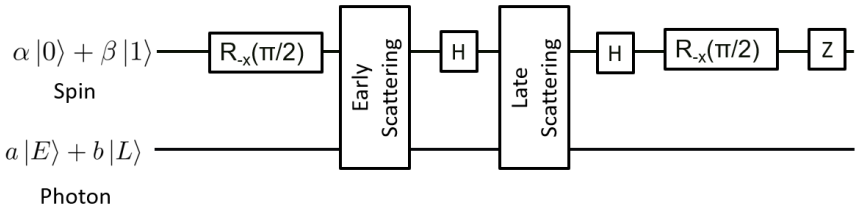

Figure 3.2: Circuit representation of the photon-spin entangling protocol. The "Early scattering" and "Late scattering" blocks symbolize photon scattering off the cavity.

We apply a Hadamard gate on the spin before and after late scattering, and we apply another gate to the spin before and after the photon-spin interaction. The $R_{-X}(\pi/2)$ gate is a rotation of $\pi/2$ about the negative X-axis on the Bloch sphere, and it is given by:

$$R_{-X}(\pi/2) = \frac{1}{\sqrt{2}}\begin{bmatrix} 1 & i \\ i & 1 \end{bmatrix} \tag{3.2}$$

Applying this rotation to $|0\rangle$ and $|1\rangle$ states results in $|i\rangle$ and $|-i\rangle$ states respectively, as shown below,

$$\begin{aligned} R_{-X}(\pi/2)|0\rangle &= \frac{1}{\sqrt{2}}(|0\rangle + i|1\rangle) \\ R_{-X}(\pi/2)|1\rangle &= \frac{i}{\sqrt{2}}(|0\rangle - i|1\rangle) \end{aligned} \tag{3.3}$$

Now that we have introduced all the single-qubit gates necessary to entangle photons with the spin, we will see how the photon-spin state evolves under all these operations to give out an entangled state. We start with an arbitrary unentangled photon-spin state $|\Psi_{ps}\rangle$, given by

$$\begin{aligned} |\Psi_{ps}\rangle &= (a|E\rangle + b|L\rangle) \otimes (\alpha|0\rangle + \beta|1\rangle) \\ &= a\alpha|E\rangle|0\rangle + a\beta|E\rangle|1\rangle + b\alpha|L\rangle|0\rangle + b\beta|L\rangle|1\rangle \end{aligned} \tag{3.4}$$

Applying $R_{-X}(\pi/2)$ rotation on the spin gives us

$$|\Psi_{ps}\rangle = (a|E\rangle + b|L\rangle)\left(\frac{\alpha}{\sqrt{2}}(|0\rangle + i|1\rangle) + \frac{i\beta}{\sqrt{2}}(|0\rangle - i|1\rangle)\right) \tag{3.5}$$

After early scattering the state becomes

$$\begin{aligned}|\Psi_{ps}\rangle =& a|E\rangle\left(\frac{\alpha}{\sqrt{2}}(r_0|0\rangle + ir_1|1\rangle) + \frac{i\beta}{\sqrt{2}}(r_0|0\rangle - ir_1|1\rangle)\right)\\ &+ b|L\rangle\left(\frac{\alpha}{\sqrt{2}}(|0\rangle + i|1\rangle) + \frac{i\beta}{\sqrt{2}}(|0\rangle - i|1\rangle)\right)\end{aligned} \tag{3.6}$$

After the Hadamard gate on the spin, the photon-spin state transforms to the following state

$$\begin{aligned}|\Psi_{ps}\rangle =& a|E\rangle\left(\frac{\alpha}{2}((r_0+ir_1)|0\rangle + (r_0-ir_1)|1\rangle) + \frac{i\beta}{2}((r_0-ir_1)|0\rangle + (r_0+ir_1)|1\rangle)\right)\\ &+ b|L\rangle\left(\frac{\alpha}{2}((1+i)|0\rangle + (1-i)|1\rangle) + \frac{i\beta}{2}((1-i)|0\rangle + (1+i)|1\rangle)\right)\end{aligned} \tag{3.7}$$

Scattering the late time-bin gives us

$$\begin{aligned}|\Psi_{ps}\rangle =& a|E\rangle\left(\frac{\alpha}{2}((r_0+ir_1)|0\rangle + (r_0-ir_1)|1\rangle) + \frac{i\beta}{2}((r_0-ir_1)|0\rangle + (r_0+ir_1)|1\rangle)\right)\\ &+ b|L\rangle\left(\frac{\alpha}{2}((1+i)r_0|0\rangle + (1-i)r_1|1\rangle) + \frac{i\beta}{2}((1-i)r_0|0\rangle + (1+i)r_1|1\rangle)\right)\end{aligned} \tag{3.8}$$

Applying Hadamard gate on the spin results in

$$\begin{aligned}|\Psi_{ps}\rangle =& a|E\rangle\left(\frac{\alpha}{\sqrt{2}}(r_0|0\rangle + ir_1|1\rangle) + \frac{i\beta}{\sqrt{2}}(r_0|0\rangle - ir_1|1\rangle)\right)\\ &+ b|L\rangle\frac{\alpha}{2}\left(\frac{r_0(1+i)+r_1(1-i)}{2}|0\rangle + \frac{r_0(1+i)-r_1(1-i)}{2}|1\rangle\right)\\ &+ b|L\rangle\frac{i\beta}{2}\left(\frac{r_0(1-i)+r_1(1+i)}{2}|0\rangle + \frac{r_0(1-i)-r_1(1+i)}{2}|1\rangle\right)\end{aligned} \tag{3.9}$$

Applying $R_{-X}(\pi/2)$ rotation on the spin would give us the output state as

$$\begin{aligned}|\Psi_{ps}\rangle =& \frac{a\alpha}{2}|E\rangle((r_0-r_1)|0\rangle + i(r_0+r_1)|1\rangle)\\ &+ \frac{ia\beta}{2}|E\rangle((r_0+r_1)|0\rangle + i(r_0-r_1)|1\rangle)\\ &+ \frac{ib\alpha}{2}|L\rangle((r_0-r_1)|0\rangle + (r_0+r_1)|1\rangle)\\ &+ \frac{ib\beta}{2}|L\rangle((r_0+r_1)|0\rangle + (r_0-r_1)|1\rangle)\end{aligned} \tag{3.10}$$

Applying Z gate on the spin

$$\begin{aligned}|\Psi_{ps}\rangle =& \frac{a\alpha}{2}|E\rangle((r_0-r_1)|0\rangle - i(r_0+r_1)|1\rangle)\\ &+ \frac{ia\beta}{2}|E\rangle((r_0+r_1)|0\rangle - i(r_0-r_1)|1\rangle)\\ &+ \frac{ib\alpha}{2}|L\rangle((r_0-r_1)|0\rangle - (r_0+r_1)|1\rangle)\\ &+ \frac{ib\beta}{2}|L\rangle((r_0+r_1)|0\rangle - (r_0-r_1)|1\rangle)\end{aligned} \tag{3.11}$$

This is the final state of the protocol for arbitrary initial unentangled states of photon and spin, and for arbitrary reflection coefficients, r_0 and r_1.

Ideally, we would like to have perfect reflection so that the magnitude of reflection coefficients is unity, $|r_0| = |r_1| = 1$, and the phase difference between r_0 and r_1 is π. Simply, we want $r_0 = -1$ and $r_1 = 1$. If we put these values in the entangled photon-spin state, we get the following entangled state.

$$\begin{aligned} |\Psi_{ps}\rangle &= -a\alpha\,|E\rangle\,|0\rangle - a\beta\,|E\rangle\,|1\rangle - ib\alpha\,|L\rangle\,|0\rangle + ib\beta\,|L\rangle\,|1\rangle \\ &= -\left[a\,|E\rangle\,(\alpha\,|0\rangle + \beta\,|1\rangle) + ib\,|L\rangle\,(\alpha\,|0\rangle - \beta\,|1\rangle)\right] \\ &= -\left[(a\,|E\rangle + ib\,|L\rangle)\alpha\,|0\rangle + (a\,|E\rangle - ib\,|L\rangle)\beta\,|1\rangle\right] \end{aligned} \tag{3.12}$$

We can ignore the global phase to get the following final photon-spin state

$$|\Psi_{ps}\rangle = \left[(a\,|E\rangle + ib\,|L\rangle)\alpha\,|0\rangle + (a\,|E\rangle - ib\,|L\rangle)\beta\,|1\rangle\right] \tag{3.13}$$

For $a = \alpha = \beta = 1/\sqrt{2}$ and $b = -i/\sqrt{2}$ the initial state is

$$\begin{aligned} |\Psi_{ps}\rangle &= \frac{1}{\sqrt{2}}(|E\rangle - i\,|L\rangle) \otimes \frac{1}{\sqrt{2}}(|0\rangle + |1\rangle) \\ &= |-i\rangle \otimes |+\rangle \end{aligned} \tag{3.14}$$

the final state after photon-spin entangling protocol for this initial state would be

$$\begin{aligned} |\Psi_{ps}\rangle &= \frac{1}{2}(|E\rangle + |L\rangle)\,|0\rangle - \frac{1}{2}(|E\rangle - |L\rangle)\,|1\rangle \\ &= \frac{1}{\sqrt{2}}(|+\rangle\,|0\rangle + |-\rangle\,|1\rangle) \end{aligned} \tag{3.15}$$

Therefore, the protocol takes the initial photon-spin state $|-i\rangle\,|+\rangle$ to a state which is the resulting state of CZ between $|+\rangle$ and a $|+\rangle$ which is a maximally entangled state between photon and spin. If the spin and the photon are two vertices of a graph state, this protocol forms an edge between them.

This protocol can entangle an arbitrary state of spin with a state of the photon. Coefficients of $|0\rangle$ state and $|1\rangle$ state of spin do not change after the protocol, as shown in eq. 3.13. Consequently, this protocol can entangle a photon to a spin that is already entangled with other photons. The coefficients α and β could contain information about the states of other photons entangled with the spin. And this protocol does not result in a state with a sum of the coefficients α and β in it. Thus, entangling a new photon does not change the states of the other photons entangled to the spin. Therefore, it can be used to generate graph states or tree-cluster states. The aim of this thesis is the generation of tree-cluster states, and the protocol for tree generation is discussed in Chapter 4. The next section will model the single-photon source, the Emitter, which is the first of our two spin-cavity systems.

3.2. Emitter Dynamics

Our system consists of two spins coupled to cavities, the Emitter and the Gate. In this section, the dynamics of the Emitter system are explained. We will discuss how to generate single-photons and the state of the time-bin qubits. After that, we will explore the different errors that can occur during the photon generation in the next section.

3.2.1. The Emitter system

The system is a three-level Λ system with two ground states $|g\rangle$ and $|f\rangle$, and an excited state $|e\rangle$ (fig. 3.3). The Jaynes-Cummings Hamiltonian in a suitable rotating frame is given by eq. 2.6. Here, Ω is the amplitude of the driving laser that takes the spin from the ground state $|g\rangle$ to the excited state $|e\rangle$. The driving laser could be time-dependent or time-independent. For our analysis we will consider that the drive is a square pulse. The transition $|e\rangle$ to $|f\rangle$ is coupled to the cavity with a single-photon

Rabi frequency g. When the spin makes a transition from the excited state $|e\rangle$ to the ground state $|f\rangle$, the spin releases energy in the form of a photon in the cavity mode. (In our analysis, we have assumed $\hbar = 1$)

$$\hat{H}_{JC} = \Delta |e\rangle\langle e| + \delta \hat{c}^\dagger \hat{c} + (g|e\rangle\langle f| c + H.C.) + (\Omega |e\rangle\langle g| + H.C.) \tag{3.16}$$

where Ω is the amplitude of the laser pulse. Δ is the detuning between the laser frequency and the $|g\rangle \rightarrow |e\rangle$ transition. δ is the two-photon detuning and we will assume that it is zero throughout this analysis.

$$\Delta = \omega_e - \omega_g - \omega_L$$
$$\delta = \omega_f + \omega_c - \omega_g - \omega_L$$

The choice of basis for our analysis are the following three spin-photon states, $|g\rangle|0\rangle$, $|e\rangle|0\rangle$ and $|f\rangle|1\rangle$. Where, $|g\rangle$, $|f\rangle$ and $|e\rangle$ are the states of the spin and $|0\rangle$ and $|1\rangle$ are the states of the photon in cavity mode. Therefore, $|f\rangle|1\rangle$ state has a photon in the cavity mode and the spin in the ground state $|f\rangle$, while $|g\rangle|0\rangle$ and $|e\rangle|0\rangle$ do not have a photon inside the cavity.

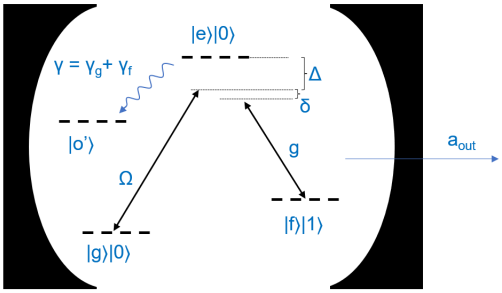

Figure 3.3: Level structure of the Emitter with dump-state and detunings

The photon in the cavity mode could escape the cavity in the output mode with a rate given by κ. This photon is in the desired output mode, and it goes on to entangle with the Gate. Besides generating a photon in the cavity mode, the spin could emit a photon by spontaneously decaying to one of the two ground states from the excited state. If a spontaneous decay occurs, we will lose the emitted photon to the environment, leading to errors. The rates of spontaneous emission are denoted by γ_g for the $|g\rangle$ ground state and γ_f for the $|f\rangle$ ground state. These transitions are included in the dynamics as jump operators in the Lindblad equation, summarized in eq. 3.18.

To understand the evolution of the system according to the Hamiltonian, we solve the Lindblad equation (introduced in sec. 2.2), given by:

$$\dot{\rho} = -i[\hat{H}_{JC}, \rho] + \sum_x \left(L_x \rho L_x^\dagger - \frac{1}{2}\{L_x^\dagger L_x, \rho\} \right) \tag{3.17}$$

L_x are the jump operators which are given by,

$$\begin{aligned} \hat{L}_{\gamma_g} &= \sqrt{\gamma_g}\,|g\rangle\langle e| \\ \hat{L}_{\gamma_f} &= \sqrt{\gamma_f}\,|f\rangle\langle e| \\ \hat{L}_\kappa &= \sqrt{\kappa}\,\hat{c} \end{aligned} \tag{3.18}$$

To find out the output mode of the photon, we use the input-output relations of the cavity. The input-output relations [41, 42] give us the output mode in terms of the cavity mode (the generated photon in the cavity mode escapes in the output mode with a rate κ).

$$\hat{a}_{out} = \sqrt{\kappa}\,\hat{c} \tag{3.19}$$

Solving the Lindblad equation involves solving the density matrix. To reduce the amount of computation required, we will use the method of the stochastic Hamiltonian (2.3). However, first, we need to define the wavefunction of the system. To define the wavefunction we go back to the basis states, those states are $|g0\rangle$, $|e0\rangle$ and $|f1\rangle$. We can define a time-dependent wavefunction $|\psi(t)\rangle$ which would be a linear combination of the basis states with time-dependent coefficients. The wavefunction is described as

$$|\psi(t)\rangle = c_0(t)\,|g0\rangle + c_1(t)\,|e0\rangle + c_2(t)\,|f1\rangle \tag{3.20}$$

We are interested in solving the time dependence of this wavefunction. Specifically, we want to find out the evolution of the $|f1\rangle$ state, thus the coefficient $c_2(t)$. The evolution of a wavefunction according to the effective Hamiltonian is given by eq. 3.17. At $t = 0$ the spin is in the ground state $|g\rangle$, and there is no excitation in the cavity, that is, the cavity is empty. The Schrödinger equation for solving the evolution of the wavefunction evolving according to the stochastic Hamiltonian is

$$\frac{d}{dt}|\psi(t)\rangle = -i\hat{H}_{eff}\,|\psi(t)\rangle \tag{3.21}$$

where stochastic Hamiltonian for the system is defined as,

$$\begin{aligned}\hat{H}_{eff} =& \Delta\,|e\rangle\langle e| + \delta\hat{c}^{\dagger}\hat{c} + (g\,|e\rangle\langle f|\,c + H.C.) + (\Omega\,|e\rangle\langle g| + H.C.)\\ &- \frac{i}{2}\left(\gamma\,|e\rangle\langle e| + \kappa\hat{c}^{\dagger}\,|f\rangle\langle f|\,\hat{c}\right)\end{aligned} \tag{3.22}$$

where, $\gamma = \gamma_g + \gamma_f$ is the total decay rate. We will solve the differential equation using the method of stochastic Hamiltonian. Therefore any spontaneous emission results in a population loss to dump states, as shown in fig. 3.3.

3.2.2. Output mode of the photon

To find the mode of the outgoing photon, we first have to solve the equation 3.21 to find the time dependence of the coefficient of the $|f1\rangle$ state, $c_2(t)$. The time-dependent Schrödinger equation gives us three correlated differential equations in time-dependent coefficients c_0, c_1 and c_2.

$$\begin{aligned} i\dot{c}_0 &= c_1\Omega^*\\ i\dot{c}_1 &= c_0\Omega + c_1\left(\Delta - \frac{i}{2}\gamma\right) + c_2 g\\ i\dot{c}_2 &= c_1 g^* + c_2\delta - \frac{i}{2}\kappa c_2\end{aligned} \tag{3.23}$$

In order to get the solution of these equations analytically, we first make a few assumptions and then make adiabatically elimination.

- Assumption 1: we are in the weak driving regime and we are far detuned from the level

$$\Omega \ll \Delta$$

- Assumption 2: the rate of photon emission is large compared to the rate of generation of photon inside the cavity. Furthermore, the rate of spontaneous emission is negligible compared to single-photon Rabi frequency.

$$\gamma \ll g \ll \kappa$$

- Assumption 3: We have already introduced this assumption earlier, to group all the assumptions together we do it again here. δ is zero

$$\delta = 0$$

Now we adiabatically eliminate the third differential equation by putting the second and the third assumptions to use,

$$i\dot{c}_2 = c_1 g^* + c_2\delta - \frac{i}{2}\kappa c_2 \approx 0$$

which gives us the relation between $c_2(t)$ and $c_1(t)$,

$$c_2 = -\frac{2ig^*}{\kappa}c_1 \tag{3.24}$$

Substituting $c_2(t)$ in the second differential equation and adiabatically eliminating would give us a relation between $c_1(t)$ and $c_0(t)$,

$$\begin{aligned} i\dot{c}_1 &= c_0\Omega + c_1\left(\Delta - \frac{i}{2}\gamma\right) + c_2 g \\ &= c_0\Omega + c_1\left(\Delta - \frac{i}{2}\gamma\right) - \frac{2i|g|^2}{\kappa}c_1 \\ &= c_0\Omega + c_1\left(\Delta - \frac{i\gamma}{2}(1+4C)\right) \approx 0 \end{aligned}$$

$$c_1 = \frac{-\Omega}{\Delta - \frac{i\gamma}{2}(1+4C)}c_0 \tag{3.25}$$

Here, C is the cooperativity of the system given by $C = \frac{|g|^2}{\kappa\gamma}$. Substituting $c_1(t)$ in the first differential equation would give us a differential equation in $c_0(t)$.

$$\dot{c}_0 = \frac{i|\Omega|^2}{\Delta - \frac{i\gamma}{2}(1+4C)}c_0 = bc_0 \tag{3.26}$$

where

$$b = \frac{i|\Omega|^2(\Delta + \frac{i\gamma}{2}(1+4C))}{\Delta^2 + \frac{\gamma^2}{4}(1+4C)^2} \tag{3.27}$$

The solution of this equation is an exponential in time and using the initial conditions we can find $c_0(t)$ thus the $|\psi(t)\rangle$,

$$c_0(t) = e^{bt} \tag{3.28}$$

We know the relations between $c_0(t)$, $c_1(t)$ and $c_2(t)$ from before, we can write down the wavefunction of the system in terms of the parameter b (eq. 3.27).

$$|\psi(t)\rangle = e^{bt}|g0\rangle - \frac{\Omega(\Delta + \frac{i\gamma}{2}(1+4C))}{\Delta^2 + \frac{\gamma^2}{4}(1+4C)^2}e^{bt}|e0\rangle + \frac{2i\Omega g^*\left(\Delta + \frac{i\gamma}{2}(1+4C)\right)}{\kappa\left(\Delta^2 + \frac{\gamma^2}{4}(1+4C)^2\right)}e^{bt}|f1\rangle \tag{3.29}$$

In terms of b (eq. 3.27), it is

$$|\psi(t)\rangle = e^{bt}|g0\rangle + e^{bt}\frac{ib}{\Omega^*}|e0\rangle + e^{bt}\frac{2g^*b}{\Omega^*\kappa}|f1\rangle$$

This is the solution for a drive that is constant in time. In case we do not turn off the drive, the population in the $|g0\rangle$ state will get slowly transferred to the $|f1\rangle$ state. The $|f1\rangle$ state emits

the photon simultaneously, and as a result, it decays to the $|f0\rangle$ state. Having a significantly large cavity decay rate (κ) compared to the spin-cavity coupling (g) implies that as the spin undergoes the cavity coupled transition, generating a photon in the cavity mode, which escapes the cavity instantaneously. At longer times, the whole population of $|g0\rangle$ state is transferred to the $|f1\rangle$ via the excited state, which in turn decays to the $|f0\rangle$ state giving out a photon. The rate of decay from the excited is low because we are in the weak driving regime ($\Omega \ll \Delta$).

3.2.3. Drive for generating time-bin photon

So far, we have only considered a drive that is constant in time. However, to generate time-bin photons, we have to turn the drive off for some time and then turn it back on again. In this subsection, we will discuss the evolution of our system after the driving is stopped. First let us assume that the drive is on from time $t = 0$ to $t = T_1$ and from time $t = T_1$ to $t = T_2$ it is zero. For the time after $t = T_2$, it is on again. We will first find the solution for the wavefunction from time $t = T_1$ to $t = T_2$ and then we will solve for time $T_2 < t$.

For the analysis from $t = T_1$ to $t = T_2$, we can put the value of Ω to zero in the differential equations, resulting in the following equation

$$\begin{aligned} i\dot{c}_0 &= 0 \\ i\dot{c}_1 &= c_1\left(\Delta - \frac{i}{2}\gamma\right) + c_2 g \\ i\dot{c}_2 &= c_1 g^* + c_2\delta - \frac{i}{2}\kappa c_2 \end{aligned} \tag{3.30}$$

We know that the drive was on from $t = 0$ to $t = T_1$, therefore the initial condition for solving the set of differential equations 3.30 is the wavefunction at $t = T_1$. In terms of b (eq. 3.27), it is

$$|\psi(t = T_1)\rangle = e^{bT_1}|g0\rangle + e^{bT_1}\frac{ib}{\Omega^*}|e0\rangle + e^{bT_1}\frac{2g^* b}{\Omega^*\kappa}|f1\rangle$$

To solve the set of differential equations, we will again make use of our assumptions about the various parameters, as discussed in the previous subsection. We can therefore adiabatically eliminate the third differential equation and find the relation between $c_2(t)$ and $c_1(t)$.

$$\begin{aligned} i\dot{c}_2 &= c_1 g^* + c_2\delta - \frac{i}{2}\kappa c_2 \approx 0 \\ c_2 &= -\frac{2ig^*}{\kappa}c_1 \end{aligned} \tag{3.31}$$

where δ was assumed earlier to be zero. substituting $c_2(t)$ in the second equation gives an ordinary differential equation in c_1, as shown in equation 3.32

$$\begin{aligned} i\dot{c}_1 &= c_1\left(\Delta - \frac{i}{2}\gamma\right) + \frac{-2i|g|^2}{\kappa}c_1 \\ \dot{c}_1 &= -i\left(\Delta - \frac{i\gamma}{2}(1+4C)\right)c_1 \end{aligned} \tag{3.32}$$

The solution of this differential equation is an exponential decay. After taking into account the initial conditions, we get that for time $T_1 < t < T_2$,

$$\begin{aligned} |\psi(t)\rangle =& c_0(T_1)|g0\rangle + c_1(T_1)e^{-i\left(\Delta - \frac{i\gamma}{2}(1+4C)\right)(t-T_1)}|e0\rangle \\ &- \frac{2ig^* c_1(T_1)}{\kappa}e^{-i\left(\Delta - \frac{i\gamma}{2}(1+4C)\right)(t-T_1)}|f1\rangle \end{aligned} \tag{3.33}$$

where,

$$c_1(T_1) = -\frac{\Omega(\Delta + \frac{i\gamma}{2}(1+4C))}{\Delta^2 + \frac{\gamma^2}{4}(1+4C)^2} e^{bT_1} \tag{3.34}$$

$$c_0(T_1) = e^{bT_1} \tag{3.35}$$

For sanity check, let us look at this solution at $t = T_1$. The exponential terms in the expression dependent on t would become unity, and we are just left with:

$$|\psi(t = T_1)\rangle = c_0(T_1)|g0\rangle + c_1(T_1)|e0\rangle - \frac{2ig^* c_1(T_1)}{\kappa}|f1\rangle \tag{3.36}$$

This is the same as the initial wavefunction, thus confirming that the wavefunction does not have a discontinuity.

At this point, we can make a couple of observations. First, after the driving is stopped, c_0 remains constant. It makes sense as the population in the state $|g0\rangle$ is not pumped to the excited state anymore. Second, $c_2(t)$ is an exponential decay, and it goes to zero with a rate roughly equal to $\gamma(1+4C)/2$. This makes sense as no population is added to the $|e0\rangle$ state, and the remaining population only undergoes the transition to the $|f1\rangle$ state with a Purcell enhanced decay rate $\gamma(1+4C)/2$.

If we make sure that $T_2 - T_1$ is large enough such that the coefficients of states $|e0\rangle$ and $|f1\rangle$ are negligible at $t = T_2$, then we can see that the wavefunction at a time just before T_2 is given by:

$$|\psi(t = T_1)\rangle = c_0(T_1)|g0\rangle \tag{3.37}$$

Mathematically the condition on T_2 in terms of the rate of decay is therefore

$$\frac{1}{\gamma(1+4C)} \ll (T_2 - T_1) \tag{3.38}$$

For time $T_2 < t$, the drive is on, therefore, the differential equations would look the same as the differential equations for time $0 < t < T_1$, given by equation 3.23. The only difference is that this time we will have different initial conditions.

$$|\psi(t = T_2)\rangle = c_0(T_1)|g0\rangle \tag{3.39}$$

If we include these initial conditions in our solution for the differential equation, eq. 3.23, the solution for $T_2 < t$ would therefore be,

$$|\psi(t)\rangle = c_0(T_1)e^{b(t-T_2)}|g0\rangle + c_0(T_1)e^{b(t-T_2)}\frac{ib}{\Omega^*}|e0\rangle + c_0(T_1)e^{b(t-T_2)}\frac{2g^* b}{\Omega^* \kappa}|f1\rangle \tag{3.40}$$

where b is defined in eq. 3.27. We can observe that this solution is also continuous at $t = T_2$.

In conclusion, for a drive that is on only from $t = 0$ to $t = T_1$ and for $T_2 < t$ we have the solution for the wavefunction of the system. For $0 < t < T_1$,

$$\begin{aligned}
|\psi(t)\rangle =& e^{bt}|g0\rangle + e^{bt}\frac{ib}{\Omega^*}|e0\rangle + e^{bt}\frac{2g^* b}{\Omega^* \kappa}|f1\rangle, && \text{for} \quad 0 < t < T_1, \\
|\psi(t)\rangle =& c_0(T_1)|g0\rangle + c_1(T_1)e^{-i\left(\Delta - \frac{i\gamma}{2}(1+4C)\right)(t-T_1)}|e0\rangle \\
& - \frac{2ig^* c_1(T_1)}{\kappa}e^{-i\left(\Delta - \frac{i\gamma}{2}(1+4C)\right)(t-T_1)}|f1\rangle, && \text{for} \quad T_1 < t < T_2, \\
|\psi(t)\rangle =& c_0(T_1)e^{b(t-T_2)}|g0\rangle + c_0(T_1)e^{b(t-T_2)}\frac{ib}{\Omega^*}|e0\rangle \\
& + c_0(T_1)e^{b(t-T_2)}\frac{2g^* b}{\Omega^* \kappa}|f1\rangle, && \text{for} \quad T_2 < t
\end{aligned} \tag{3.41}$$

where b is defined in eq. 3.27.

3.2.4. Defining early and late time-bin

In this subsection, we will introduce the state of the output photon. We know the dynamics of the spin and the cavity photon, and we have a solution for the spin-photon wavefunction. Furthermore, from the wavefunction, we know how the different states of the spin-photon system evolve as a function of time.

For the mode of the generated photon inside the cavity, we focus on the dynamics of the $|f1\rangle$ state. The coefficient of the $|f1\rangle$ state is $c_2(t)$, and from our previous analysis, we know its form for our drive. In addition, we stop the drive for some time in order to separate the two states of the time-bin, $|E\rangle$ and $|L\rangle$. We can define the early and late time-bins in terms of the coefficient $c_2(t)$ before and after $t = T_2$ respectively. We define two new coefficients $c_{2,E}$ and $c_{2,L}$ to separate the modes of the two time-bins. For the early time-bin, $c_{2,E}$ is of the form,

$$\begin{aligned} c_{2,E}(t) &= \frac{2g^* b}{\Omega^* \kappa} e^{bt}, && \text{for} \quad 0 < t < T_1, \\ &= \frac{-2ig^* c_1(T_1)}{\kappa} e^{-i\left(\Delta - \frac{i\gamma}{2}(1+4C)\right)(t-T_1)}, && \text{for} \quad T_1 < t < T_2 \end{aligned} \tag{3.42}$$

Similarly, for the late time-bin, $c_{2,L}$ is of the form,

$$c_{2,L}(t) = c_0(T_1) \frac{2g^* b}{\Omega^* \kappa} e^{b(t-T_2)} \qquad \text{for} \qquad T_2 < t \tag{3.43}$$

From the input output relation, equation 3.19, the output mode of the photon in terms of the cavity mode is known. Furthermore, we know the cavity mode from $c_2(t)$. It is therefore possible to define an operator $\hat{A}$ which generates the output photon in terms of κ, $c_2(t)$ and $\hat{c}$, as defined by Tiurev et al. in [43].

$$\hat{A}^\dagger(t) = \int_0^t \sqrt{\kappa} c_2(t') \hat{c}^\dagger(t')\, dt' \tag{3.44}$$

where the operator $\hat{c}^\dagger(t')$ generates a photon in the cavity mode at time t' and obeys the Bosonic operator commutation relations, $[\hat{c}(t), \hat{c}^\dagger(t')] = \delta_{tt'}$.

For the early and late time-bins we define operators $\hat{A}_E^\dagger$ and $\hat{A}_L^\dagger$ respectively in terms of $c_{2,E}$ and $c_{2,L}$. We can write the output-mode creation operator in terms of the cavity creation operator.

$$\begin{aligned} \hat{A}_E^\dagger &= \int_0^{T_2} \sqrt{\kappa} c_{2,E}(t') \hat{c}^\dagger(t')\, dt' \\ \hat{A}_L^\dagger &= \int_{T_2}^{\infty} \sqrt{\kappa} c_{2,L}(t') \hat{c}^\dagger(t')\, dt' \end{aligned} \tag{3.45}$$

the operator $\hat{c}^\dagger(t')$ generates a photon in the cavity mode at time $t = t'$. $\hat{A}_E^\dagger$ and $\hat{A}_L^\dagger$ operators create the photon in the output-mode in early and late time-bins.

We have assumed that the quantity $T_2 - T_1$ large as compared to the rate of the exponential decay, as shown in eq. 3.38. Therefore, we can make an approximation in our definition of $\hat{A}_E^\dagger$.

$$\hat{A}_E^\dagger \approx \int_0^{\infty} \sqrt{\kappa} c_{2,E}(t') \hat{c}^\dagger(t')\, dt' \tag{3.46}$$

We can also simplify the definition of $\hat{A}_L^\dagger$ so that it starts at $t = 0$ and goes on till infinity. Notice in the definition of $c_{2,L}(t')$ that it depends only on the quantity $t - T_2$. In the integral for $\hat{A}_L^\dagger$, we can make a variable change in the exponential in the term $c_{2,L}(t')$. If we write the integral in terms of t'', where $t'' = t' - T_2$, and if we also make suitable changes to the limits, the operator $\hat{A}_L^\dagger$ can be re-written as:

$$\begin{aligned}\hat{A}_L^\dagger &= \int_0^\infty \sqrt{\kappa} c_0(T_1) \frac{2g^* b}{\Omega^* \kappa} e^{bt''} \hat{c}^\dagger(t'')\, dt'' \\ &= \int_0^\infty \sqrt{\kappa} c_{2,L}(t'') \hat{c}^\dagger(t'')\, dt''\end{aligned} \tag{3.47}$$

Defining the operators $\hat{A}_{E/L}^\dagger$ now allows us to define the early and late time-bins. Applying these operators on the vacuum state gives us the early and late states,

$$|E\rangle = \hat{A}_E^\dagger |vac\rangle = \int_0^\infty \sqrt{\kappa} c_{2,E}(t') \hat{c}^\dagger(t')\, dt' |vac\rangle \tag{3.48}$$

$$-i|L\rangle = \hat{A}_L^\dagger |vac\rangle = \int_0^\infty \sqrt{\kappa} c_{2,L}(t'') \hat{c}^\dagger(t'')\, dt'' |vac\rangle \tag{3.49}$$

We define the late state $|L\rangle$ with a phase because of our photon-spin entangling protocol. Recall that the protocol takes the photon in $|-i\rangle$ state to give out an entangled photon-spin state. Note that the form of the integrals give us an illusion that there is a finite overlap between the early and late time-bins. But we have to keep in mind that t'' is always greater than t' by T_2 and the value of $c_{2,E}(T_2)$ goes to zero for large enough T_2, i.e. $c_{2,E}(T_2) \approx 0$.

3.2.5. Probability of getting output photon

So far, we have defined the states $|E\rangle$ and $|L\rangle$ of the early and late time-bins. Now we will look at the probability of generating those time-bins. The probability of photon being in the early time-bin is given by,

$$\begin{aligned}\langle E|E\rangle &= \langle vac| \hat{A}_E \hat{A}_E^\dagger |vac\rangle \\ &= \int_0^\infty \int_0^\infty \kappa \langle vac| \hat{c}(t') c_{2,E}^*(t') c_{2,E}(t_1') \hat{c}^\dagger(t_1') |vac\rangle\, dt'\, dt_1' \\ &= \int_0^\infty \kappa |c_{2,E}(t')|^2\, dt'\end{aligned} \tag{3.50}$$

The integral of $|c_{2,E}(t_1')|^2$ can be split into two separate integrals, one from $t = 0$ to $t = T_1$ and the other for $t > T_1$.

$$\begin{aligned}\langle E|E\rangle &= \int_0^{T_1} \kappa |c_{2,E}(t')|^2 + \int_{T_1}^\infty \kappa |c_{2,E}(t')|^2\, dt' \\ &= \kappa \int_0^{T_1} \frac{4|g|^2|\Omega|^2}{\kappa^2(\Delta^2 + \frac{\gamma^2(1+4C)^2}{4})} e^{-\frac{|\Omega|^2\gamma(1+4C)}{\Delta^2 + \frac{\gamma^2(1+4C)^2}{4}} t'}\, dt' \\ &\quad + \kappa \int_{T_1}^\infty |c_{2,E}(T_1)|^2 e^{-\gamma(1+4C)t'}\, dt'\end{aligned} \tag{3.51}$$

to make the expression a bit clearer, we define a new parameter A as,

$$A = -\frac{|\Omega|^2\gamma(1+4C)}{2\left(\Delta^2 + \frac{\gamma^2(1+4C)^2}{4}\right)} \tag{3.52}$$

the expression for $\langle E|E\rangle$ in terms of A thus becomes,

$$\begin{aligned}\langle E|E\rangle &= \kappa\int_0^{T_2}\frac{4|g|^2|\Omega|^2}{\kappa^2(\Delta^2+\frac{\gamma^2(1+4C)^2}{4})}e^{2At'}+\kappa\int_{T_1}^{\infty}|c_{2,E}(T_1)|^2e^{-\gamma(1+4C)t'}\,dt'\\ &= \frac{4C}{1+4C}\left(1-e^{2AT_1}\right)+\frac{\kappa}{\gamma(1+4C)}|c_{2,E}(T_1)|^2\\ &= \frac{4C}{1+4C}\left(1-e^{2AT_1}\right)+\frac{\kappa}{\gamma(1+4C)}\frac{4|g|^2|\Omega|^2}{\kappa^2(\Delta^2+\frac{\gamma^2(1+4C)^2}{4})}e^{2AT_1}\\ &= \frac{4C}{1+4C}\left(1-e^{2AT_1}\right)+\frac{4C}{1+4C}\left(\frac{|\Omega|^2e^{2AT_1}}{\Delta^2+\frac{\gamma^2}{4}(1+4C)^2}\right)\end{aligned} \tag{3.53}$$

previously, we assumed that we are in the weak driving regime. We can therefore assume that the second term in the final expression of $\langle E||E\rangle$ is negligible in comparison with the first term. The final expression thus becomes,

$$\langle E|E\rangle \approx \frac{4C}{1+4C}\left(1-e^{2AT_1}\right) \tag{3.54}$$

Similarly the probability of finding the photon in the late time-bin in terms of A is,

$$\begin{aligned}\langle L|L\rangle &= \langle vac|\,\hat{A}_L\hat{A}_L^{\dagger}\,|vac\rangle\\ &= \int_0^{\infty}\int_0^{\infty}\kappa\,\langle vac|\,\hat{c}(t')c_{2,L}^{*}(t')c_{2,L}(t_1')\hat{c}^{\dagger}(t_1')\,|vac\rangle\,dt'\,dt_1'\\ &= \int_0^{\infty}\kappa|c_{2,L}(t')|^2\,dt'\\ &= \kappa\int_0^{\infty}\frac{4|g|^2|\Omega|^2}{\kappa^2(\Delta^2+\frac{\gamma^2(1+4C)^2}{4})}e^{2AT_1}e^{2At'}\,dt'\\ &= \frac{4C}{1+4C}e^{2AT_1}\end{aligned} \tag{3.55}$$

From the expressions of the respective probabilities of the photon being in the early or late time-bin, we can make a few conclusions. First, the probabilities depends only on the time when the driving was stopped, assuming that we are in the weak driving regime and the driving is restarted after waiting for enough time so the spin can relax. Second, the probability of emitting the photon depends on the cooperativity of the system. Higher cooperativity implies that the spin-cavity coupling is strong, thus the spin undergoes the desired transition from the excited state $|e\rangle$ to the ground state $|f\rangle$ rather than decaying spontaneously. Adding the two probabilities, we can get the total probability (P) of getting the photon in the time-bins.

$$\begin{aligned}P &= \langle E||E\rangle+\langle L||L\rangle\\ &= \frac{4C}{1+4C}\left(1-e^{2AT_1}\right)+\frac{4C}{1+4C}e^{2AT_1}\\ &= \frac{4C}{1+4C}\end{aligned} \tag{3.56}$$

We can also choose the time T_1 such that the relative probabilities of early and late photons are different. For an equal superposition of early and late time-bins we can find T_1 such that

$$e^{2AT_1}=\frac{1}{2}$$

therefore we can find,

$$T_1 = \frac{-\log 2}{2A} \tag{3.57}$$

where,

$$A = -\frac{|\Omega|^2 \gamma(1+4C)}{2\left(\Delta^2 + \frac{\gamma^2(1+4C)^2}{4}\right)}$$

For this T_1, we can normalize the early and late time-bin states, such that

$$\langle E|E\rangle = \langle L|L| = 1$$

$$\begin{aligned} |E\rangle &= \sqrt{\frac{1+4C}{2C}} \int_0^\infty \sqrt{\kappa} c_{2,E}(t') \hat{c}^\dagger(t')\, dt' \,|vac\rangle \\ |L\rangle &= i\sqrt{\frac{1+4C}{2C}} \int_0^\infty \sqrt{\kappa} c_{2,L}(t'') \hat{c}^\dagger(t'')\, dt'' \,|vac\rangle \end{aligned} \tag{3.58}$$

In terms of these normalized $|E\rangle$ and $|L\rangle$ states, the output state of the photon for a drive that is on from time $t = 0$ to $t = T_1$ and for $t > T_2$

$$|\psi_{ph}\rangle = \frac{1}{\sqrt{2}}\left(|E\rangle - i\,|L\rangle\right) \tag{3.59}$$

3.3. Errors in the Emitter

In the previous section, we solved the dynamics of the spin-cavity system, and we found the state of the emitted photon. This section will introduce the possible errors that can occur during photon generation, and we will analyze the system in case these errors happen. Our goal is to find the respective probabilities of these errors and possibly mitigate those errors.

During the photon generation, it is possible that the spin undergoes a spontaneous emission of a photon and decays to one of the ground states. This photon is not in the cavity mode. Hence it could escape the cavity, resulting in the loss of the photon to the environment. Spontaneous emission could happen while the spin is in the excited state. We do not care about the state of the spin just before it happens because the photon is lost to the environment, and the spin losses its coherence. Instead, we care about the state of the spin after spontaneous emission, and we care about the ground state to which the spin collapses.

The previous section assumed spontaneous emissions as "jumps" to ground states. We introduced two jump operators $\hat{L}_{\gamma_g}$ and $\hat{L}_{\gamma_f}$ to capture the effect of spontaneous emissions on the dynamics of the system. However, we used the stochastic Hamiltonian method to solve the dynamics of the system. As discussed earlier, this means that we do not take in the contribution of a jump operator to its target state. Hence we introduced a dump state in our system earlier. However, now that we are interested in decay to one of the ground states, in our analysis in this section, we cannot use the method of stochastic Hamiltonian anymore.

We need to distinguish the two different decays the spin could undergo. If the spin decays to the $|g\rangle$ state, it could generate a photon in the cavity mode by driving to the excited state. If the spin instead collapses to the $|f\rangle$ state, there is no way that it can emit a photon. Therefore, the analysis in this section is divided into two parts. First, we will see what happens in case of decay to the $|g\rangle$ state, and later, we will consider the case of decay to the $|f\rangle$ state.

3.3.1. Decay to $|g\rangle$ state

A decay to $|g\rangle$ state could generate a photon in the cavity mode. It will happen if the decay to $|g\rangle$ state happens when the driving is still on. In this case, the spin could go back to the excited state

because of the drive. This could give out a photon (in the cavity mode), but it would be after the system has lost all its coherence. The cycle of decay to $|g\rangle$ state and excitation to the excited state may repeat itself multiple times, and later we get a photon out in the cavity mode. This would also result in a photon in the cavity mode, but it would not be in coherence with either of the $|E\rangle$ and $|L\rangle$ states.

Our analysis will distinguish between systems that have had one spontaneous decay from the system without any spontaneous decay. For that, we will modify the jump operators $\hat{L}_{\gamma_g}$ and $\hat{L}_{\gamma_f}$ so that they carry the information about a decay if it occurs. When a spontaneous decay occurs, we collapse to a different system, which we refer to as the "Dash system". The system carries the information that we have decayed and is orthogonal to our original system (system with no spontaneous decay).

$$|g'\rangle = |g\rangle\,|decay\rangle \tag{3.60}$$

$$\langle g|g'\rangle = 0 \tag{3.61}$$

We go from the original system to the Dash system only when a spontaneous emission occurs. So, to model a change in systems, we introduce a slight change to the jump operators. Jump operators now take us from the excited state of the original system to the ground states of the Dash system.

$$\begin{aligned}\hat{L}_{\gamma_g} &= \sqrt{\gamma_g}\,|g\rangle\,|decay\rangle\,\langle e| \\ &= \sqrt{\gamma_g}\,|g'\rangle\,\langle e| \\ \hat{L}_{\gamma_f} &= \sqrt{\gamma_f}\,|f\rangle\,|decay\rangle\,\langle e| \\ &= \sqrt{\gamma_f}\,|f'\rangle\,\langle e|\end{aligned} \tag{3.62}$$

In our analysis, we will limit ourselves to only one spontaneous emission and decay to $|g\rangle$ state. We will assume that the probability of having multiple decays is minuscule. Thus we can neglect the cases with more than one spontaneous decay. A spontaneous decay can happen anytime during the early time-bin generation or the late time-bin generation. Therefore, to reduce the complexity of the problem, we will assume that we do not switch off our drive and that our drive is a step-function with amplitude Ω. The assumptions we made in the last section still hold for our analysis in this section because we are physically in the same system. Furthermore, we will still keep dump states, meaning that in case the decay happens again, we will go into a dump state, and therefore, we can ignore the addition of population to $|g\rangle$ state or $|f\rangle$ state because of spontaneous decays while writing the differential equations.

$$\hat{H} = \Delta\,|e'\rangle\,\langle e'| + \left(\Omega\,|e'\rangle\,\langle g'| + H.C.\right) + \left(g\,|e'\rangle\,\langle f'1| + H.C.\right) \tag{3.63}$$

$$\begin{aligned}\hat{L}_1 &= \sqrt{\gamma_g}\,|g'\rangle\,\langle e| \\ \hat{L}_2 &= \sqrt{\gamma_g}\,|g'\rangle\,\langle e'| \\ \hat{L}_3 &= \sqrt{\gamma_f}\,|f'\rangle\,\langle e'| \\ \hat{L}_\kappa &= \sqrt{\kappa}\hat{c}\end{aligned}$$

$$\dot{A} = i[\hat{H}_{JC}, A] + \sum_x L_x^\dagger A L_x - \frac{1}{2}\{L_x^\dagger L_x, A\} \tag{3.64}$$

Solving the master equation and adiabatically eliminating some of the parameters, we get the probability of getting a photon out as:

$$
\begin{aligned}
\frac{d}{dt}\left(|g'\rangle\langle g'|\right) &= i(\Omega|e'\rangle\langle g'| - \Omega^*|g'\rangle\langle e'|) + \gamma_g|e\rangle\langle e| \\
\frac{d}{dt}\left(|f'1\rangle\langle f'1|\right) &= i(g|e'\rangle\langle f'1| - g^*|f'1\rangle\langle e'|) - \kappa|f'1\rangle\langle f'1| \\
\frac{d}{dt}\left(|e'\rangle\langle e'|\right) &= -i(\Omega|e'\rangle\langle g'| - \Omega^*|g'\rangle\langle e'|) - i(g|e'\rangle\langle f'1| - g^*|f'1\rangle\langle e'|) - \gamma|e'\rangle\langle e'| \\
\frac{d}{dt}\left(|g'\rangle\langle f'1|\right) &= i(\Omega|e'\rangle\langle f'1| - g^*|g'\rangle\langle e'|) - \frac{\kappa}{2}|g'\rangle\langle f'1| \\
\frac{d}{dt}\left(|e'\rangle\langle g'|\right) &= i(\Delta|e'\rangle\langle g'| + g^*|f'1\rangle\langle g'| + \Omega^*|g'\rangle\langle g'| - \Omega^*|e'\rangle\langle e'|) - \frac{\gamma}{2}|e'\rangle\langle g'| \\
\frac{d}{dt}\left(|e'\rangle\langle f'1|\right) &= i(\Delta|e'\rangle\langle f'1| + g^*|f'1\rangle\langle f'1| + \Omega^*|g'\rangle\langle f'1| - g^*|e'\rangle\langle e'|) - \frac{1}{2}(\gamma+\kappa)|e'\rangle\langle f'1|
\end{aligned}
\tag{3.65}
$$

Solve the set of differential equations, we adiabatically eliminate the equations to find relations between $|g'\rangle\langle g'|$, $|f'1\rangle\langle f'1|$ and $|e'\rangle\langle e'|$. The calculations are shown in appendix A.

To make the adiabatic eliminations, we make a few assumptions. First, we assume that the driving is weak compared to the detuning $\Omega \ll \Delta$. Second, we are in the Purcell regime, i.e., $\gamma \ll g \ll \kappa$. These are the assumptions we had made earlier for solving dynamic of the system with no spontaneous emissions. In this section, we will make another assumption that the detuning is small compared to the cavity decay rate, $\Delta \ll \kappa$. Using these assumptions, we get the following differential equation

$$
\frac{d}{dt}|g'\rangle\langle g'| = -\frac{|\Omega|^2\gamma(1+4C)}{\Delta^2 + \frac{\gamma^2}{4}(1+4C)^2}|g'\rangle\langle g'| + \gamma_g|e\rangle\langle e| \tag{3.66}
$$

We know the time dependence of $|e\rangle$ state from our analysis of the system without any spontaneous decay in the previous section. The state $|e\rangle\langle e|$ as a function of time is

$$
|e\rangle\langle e| = \frac{|\Omega|^2}{\Delta^2 + \frac{\gamma^2}{4}(1+4C)^2} e^{-\frac{|\Omega|^2\gamma(1+4C)}{\Delta^2+\frac{\gamma^2}{4}(1+4C)^2}t} \tag{3.67}
$$

To simplify the expressions, we define a new parameter Q as

$$
Q = \frac{|\Omega|^2}{\Delta^2 + \frac{\gamma^2}{4}(1+4C)^2} \tag{3.68}
$$

Therefore, the differential equation now becomes,

$$
\frac{d}{dt}|g'\rangle\langle g'| = -Q\gamma(1+4C)|g'\rangle\langle g'| + \gamma_g Q e^{-Q\gamma(1+4C)t} \tag{3.69}
$$

Solving this differential equation gives us

$$
|g'\rangle\langle g'|(t) = \gamma_g Q t e^{-Q\gamma(1+4C)t} \tag{3.70}
$$

We know the relations between $|g'\rangle\langle g'|$ and $|e'\rangle\langle e'|$, and $|e'\rangle\langle e'|$ and $|f'1\rangle\langle f'1|$ (A). From those relations, we can find the $|f'1\rangle\langle f'1|(t)$.

$$
|f'1\rangle\langle f'1|(t) = \frac{4|g|^2\gamma_g Q^2}{\kappa^2} t e^{-Q\gamma(1+4C)t} \tag{3.71}
$$

To find the mode of the output photon, we will analyse the evolution of the $|f'0\rangle\langle f'0|$ state. We have assumed that we end up in a dump state if we decay again, therefore, any population in this

state can only be due to the emission of the photon in the output mode. The differential equation for the $|f'0\rangle\langle f'0|$ is,

$$\frac{d}{dt}|f'0\rangle\langle f'0| = \kappa|f'1\rangle\langle f'1| \tag{3.72}$$

therefore,

$$|f'0\rangle\langle f'0|(t) = \kappa\int_0^t |f'1\rangle\langle f'1|(t_e)\,dt_e \tag{3.73}$$

Therefore the probability of emitting a photon after decaying to $|g\rangle$ state (P_g) once is,

$$\begin{aligned} P_g &= \kappa\int_0^\infty \frac{4|g|^2\gamma_g Q^2}{\kappa^2} te^{-Q\gamma(1+4C)t}\,dt \\ &= \frac{4|g|^2\gamma_g Q^2}{\kappa}\int_0^\infty te^{-Q\gamma(1+4C)t}\,dt \\ &= \frac{4|g|^2\gamma_g Q^2}{\kappa}\frac{1}{(Q\gamma(1+4C))^2} \\ &= \frac{4\gamma_g C}{\gamma(1+4C)^2} \end{aligned} \tag{3.74}$$

This is a surprising result because this expression could have been found by naively multiplying probabilities of the following three steps. First step would be failing to emit a photon in either early or late time-bin. Second step would be decaying to the $|g\rangle$ state, given that we decay to one of the ground states. The third step would be emitting a photon after excitation because of the driving laser. Mathematically we can write the probability in terms of probabilities of all three steps. The naive probability of emitting a photon after only one decay to $|g\rangle$ state is,

$$P_{naive} = \frac{1}{1+4C}\times\frac{\gamma_g}{\gamma}\times\frac{4C}{1+4C} \tag{3.75}$$

This naive approach gives the same result as the extensive analysis because we still assume that the dump states exist. Therefore, to find the probability of emission of photon in case of multiple decays we can use the naive approach. Probability of emitting a photon in the output mode after n number of decays to the $|g\rangle$ state is,

$$P_{naive} = \left(\frac{1}{1+4C}\times\frac{\gamma_g}{\gamma}\right)^n\times\frac{4C}{1+4C} \tag{3.76}$$

This probability can be verified by extending the analysis that we have done in this section. To find the probability of emitting (or not emitting) a photon after k decays we use the the evolution of the excited state of the system with $k-1$ decays for $k \geq 1$. Thus, we can go from the system without any decay to a system with k decays find solving sequentially. However, we will not verify the naive probability in this report. We would like to reiterate that this solution is for a drive that is a step function in time.

To summarize, the output state of the photon after the spin decays once to $|g\rangle$ can be written as,

$$\rho_g = \frac{4\gamma_g C}{\gamma(1+4C)^2}|\tilde{\psi}_{ph}\rangle\langle\tilde{\psi}_{ph}| \tag{3.77}$$

we do not care what form $|\tilde{\psi}_{ph}\rangle$ takes, because it is an error term, but it should be normalized.

$$\langle\tilde{\psi}_{ph}|\tilde{\psi}_{ph}\rangle = 1 \tag{3.78}$$

3.3.2. Decay to $|f\rangle$ state

In case the spin decay is to the $|f\rangle$ state, we would fail to get an output photon. We are driving the population only from the $|g\rangle$ state to $|e\rangle$ state, so once the spin decays to $|f\rangle$ state, the population cannot be pumped to other states by our drive. Unlike a decay to $|g\rangle$ state, this would not give a photon in the output mode, therefore, the output state in this case would just be a vacuum state. To find the probability of this happening, we will use the naive approach. The probability of not emitting a photon in the early and late time bin is given by,

$$\begin{aligned} P_{\text{fail}} &= 1 - \frac{4C}{1+4C} \\ &= \frac{1}{1+4C} \end{aligned} \tag{3.79}$$

we call this probability of failure because if this happens, it will result in an error, thus failure. The probability of decaying to $|f\rangle$ state, given that a decay happened is,

$$P = \frac{\gamma_f}{\gamma} \tag{3.80}$$

The probability of ending up in $|f\rangle$ state after spontaneous emission (P_f) is therefore,

$$P_f = \frac{\gamma_f}{\gamma(1+4C)} \tag{3.81}$$

The output state can be written in a form of a density matrix as:

$$\rho_f = \frac{\gamma_f}{\gamma(1+4C)} |vac\rangle\langle vac| \tag{3.82}$$

3.3.3. Final state of the output photon

As discussed previously, we can either have a perfect operation without any spontaneous emissions or error because of spontaneous emission. We could either decay to the $|f\rangle$ state after a spontaneous emission or to the $|g\rangle$ state. In case of decay to $|f\rangle$ state, we will not get any output photon, but if we decay to the $|g\rangle$ state, we can still get a photon. It is also possible to decay to $|g\rangle$ multiple times. In case of multiple decays, the spin could get stuck in the cycle of repetitive excitation to the excited state and decay back to $|g\rangle$. After these repetitive decays and excitation, we could get a photon out by going through the cavity coupled transition, or we could spontaneously decay to $|f\rangle$ state and end up with no photon. In our analysis, we restricted ourselves only to one decay and assumed that the errors due to multiple decays are negligible. We can represent the output photon as a density matrix given below.

$$\rho_{ph} = \frac{4C}{1+4C} |\psi_{ph}\rangle\langle\psi_{ph}| + \frac{\gamma_g 4C}{\gamma(1+4C)^2} |\tilde{\psi}_{ph}\rangle\langle\tilde{\psi}_{ph}| + \frac{\gamma_f}{\gamma(1+4C)} |vac\rangle\langle vac| + error \tag{3.83}$$

where, in case of a decay to $|g\rangle$ and an emission of a photon in the output mode gives us $|\tilde{\psi}_{ph}\rangle$ which is a normalized state and,

$$|\psi_{ph}\rangle = \frac{1}{\sqrt{2}} (|E\rangle - i|L\rangle)$$

is the output state in case of no decay. The error term includes states with higher order decays.

3.4. Photon-spin entangling gate

So far in this chapter, we have introduced the protocol for entangling spin and photon. We modeled one of our spin-cavity systems and discussed the different errors that can happen in it. In the remaining two sections of this chapter, we will discuss and model the Gate and model the errors in it. This section is divided into two parts. The first part deals with dynamics of the system and the second part deals with the interaction between the photons coming from the Emitter and the Gate.

3.4.1. Dynamics of spin-cavity system

The spin-cavity system, which we call the Gate, is the system that interacts with the photons generated by the emitter. The idea is to reflect the incoming photons off this system with reflection coefficients depending on the state of the spin. The system has spin with four levels, two ground states with their respective excited states, coupled to a cavity as shown in fig. 3.4.

The Hamiltonian of the system in a suitable rotating frame with respect to the cavity frequency is given by,

$$\hat{H}_{JC} = \Delta_0 |e_0\rangle\langle e_0| + \Delta_1 |e_1\rangle\langle e_1| + \left(g_0 |e_0\rangle\langle 0|\,\hat{c} + H.C.\right) + \left(g_1 |e_1\rangle\langle 1|\,\hat{c} + H.C.\right) \tag{3.84}$$

where Δ_0 and Δ_1 are detuning between levels and the cavity frequency, g_0 and g_1 are the single-photon Rabi frequency of the levels. Δ_0 and Δ_1 are given by

$$\begin{aligned} \Delta_0 &= \omega_{e_0} - \omega_0 - \omega_c \\ \Delta_1 &= \omega_{e_1} - \omega_1 - \omega_c \end{aligned} \tag{3.85}$$

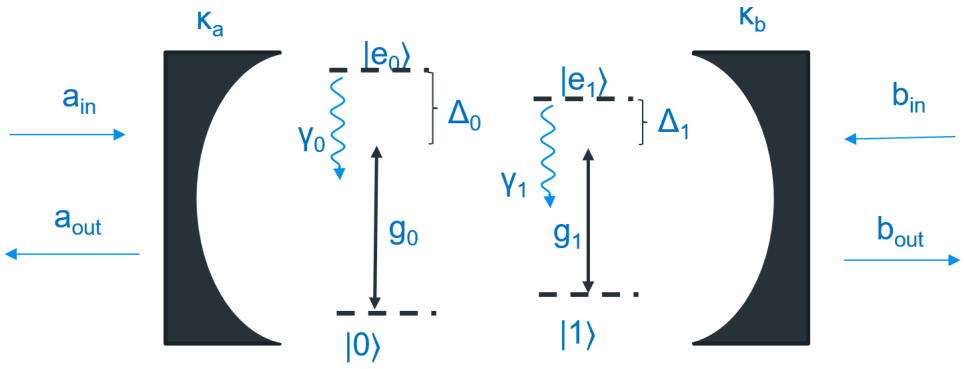

Figure 3.4: Level structure of the Gate with spontaneous decay rates

To solve for the dynamics of the system during the photon-spin interaction, we will solve the master equation in the Heisenberg picture. As described in section 2.2.1 we will ignore the contribution of the Langevin noise operator. The Heisenberg-Langevin equations of motion for an observable $\hat{A}$ are given by,

$$\dot{A} = i[\hat{H}_{JC}, A] + \sum_x L_x^\dagger A L_x - \frac{1}{2}\{L_x^\dagger L_x, A\} \tag{3.86}$$

During the photon-spin interaction, the spin could undergo a spontaneous decay from the excited states to the ground states. This could result in the loss of the photon to the environment. These decays are treated as jump operators while solving for the dynamics of the system. The Lindblad jump operators for the spontaneous emission are,

$$\begin{aligned} L_0 &= \sqrt{\gamma_0}\,|0\rangle\langle e_0| = \sqrt{\gamma_0}\,\sigma_0^- \\ L_1 &= \sqrt{\gamma_1}\,|1\rangle\langle e_1| = \sqrt{\gamma_1}\,\sigma_1^- \end{aligned} \tag{3.87}$$

where γ_0 and γ_1 are rates of decay of excited states. We define σ_j^- as $\sigma_j^- = |j\rangle\langle e_j|$, where $j \in \{0,1\}$. The input-output relations for the cavity for incoming fields $\hat{a}$ and $\hat{b}$ are [41, 42],

$$\begin{aligned}\hat{a}_{out} &= \hat{a}_{in} - \sqrt{\kappa_a}\hat{c} \\ \hat{b}_{out} &= \hat{b}_{in} - \sqrt{\kappa_b}\hat{c} \\ \dot{\hat{c}} &= i[\hat{H}_{JC}, \hat{c}] - \frac{\kappa\hat{c}}{2} + \sqrt{\kappa_a}\hat{a}_{in} + \sqrt{\kappa_b}\hat{b}_{in}\end{aligned} \tag{3.88}$$

κ_a and κ_b are the rates of cavity decay for the two mirrors, and κ is the total cavity decay rate. Simplifying the differential equation involving the cavity annihilation operator gives us the following equation,

$$\dot{\hat{c}} = -i(g_0^*\sigma_0^- + g_1^*\sigma_1^-) - \frac{\kappa}{2}\hat{c} + \sqrt{\kappa_a}\hat{a}_{in} + \sqrt{\kappa_b}\hat{b}_{in} \tag{3.89}$$

we have used the commutation relation between $\hat{c}$ and $\hat{c}^\dagger$, $[\hat{c}, \hat{c}^\dagger] = 1$. Since the evolution of $\hat{c}$ depends on the observables σ_0^- and σ_1^-, we will next look at the evolution of these observables. The differential equations from the master equation are,

$$\begin{aligned}\dot{\sigma_0^-} &= i[\hat{H}_{JC}, \sigma_0^-] + \sum_x L_x^\dagger \sigma_0^- L_x - \frac{1}{2}\{L_x^\dagger L_x, \sigma_0^-\} \\ &= -ig_0\sigma_{0,z}c - (\frac{1}{2}\gamma_0 + i\Delta_0)\sigma_0^- \\ \dot{\sigma_1^-} &= -ig_1\sigma_{1,z}c - (\frac{1}{2}\gamma_1 + i\Delta_1)\sigma_1^-\end{aligned} \tag{3.90}$$

where, $\sigma_{0,z} = |0\rangle\langle 0| - |e_0\rangle\langle e_0|$ and $\sigma_{1,z} = |1\rangle\langle 1| - |e_1\rangle\langle e_1|$.

These equations depend on $\sigma_{j,z}(t)$ $(j \in \{0,1\})$, thus we also have to find its time evolution. To simplify the calculations, we assume that we are in a weak driving regime. This means that at any point during the photon-spin interaction, the incoming photon field is so weak that the excitation in the population the spin is negligible compared to the respective ground state population. Therefore the $\sigma_{j,z}(t)$ can be approximated as,

$$\begin{aligned}\hat{\sigma}_{j,z} &= |j\rangle\langle j| - |e_j\rangle\langle e_j| \\ &\approx |j\rangle\langle j| = \hat{P}_j\end{aligned} \tag{3.91}$$

where $\hat{P}_j$ is the projector onto the ground state $|j\rangle$, $j \in \{0,1\}$.

We have now established the differential equations that govern the dynamics of the photon-spin interaction. These are 3.89 and 3.90. To solve the set of these equations we will go into the Fourier domain by taking the Fourier transform on both sides of the equations. We can then use the property of Fourier transform to simplify the differential equations.

Fourier transform of an observable $\hat{A}$ is given by:

$$\hat{A}(\omega) = \frac{1}{\sqrt{2\pi}}\int \hat{A}(t)e^{-i\omega t}\,dt \tag{3.92}$$

we use the property of the Fourier transform that the Fourier transform of derivative of a function $f(t)$ can be written as

$$f(t) \xrightarrow{\mathscr{F}} F(\omega)$$

$$\dot{f}(t) \xrightarrow{\mathscr{F}} i\omega F(\omega)$$

Therefore, in the Fourier domain the set of equations are of the following form,

$$\begin{aligned} i\omega\hat{c}(\omega) &= -i\left(g_0^*\sigma_0^-(\omega)+g_1^*\sigma_1^-(\omega)\right)-\frac{\kappa}{2}\hat{c}(\omega)+\sqrt{\kappa_a}\hat{a}_{in}(\omega)+\sqrt{\kappa_b}\hat{b}_{in}(\omega) \\ i\omega\sigma_0^-(\omega) &= -ig_0\hat{P}_0\hat{c}(\omega)-\left(i\Delta_0+\frac{\gamma_0}{2}\right)\sigma_0^-(\omega) \\ i\omega\sigma_1^-(\omega) &= -ig_1\hat{P}_1\hat{c}(\omega)-\left(i\Delta_1+\frac{\gamma_1}{2}\right)\sigma_1^-(\omega) \end{aligned} \tag{3.93}$$

we can rewrite $\sigma_j^-(\omega)$ ($j\in\{0,1\}$) in terms of $\hat{c}(\omega)$ from the second and the third equations. This will give a relation between $\sigma_j^-(\omega)$ ($j\in\{0,1\}$) and $\hat{c}(\omega)$ as shown below,

$$\begin{aligned} \sigma_0^-(\omega) &= \frac{-ig_0\hat{P}_0\hat{c}(\omega)}{\left(i\omega+i\Delta_0+\frac{\gamma_0}{2}\right)} \\ \sigma_1^-(\omega) &= \frac{-ig_1\hat{P}_1\hat{c}(\omega)}{\left(i\omega+i\Delta_1+\frac{\gamma_1}{2}\right)} \end{aligned} \tag{3.94}$$

Substituting these in the equation for $\hat{c}(\omega)$ and solving for $\hat{c}(\omega)$ gives us the solution for $\hat{c}(\omega)$,

$$\hat{c}(\omega)=\frac{\sqrt{\kappa_a}\hat{a}_{in}(\omega)+\sqrt{\kappa_b}\hat{b}_{in}(\omega)}{\left(i\omega+\frac{\kappa}{2}+\sum_{j=0}^{1}\frac{|g_j|^2\hat{P}_j}{i(\omega+\Delta_j)+\frac{\gamma_j}{2}}\right)} \tag{3.95}$$

where, j in the sum corresponds to two ground states ($j\in\{0,1\}$). The operator $\hat{P}_j$ is the projector to the ground state $|j\rangle$ ($j\in\{0,1\}$).

For our protocol we are considering only single-sided cavities for entanglement generation. Therefore, the contribution from the $\hat{b}$ field can be ignored, resulting in the following equation.

$$\hat{c}(\omega)=\frac{\sqrt{\kappa_a}\hat{a}_{in}(\omega)}{\left(i\omega+\frac{\kappa}{2}+\sum_{j=0}^{1}\frac{|g_j|^2\hat{P}_j}{i(\omega+\Delta_j)+\frac{\gamma_j}{2}}\right)} \tag{3.96}$$

we can now substitute $\hat{c}(\omega)$ in the input-output relations to get $\hat{a}_{out}$ in terms of $\hat{a}_{in}$.

$$\hat{a}_{out}(\omega)=\left[1-\frac{\kappa_a}{i\omega+\frac{\kappa}{2}+\sum_{j=0}^{1}\frac{|g_j|^2\hat{P}_j}{i(\omega+\Delta_j)+\frac{\gamma_j}{2}}}\right]\hat{a}_{in}(\omega) \tag{3.97}$$

3.4.2. Photon-spin interaction

In the previous section, we solved the dynamics of the system during the photon-spin interaction, and we found the outgoing field in terms of the incoming field. In this part of the report, we will investigate the output mode of the reflected photon. The photon generated by the Emitter comes in and interacts with the Gate. Therefore the output mode of the photon from the Emitter will be the input mode to the Gate. From our analysis of the Emitter, the input mode for the gate is given by equations 3.102 and **??** for the early time-bin, and equation 3.103 for late time-bin. Furthermore, the reflection coefficient of the Gate in the Fourier Domain is given by,

$$r(\omega)=\left[1-\frac{\kappa_a}{-i\omega+\frac{\kappa}{2}+\sum_{j=0}^{1}\frac{|g_j|^2\hat{P}_j}{-i(\omega+\Delta_j)+\frac{\gamma_j}{2}}}\right] \tag{3.98}$$

One thing to keep in mind is that we are in different rotating frames for the Emitter and the Gate. We need to be in the same frame in order to analyse the interaction between cavity and photon.

We will move to the same rotating frame by introducing the detuning between the Gate cavity and incoming photon, ω_d.

$$\omega_d = \omega_c - \omega_{ph} \tag{3.99}$$

where ω_c is the frequency of the cavity mode of the gate. This will modify the reflection coefficient a bit, the new reflection coefficient is given by,

$$r(\omega_{ph}) = \left[1 - \frac{\kappa_a}{-i(\omega_{ph}+\omega_d) + \frac{\kappa}{2} + \sum_{j=0}^{1} \frac{|g_j|^2 \hat{P}_j}{-i(\omega_{ph}+\omega_d+\Delta_j)+\frac{\gamma_j}{2}}}\right] \tag{3.100}$$

Rewriting the reflection coefficient in terms of the cooperativity of the system,

$$r(\omega_{ph}) = \left[1 - \frac{\kappa_a/\kappa}{\frac{-i(\omega_{ph}+\omega_d)}{\kappa} + \frac{1}{2} + \sum_{j=0}^{1} \frac{C_j \hat{P}_j}{\frac{-i}{\gamma_j}(\omega_{ph}+\omega_d+\Delta_j)+\frac{1}{2}}}\right] \tag{3.101}$$

The input mode of photon to the Gate after ignoring the contribution from the decay of the excited state $|e\rangle$ of the emitter to the early time-bin is

$$c_{2,E}(t) = \frac{2g^* b}{\Omega^* \kappa} e^{bt} (H(t) - H(T_1)) \tag{3.102}$$

for $T_1 < t < T_2$. Similarly, for the late time-bin, $c_{2,L}$ is of the form,

$$c_{2,L}(t) = c_0(T_1) \frac{2g^* b}{\Omega^* \kappa} e^{b(t-T_2)} H(T_2) \tag{3.103}$$

for $T_2 < t$. where we have expressed the modes in terms of b, eq. 3.27.

For the photon-spin interaction we find Fourier transform of the photon modes. Recall that we have already assumed that the decay of the early time-bin in instantaneous when the driving is turned off. Thus we will ignore the contribution of $c_{2,E}(t)$ for $t > T_1$. The Fourier transform of the input modes is

$$\begin{aligned} v_{E/L}(\omega_{ph}) &= \frac{1}{\sqrt{2\pi}} \int v_{E/L}(t) e^{-i\omega_{ph} t}\, dt \\ v_{E/L}(\omega_{ph}) &= \sqrt{\frac{\kappa_e}{2\pi}} \int c_{2,E/L}(t) e^{-i\omega_{ph} t}\, dt \end{aligned} \tag{3.104}$$

We will split b into real and imaginary parts, $b = A + iB$. Where A is given in eq. 3.52. We will rename the cavity decay rate of the Emitter to κ_e to distinguish it from the cavity decay rate of the Gate.

$$v_E(\omega_{ph}) = \frac{2g^* b}{\Omega^* \kappa_e} \sqrt{\frac{\kappa_e}{2\pi}} \left(\frac{1}{A + (B - \omega_{ph})i}\right) (e^{(A+(B-\omega_{ph})i)T_1} - 1) \tag{3.105}$$

$$|v_E(\omega)|^2 = \frac{4|g|^2|b|^2}{2\pi|\Omega|^2\kappa_e} \left(\frac{3/2 - \sqrt{2}\cos T_1(B-\omega_{ph})}{A^2 + (B-\omega_{ph})^2}\right) \tag{3.106}$$

We put the value of $e^{2AT_1} = 1/2$. The function $|v(\omega)|^2$ assumes its maximum value at $\omega = B$. This function is bounded by two functions,

$$\frac{4|g|^2|b|^2}{2\pi|\Omega|^2\kappa_e}\left(\frac{3/2-\sqrt{2}}{A^2+(B-\omega_{ph})^2}\right)\leq|v_E(\omega_{ph})|^2\leq\frac{4|g|^2|b|^2}{2\pi|\Omega|^2\kappa_e}\left(\frac{3/2+\sqrt{2}}{A^2+(B-\omega_{ph})^2}\right) \tag{3.107}$$

The full width at half maximum (FWHM) of these functions is

$$FWHM=2A \tag{3.108}$$

We can safely assume that the FWHM of $|v_E(\omega_{ph})|^2$ must be of the order of A. A and B are small quantities because we are in the weak driving and high cooperativity regime. They depend on $(\Omega/\Delta)^2$, which makes the values of A and B small. Hence, the FWHM and the frequency corresponding to the maximum are small. Therefore, we are going to treat $|v(\omega_{ph})|$ as a δ function.

$$\begin{aligned}v_E(\omega_{ph})&=\frac{2g^*b}{\Omega^*\kappa_e}\sqrt{\frac{\kappa_e}{2\pi}}\left(e^{AT_1}-1\right)\delta(\omega_{ph})\\&=C_v\delta(\omega_{ph})\end{aligned} \tag{3.109}$$

$$C_v=\frac{2g^*b}{\Omega^*\kappa_e}\sqrt{\frac{\kappa_e}{2\pi}}\left(e^{AT_1}-1\right)$$

Where C_v is the coefficient of the δ function. The output mode of the photon, $g(\omega_{ph})$, is known in terms of the reflection coefficient, $r(\omega_{ph})$, and the input mode, $v(\omega_{ph})$, ref. [44].

$$\begin{aligned}g_E(\omega_{ph})&=r(\omega_{ph})v_E(\omega_{ph})\\&=\left[1-\frac{\kappa_a/\kappa}{\frac{-i(\omega_{ph}+\omega_d)}{\kappa}+\frac{1}{2}+\sum_{j=0}^{1}\frac{C_j\hat{P}_j}{\frac{-i}{\gamma_j}(\omega_{ph}+\omega_d+\Delta_j)+\frac{1}{2}}}\right]C_v\delta(\omega_{ph})\\&=\left[1-\frac{\kappa_a/\kappa}{\frac{-i(\omega_d)}{\kappa}+\frac{1}{2}+\sum_{j=0}^{1}\frac{C_j\hat{P}_j}{\frac{-i}{\gamma_j}(\omega_d+\Delta_j)+\frac{1}{2}}}\right]C_v\delta(\omega_{ph})\\&=R(0)v_E(\omega_{ph})\end{aligned} \tag{3.110}$$

In time-domain the the output mode of the photon is input mode times the value of reflection coefficient, $r(\omega_{ph})$, at $\omega_{ph}=0$.

$$g_E(t)=r(0)v_E(t) \tag{3.111}$$

A similar analysis can be done for late time-bin by treating $v_L(\omega_{ph})$ as a δ function because of it is a similar function to $v_E(\omega_{ph})$. After the interaction between the late time-bin and the spin, the output mode can be written in terms of $R(0)$ and the input mode.

$$g_L(t)=r(0)v_L(t) \tag{3.112}$$

3.4.3. Ideal values of reflection coefficient

The reflection coefficient is a function of the projector operators onto the ground states, $\hat{P}_0$ and $\hat{P}_1$. This means that during the spin photon interaction it can take two values depending on the state of the spin. If the Gate spin is initialized to $|0\rangle$ state, then the reflection coefficient takes the value,

$$r_0=\left[1-\frac{\kappa_a/\kappa}{\frac{-i\omega_d}{\kappa}+\frac{1}{2}+\frac{C_0}{\frac{-i}{\gamma_0}(\omega_d+\Delta_0)+\frac{1}{2}}}\right] \tag{3.113}$$

similarly if it is initialized to the $|1\rangle$ state then the reflection coefficient is,

$$r_1 = \left[1 - \frac{\kappa_a/\kappa}{\frac{-i\omega_d}{\kappa} + \frac{1}{2} + \frac{C_1}{\frac{-i}{\gamma_1}(\omega_d+\Delta_1)+\frac{1}{2}}}\right] \tag{3.114}$$

Their values depend on the coupling of the levels to the cavity, loss in the cavity, the respective detunings of levels, and the detuning between incoming photon field and cavity field.

In the ideal scenario, we want the $|0\rangle$ ground state to be decoupled from the cavity ($g_0 = 0$) or to have a really large detuning compared to the cooperativity, $C_0 \ll \Delta_0$. Furthermore, we prefer that the $|1\rangle \rightarrow |e_1\rangle$ transition is on resonance with the cavity field, and the cooperativity is really large, $C_1 >> \Delta_1 \approx 0$ $0 \approx \Delta_1 \gg C_1$. Moreover, we want to drive the Emitter such that the photons are on resonance with the cavity field of the Gate i.e., $\omega_d \approx 0$. If we apply all these conditions to the reflection coefficients, they take the following form

$$r_0 = \left[1 - \frac{2\kappa_a}{\kappa}\right], \quad r_1 = \left[1 - \frac{\kappa_a}{2\kappa C_1}\right] \tag{3.115}$$

Assuming that there is no cavity loss, $\kappa_a = \kappa$, and ignoring the terms with $1/C_1$, then the reflection coefficients take the values required for the ideal photon-spin entanglement.

$$r_0 = -1, \quad r_1 = 1 \tag{3.116}$$

3.5. Errors during the photon-spin interaction

This section will identify the sources of errors in Gate operation. We will model these errors and examine their effect on the state of the spin. We are curious what happens to the spin if these errors happen because the spin has to entangle with many photons during tree-cluster generation. There are two ways we could lose the photon during photon-spin interaction. We could lose the photon in the mirrors of the cavity because of imperfect collection efficiency, or the spin could undergo a spontaneous emission.

The rest of this section is divided into three parts. The first part deals with the case of no loss (sec. 3.5.1). In the second part 3.5.2, we will analyze the cavity losses, and in the last part, we will analyze spontaneous emissions (sec. 3.5.3). The circuit for the analysis in this section is shown in figure 3.5. We will ignore the X-rotations in this analysis and assume that all the single-qubit gates in the circuit are perfect. Thus, we will limit our analysis in the section only to a part of the photon-spin entangling protocol.

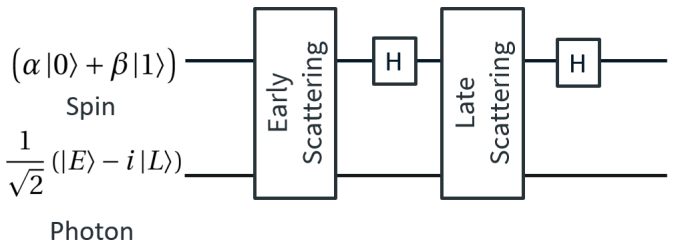

Figure 3.5: The circuit for considering errors during photon-spin interaction. We start with an arbitrary state of the spin and $|-i\rangle$ state of the photon.

3.5.1. Lossless photon-spin interaction

Ideally, when the photon interacts with the Gate, we want the photon to reflect off the cavity with reflection coefficients depending on the the state of the spin. These reflection coefficients are de-

scribed in eq. 3.113 and 3.114. We will go through the evolution of the photon-spin state for all operations in this circuit, fig. 3.5.

The starting state for this circuit is,

$$|\psi_1\rangle = \frac{1}{\sqrt{2}}(\alpha|E0\rangle + \beta|E1\rangle - i\alpha|L0\rangle - i\beta|L1\rangle) \tag{3.117}$$

The state after early scattering is,

$$|\psi_2\rangle = \frac{1}{\sqrt{2}}(r_0\alpha|E0\rangle + r_1\beta|E1\rangle - i\alpha|L0\rangle - i\beta|L1\rangle) \tag{3.118}$$

The state after the first Hadamard is,

$$|\psi_3\rangle = \frac{1}{2}\left((r_0\alpha + r_1\beta)|E0\rangle + (r_0\alpha - r_1\beta)|E1\rangle - i(\alpha+\beta)|L0\rangle - i(\alpha-\beta)|L1\rangle\right) \tag{3.119}$$

After late scattering the state becomes,

$$|\psi_4\rangle = \frac{1}{2}\left((r_0\alpha + r_1\beta)|E0\rangle + (r_0\alpha - r_1\beta)|E1\rangle - i(\alpha+\beta)r_0|L0\rangle - i(\alpha-\beta)r_1|L1\rangle\right) \tag{3.120}$$

Final state after the second Hadamard gate is,

$$|\psi_5\rangle = \frac{1}{\sqrt{2}}\left(r_0\alpha|E0\rangle + r_1\beta|E1\rangle - i\frac{(\alpha+\beta)r_0 + (\alpha-\beta)r_1}{2}|L0\rangle - i\frac{(\alpha+\beta)r_0 - (\alpha-\beta)r_1}{2}|L1\rangle\right) \tag{3.121}$$

After the loss-less operation, the final photon-spin state is given by

$$\rho = |\psi_5\rangle\langle\psi_5| \tag{3.122}$$

The probability of no-loss operation is given by,

$$\begin{aligned} P_{nl} &= Tr\left(|\psi_5\rangle\langle\psi_5|\right) \\ &= \frac{1}{2}\left[|r_0|^2|\alpha|^2 + |r_1|^2|\beta|^2 + \frac{1}{4}|(\alpha+\beta)r_0 + (\alpha-\beta)r_1|^2 + \frac{1}{4}|(\alpha+\beta)r_0 - (\alpha-\beta)r_1|^2\right] \\ &= \frac{1}{4}\left[2|r_0|^2|\alpha|^2 + 2|r_1|^2|\beta|^2 + |(\alpha+\beta)|^2|r_0|^2 + |(\alpha-\beta)|^2|r_1|^2\right] \end{aligned} \tag{3.123}$$

We can normalize the density matrix ρ using the probability P_{nl}, the normalized density matrix is given by

$$\rho_{\text{normalized}} = \left(\frac{|\psi_5\rangle\langle\psi_5|}{P_{nl}}\right) \tag{3.124}$$

The final state of no-loss in terms of the probability and the normalized density matrix is

$$\rho_{nl} = P_{nl} \times \rho_{\text{normalized}} \tag{3.125}$$

3.5.2. Cavity loss

Cavity loss are present in the system if the cavity mirrors are imperfect, i.e., $\kappa_a < \kappa$. To model the loss of photon in the cavity, we define an output mode from the Gate cavity, the loss mode, as shown in fig. 3.6.

We model the cavity loss as a transmission mode which losses the photon. Thus the rate of decay of cavity in the loss mode is given by,

$$\kappa_{loss} = \kappa - \kappa_a \tag{3.126}$$

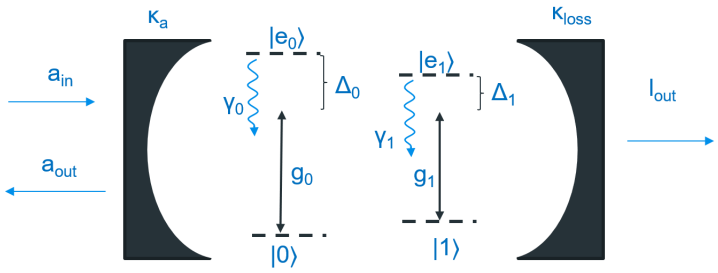

Figure 3.6: Loss mode and the output mode

In terms of this loss rate, we can write the input-output relation of the loss mode l_{out} as,

$$\hat{l}_{out}(\omega) = \sqrt{\kappa_{loss}}\hat{c}(\omega) \tag{3.127}$$

We know the expression of $\hat{c}(\omega)$ in terms of $\hat{a}_{in}(\omega)$. Using that to write the loss mode in terms of the input mode we can write

$$\hat{l}_{out}(\omega) = \frac{\sqrt{\kappa_{loss}}\sqrt{\kappa_a}}{\left(i\omega + \frac{\kappa}{2} + \sum_{j=0}^{1} \frac{|g_j|^2 \hat{P}_j}{i(\omega+\Delta_j)+\frac{\gamma_j}{2}}\right)} \hat{a}_{in}(\omega) \tag{3.128}$$

The loss coefficient similar to reflection coefficient can be found as,

$$l(\omega) = \frac{\sqrt{\kappa_{loss}}\sqrt{\kappa_a}}{\left(i\omega + \frac{\kappa}{2} + \sum_{j=0}^{1} \frac{|g_j|^2 \hat{P}_j}{i(\omega+\Delta_j)+\frac{\gamma_j}{2}}\right)} \tag{3.129}$$

Similar to reflection coefficients we can also find loss coefficients for the states $|0\rangle$ and $|1\rangle$. We will again assume that the input mode to the Gate is a delta function in the Fourier domain centered at $\omega_{ph} = 0$. The loss coefficients therefore are,

$$\begin{aligned} l_0 &= \frac{\sqrt{\kappa_{loss}}\sqrt{\kappa_a}}{\left(-i\omega_d + \frac{\kappa}{2} + \frac{|g_0|^2 \hat{P}_0}{-i(\omega_d+\Delta_0)+\frac{\gamma_0}{2}}\right)} \\ l_1 &= \frac{\sqrt{\kappa_{loss}}\sqrt{\kappa_a}}{\left(-i\omega_d + \frac{\kappa}{2} + \frac{|g_1|^2 \hat{P}_1}{-i(\omega_d+\Delta_1)+\frac{\gamma_1}{2}}\right)} \end{aligned} \tag{3.130}$$

In terms of these loss coefficients, it is possible for us to write the final loss-mode photon-spin state from circuit in fig. 3.5.

$$|\Phi\rangle = \frac{1}{\sqrt{2}}\left(\alpha l_0 |E0\rangle + \beta l_1 |E1\rangle + \frac{(\alpha+\beta)l_0 + (\alpha-\beta)l_1}{2}|L0\rangle + \frac{(\alpha+\beta)l_0 - (\alpha-\beta)l_1}{2}|L1\rangle\right) \tag{3.131}$$

We take the partial trace of the density matrix, $|\Phi\rangle\langle\Phi|$, over the photon states to get the spin state after the photon is lost. The spin state is,

$$\rho_{\text{spin}} = Tr_{ph}(|\Phi\rangle\langle\Phi|) \tag{3.132}$$

The photon-spin state after cavity loss is

$$\rho_{cl} = |vac\rangle\langle vac| \otimes \rho_{\text{spin}} \tag{3.133}$$

The probability of cavity loss happening P_{cl} can be found similar to the probability of no-loss,

$$\begin{aligned} P_{cl} &= Tr(\rho_{cl}) \\ &= \frac{1}{4}\left[2|l_0|^2|\alpha|^2 + 2|l_1|^2|\beta|^2 + |(\alpha+\beta)|^2|l_0|^2 + |(\alpha-\beta)|^2|l_1|^2\right] \end{aligned} \tag{3.134}$$

The final photon-spin state can be written in terms of the cavity loss probability and the normalized photon-spin state as

$$\rho_{cl} = P_{cl} \times \left(\frac{\rho_{cl}}{P_{cl}}\right) \tag{3.135}$$

3.5.3. Spontaneous emission

In the previous section, we found the effect of cavity loss on the photon-spin state during their interaction. In this section, we will find the photon-spin state after a spontaneous emission occurs. The spontaneous emission results in the decay of the spin to the ground state and the photon is lost to the environment. We limit our analysis only to straight decays, $|e_j\rangle \rightarrow |j\rangle$ ($j \in \{0,1\}$), and no cross transitions. The probability of a spontaneous emission occurring (P_{se}) is known in terms of the reflection and loss probabilities [45].

$$P_{se} = 1 - |r(\omega)|^2 - |l(\omega)|^2 \tag{3.136}$$

The probabilities of spontaneous emissions for the two ground state of the spin are

$$\begin{aligned} P_{se0} &= 1 - |r_0|^2 - |l_0|^2 \\ P_{se1} &= 1 - |r_1|^2 - |l_1|^2 \end{aligned} \tag{3.137}$$

The spontaneous emission could occur during the early scattering or the late scattering. Therefore, we first look at the incoming states before each scattering and then infer the final state after each decay. With probability P_{se0} (P_{se1}) the $|e_0\rangle$ ($|e_1\rangle$) state could decay to the $|0\rangle$ ($|1\rangle$) state. Therefore, the probability of ending up in any ground state is the probability of spontaneous emission times the probability of being in the corresponding excited state during scattering.

The first two expressions in the following equation represent the case where the spontaneous emission happens during the early scattering, and the last two represent the case of decay during late scattering. The final photon-spin state is

$$\begin{aligned} \rho_{se} = &P_{se0}\langle E0|\psi_1\rangle\langle\psi_1|E0\rangle|vac\rangle\langle vac|\otimes|0\rangle\langle 0| + \\ &P_{se1}\langle E1|\psi_1\rangle\langle\psi_1|E1\rangle|vac\rangle\langle vac|\otimes|1\rangle\langle 1| + \\ &P_{se0}\langle L0|\psi_3\rangle\langle\psi_3|L0\rangle|vac\rangle\langle vac|\otimes|+\rangle\langle +| + \\ &P_{se1}\langle L1|\psi_3\rangle\langle\psi_3|L1\rangle|vac\rangle\langle vac|\otimes|-\rangle\langle -| \end{aligned} \tag{3.138}$$

After spontaneous emission occurs in the early scattering, nothing happens during the late scattering because the time-bin photon is lost. That is why we have vacuum state in the final state. Only the Hadamard gates act on the spin but two Hadamard gates cancel each other's effect. Therefore the final state of the circuit is the one in eq. 3.138. Extending the similar analysis to the late scattering results in the following state

$$\begin{aligned} \rho_{se} = \frac{1}{4}\big[&2P_{se0}|\alpha|^2|vac\rangle\langle vac|\otimes|0\rangle\langle 0| + 2P_{se1}|\beta|^2|vac\rangle\langle vac|\otimes|1\rangle\langle 1| + \\ &P_{se0}|\alpha+\beta|^2|vac\rangle\langle vac|\otimes|+\rangle\langle +| + P_{se1}|\alpha-\beta|^2|vac\rangle\langle vac|\otimes|-\rangle\langle -|\big] \end{aligned} \tag{3.139}$$

Although the state of spin after decay during late scattering is $|0\rangle$ or $|1\rangle$, the Hadamard gate acts on the spin to give $|+\rangle$ or $|-\rangle$ in the final state of the circuit. The probability of having a spontaneous emission is

$$\begin{aligned} P_{se} = \frac{1}{4}\big[&2P_{se0}|\alpha|^2 + 2P_{se1}|\beta|^2 + \\ &P_{se0}|\alpha+\beta|^2 + P_{se1}|\alpha-\beta|^2\big] \end{aligned} \tag{3.140}$$

3.5.4. Final output state

The final photon-spin state after the Gate operation is summarised in the eq. 3.141

$$\begin{aligned}\rho_{ps} &= \rho_{nl} + \rho_{cl} + \rho_{se} \\ &= P_{nl} \times \rho_{\text{normalized}} + P_{cl} \times \left(\frac{\rho_{cl}}{P_{cl}}\right) + P_{se} \times \left(\frac{\rho_{se}}{P_{se}}\right)\end{aligned} \tag{3.141}$$

where, $P_{\text{nl}} = Tr\left(|\psi_5\rangle\langle\psi_5|\right)$ and $P_{cl} = Tr\left(|\Phi\rangle\langle\Phi|\right)$ are the probabilities of no-loss operation and cavity loss respectively. $\rho_{\text{normalized}}$ is the normalized density matrix after loss-less operation. $|\psi_5\rangle$ and $|\Phi\rangle$ are given in eq. 3.121 and 3.131 respectively and ρ_{se} is given in eq. 3.139.

4

Performance

In the previous chapter, we introduced the protocol for entangling spin with single-photons. We modeled the system for generating single-photons and for the photon-spin interaction. In this chapter, we first find an appropriate point of operation in the parameter space of the Gate which maximizes the Gate performance (sec. 4.1). The procedure for generating tree-cluster states is introduced in the next section (sec. 4.2). Lastly, we estimate the fidelity of the tree-cluster states created by the procedure, described in sec. 4.3.

All the simulations in this chapter are done using the QuTiP library in python.

4.1. Performance of the Gate

This section characterizes the performance of the photon-spin entangling operation using the Gate. In the previous chapter, we introduced the protocol for entangling photon and spin and the analytical expressions for the reflection coefficients for the two different ground states of the spin. This section aims to find the values of cavity parameters that yield the maximum entanglement fidelity after the photon-spin interaction.

It is possible to have imperfect single-qubit gates during the entangling protocol. However in this thesis, we assume that those gates are perfect and do not introduce any errors in the system. We limit ourselves only to imperfect photon-spin interaction by making that assumption.

The spin entangling protocol takes an arbitrary unentangled state of photon and spin and entangles them. However, for tree cluster generation, we only need to entangle $|-i\rangle$ state of the photon to a $|+\rangle$ state of the spin. Plugging in the appropriate state parameters ($\alpha = \beta = a = 1/\sqrt{2}$ and $b = -i/\sqrt{2}$) in eq. 3.11 would give us the output state in terms of general reflection coefficients as,

$$\begin{aligned} |\psi_{out}\rangle = &\frac{1}{4}|E\rangle\left((r_0 - r_1)|0\rangle - i(r_0 + r_1)|1\rangle\right) \\ &+ \frac{i}{4}|E\rangle\left((r_0 + r_1)|0\rangle - i(r_0 - r_1)|1\rangle\right) \\ &+ \frac{1}{4}|L\rangle\left((r_0 - r_1)|0\rangle - (r_0 + r_1)|1\rangle\right) \\ &+ \frac{1}{4}|L\rangle\left((r_0 + r_1)|0\rangle - (r_0 - r_1)|1\rangle\right) \end{aligned} \tag{4.1}$$

For the perfect state, $r_0 = -1$ and $r_1 = 1$. If we put these values in the above state, the prefect photon-spin state $|\Psi\rangle$ after ignoring the global phase is given by

$$|\Psi\rangle = \frac{1}{2}|E0\rangle + \frac{1}{2}|E1\rangle + \frac{1}{2}|L0\rangle - \frac{1}{2}|L1\rangle \tag{4.2}$$

The measure of fidelity for the density matrix heralded over photon detection is given by

$$F(\Psi, \rho_{\text{normalized}}) = Tr\left(|\Psi\rangle\langle\Psi|\,\rho_{\text{normalized}}\right) \tag{4.3}$$

where,

$$\rho_{\text{normalized}} = \left(\frac{|\psi_{out}\rangle\langle\psi_{out}|}{P_{nl}}\right) \tag{4.4}$$

where $|\psi\rangle$ is the photon-spin state after reflection of the photon off the cavity. The density matrix here is normalized, thus this is the fidelity heralded on photon detection. The probability of no-loss operation P_{nl}, or the success probability in terms of the reflection coefficients is given by

$$P_{nl} = \frac{1}{4}\left[3|r_0|^2| + |r_1|^2 + \right] \tag{4.5}$$

The reflection coefficients for the two ground states are given by

$$\begin{aligned} r_0 &= \left[1 - \frac{\kappa_a/\kappa}{\frac{-i\omega_d}{\kappa} + \frac{1}{2} + \frac{C_0\hat{P}_0}{\frac{-i}{\gamma_0}(\omega_d+\Delta_0)+\frac{1}{2}}}\right] \\ r_1 &= \left[1 - \frac{\kappa_a/\kappa}{\frac{-i\omega_d}{\kappa} + \frac{1}{2} + \frac{C_1\hat{P}_1}{\frac{-i}{\gamma_1}(\omega_d+\Delta_1)+\frac{1}{2}}}\right] \end{aligned} \tag{4.6}$$

We will now find the value of parameters in the reflection coefficients that can help us achieve maximum fidelity.

In the ideal reflection case, we assume that we are in the high cooperativity limit, and we assume that one of the levels ($|1\rangle$) is in resonance with the cavity field and the other level ($|0\rangle$) is far detuned. In this case we get, $r_0 = -1$ and $r_1 = 1$. In realistic cases, both the levels may be detuned from the cavity resonance by a finite amount, resulting in imperfect reflection coefficients. Moreover, it is also possible to have finite cooperativity, leading to a significantly higher probability of spontaneous emissions. Therefore, it is crucial to find operating values of the cavity parameters that maximizes the fidelity and success probability of entanglement.

For our analysis in this section we will make a few assumptions. We will assume that the two rates of decay, the two single-photon Rabi frequencies are the same for both the ground states and the Cooperativities are the same.

$$\begin{aligned} \gamma_1 &= \gamma_0 = \gamma \\ g_1 &= g_0 = g \\ C_1 &= C_0 = C \end{aligned} \tag{4.7}$$

Thus, the only different parameters for both the ground states are Δ_1 and Δ_0. It may seem that they are independent of each other, but in reality, we can find a relation between the two detuning in terms of the splitting between the levels. Hence, we define a new parameter Δ such that it is the difference between the detunings for the pair of two-level systems.

$$\begin{aligned} \Delta &= \Delta_1 - \Delta_0 \\ &= (\omega_{e1} - \omega_1 - \omega_c) - (\omega_{e0} - \omega_0 - \omega_c) \end{aligned} \tag{4.8}$$

Assuming that the two ground states are at the same energy level ($\omega_0 = \omega_1$), then Δ becomes the splitting between the two excited states, as shown in fig. 4.1.

$$\Delta = \omega_{e1} - \omega_{e0} \tag{4.9}$$

We write Δ_0 in terms of Δ_1 and Δ for our analysis in this section and optimize the system for different values of Δ.

$$\Delta_0 = \Delta_1 - \Delta \tag{4.10}$$

Δ_0 and Δ_1 are the detunings between the levels and the cavity mode, therefore, they can be negative or positive. Similarly, the detuning between the excited states, Δ, may also be negative or positive, depending on the level structure. In this analysis, we will consider that Δ is positive. Moreover, we prefer large Δ and a large cooperativity for a near-ideal operation. If Δ is large and the $|e_1\rangle$ to $|1\rangle$ transition is resonant with the cavity, then the system for $|0\rangle$ state is far detuned and therefore r_0 approaches -1 and r_1 is close to 1.

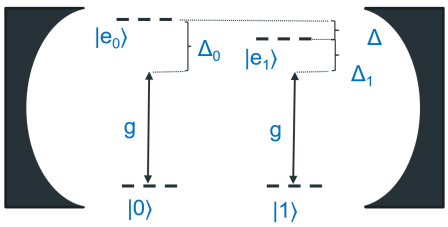

(a) Δ is negative, Δ_0 and Δ_1 are positive

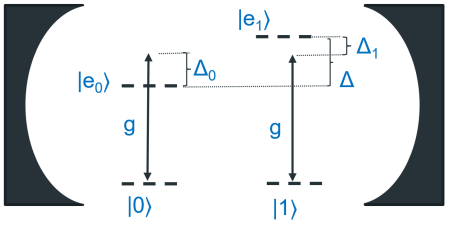

(b) Δ and Δ_1 are positive, Δ_0 is negative

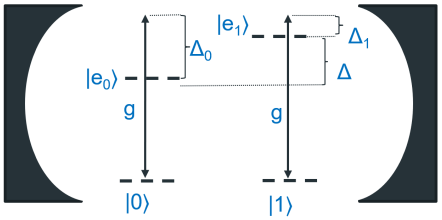

(c) Δ is positive while Δ_0 and Δ_1 are negative

Figure 4.1: Some of the configurations of Δ, Δ_0 and Δ_1, each satisfying eq. 4.10

Another parameter that we must consider is the detuning between the cavity field and the incoming photon's frequency, ω_d. We can control the frequency of the incoming photon by changing the frequency of the driving laser and changing the single-photon Rabi frequency of the Emitter. This detuning can thus also be positive or negative. Therefore, we can find the values of κ_a, κ, C, γ, ω, Δ_1 and Δ such that the entanglement fidelity is maximized. To find the maximum fidelity of the Gate, we perform a grid search over different values of these parameters. The first step towards starting the grid search is limiting some of the parameters. We solved the dynamics of the Gate assuming that we are in the Purcell regime, $\gamma \ll g \ll \kappa$. We already assumed that spontaneous emission rates for the two excited states are the same. We will assume that they are constant throughout this analysis and all the rates in the system are in terms of γ. We also fix the cavity decay rate, κ, at 100γ or simply $\kappa/\gamma = 100$.

We optimize the parameters not to maximise the fidelity of the heralded state (referred as heralded fidelity in the rest of the report), but the fidelity of entanglement. Which is the heralded fidelity multiplied with the success probability.

$$F_{ent} = F_{Heralded} \times P_{suc} \tag{4.11}$$

Note that there are two fidelities in play. First is the heralded fidelity, it is the fidelity of the state given the photon was not lost. The other is the entanglement fidelity, it is the fidelity of a state that also takes photon loss (due to cavity loss or spontaneous emission) into account by considering the success probability.

We begin by analysing the effect of varying Δ_1 and ω_d on the fidelity, we first fix other parameters and plot the entanglement fidelity, and not the heralded fidelity. The underlying idea is that we can

vary them over a range of values and find values which give us the best performance. We fix the value of the cooperativity of the system at 100, and we plot the fidelity for $\Delta = 20\gamma$, $\Delta = 50\gamma$ and $\Delta = 80\gamma$. Moreover, we assume that we have the perfect cavity mirrors and that there is no loss in the cavity, $\kappa_a = 100\gamma$. We make a contour plot of the entanglement fidelity for different values of Δ_1/γ and ω_d/γ as a starting point of our optimization.

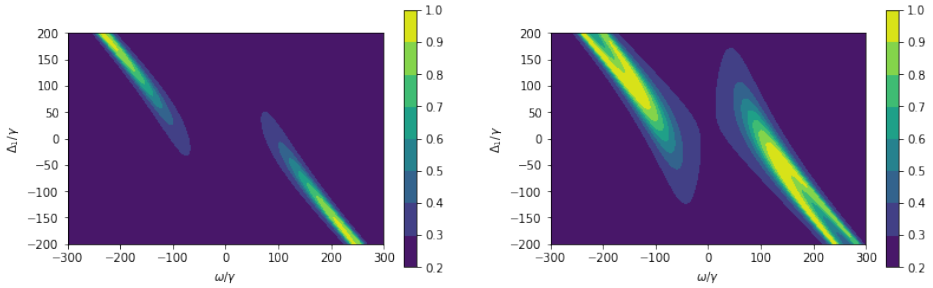

(a) $\Delta = 20\gamma$

(b) $\Delta = 50\gamma$

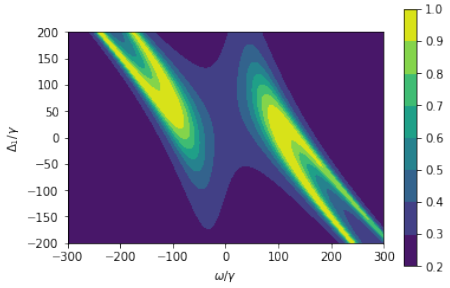

(c) $\Delta = 80\gamma$

Figure 4.2: Contour plot for entanglement fidelity vs Δ and ω_d

From the contour plots of the entanglement fidelity for different values of Δ we can make a few observations.

- The fidelity is symmetric about the point $(\Delta/2\gamma, 0)$. This is not surprising. Consider the case when Δ_1 increases from zero to Δ. Then, $|0\rangle$ state becomes less detuned to the cavity and $|1\rangle$ becomes more detuned. Finally when Δ_1 reaches the value Δ, the $|1\rangle$ state becomes far-detuned and thus r_1 assumes the value r_0 had at the beginning and vice-versa.

- The region of high fidelity is broader for higher Δ. This makes sense because as Δ becomes large the contrast between the two reflection coefficient increases. Thus a higher fidelity can be reach for wider range of values of Δ_1 and ω_d. Recalling that in the ideal case, we want the $|0\rangle$ ground state to be decoupled from the cavity or to have a really large detuning Δ_0. Having a large value of Δ helps us achieve exactly that.

- The regions of high fidelity come closer to the point $(\Delta/2\gamma, 0)$ as Δ is increased. In other words, to maximise the fidelity we do not need to have large detunings Δ_1 and ω_d for systems with large Δ.

From these observations we can limit the values ω_d/γ and Δ_1/γ can assume to optimize the search for max fidelity. For small Δ, the optimal point is far away from the point $(\Delta/2, 0)$, therefore we can safely limit Δ_1 and ω_d as

$$\begin{aligned} \Delta_1/\gamma &\in (-\infty, \Delta/2\gamma) \\ \omega_d/\gamma &\in (0, \infty) \end{aligned} \tag{4.12}$$

We do not go to infinity or negative infinity, we just vary these parameters to a large positive or from a large negative number.

In the previous plots we kept the value of cooperativity fixed at 100. We will now vary the cooperativity from 0 to 100 and keep the Δ fixed. Thus, for a given value of Δ we can find the optimal point of operation over the parameters Δ_1, ω_d and C. We plot the heralded infidelity (found by subtracting the heralded fidelity from one) and the success probability optimized over Δ_1 and ω_d for values of C.

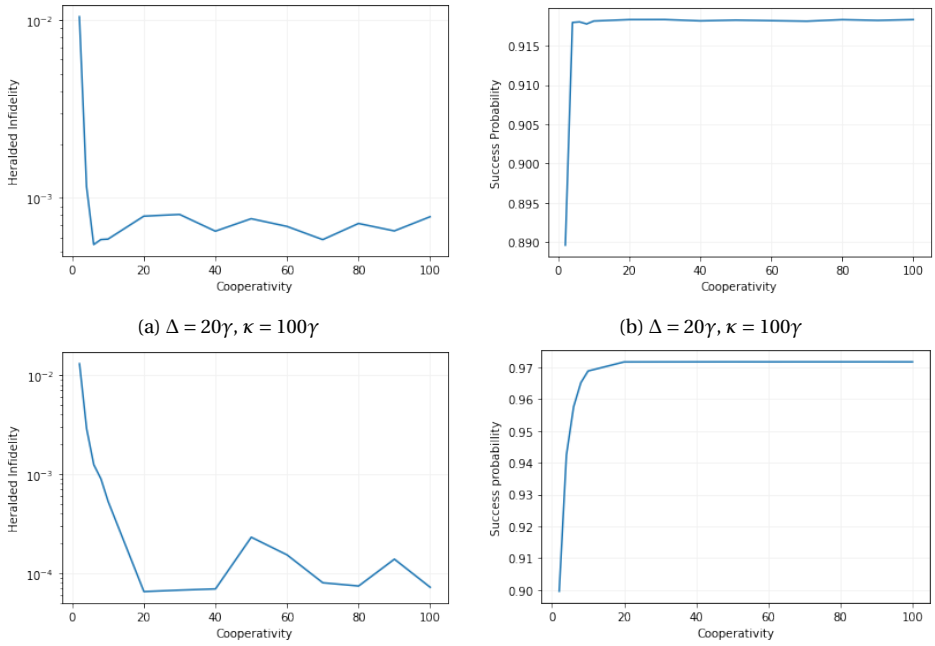

(a) $\Delta = 20\gamma$, $\kappa = 100\gamma$

(b) $\Delta = 20\gamma$, $\kappa = 100\gamma$

(c) $\Delta = 60\gamma$, $\kappa = 100\gamma$

(d) $\Delta = 60\gamma$, $\kappa = 100\gamma$

Figure 4.3: Plot of heralded infidelity and success probability for values of C

From the figures, we can observe that the heralded infidelity decreases and success probability increases for the larger Δ ($\Delta = 60\gamma$). The error in the values of infidelity decreases as well. The reason for errors in the infidelity could be because of a coarse mesh that we have used for the grid search. For a finer mesh of Δ_1 and ω_d one could decrease the errors. These errors do not affect our optimization, the errors are so small that they can be safely ignored. One crucial observation that could be made here is that the infidelity decreases rapidly at smaller cooperativity for smaller Δ. This could mean that a smaller value of cooperativity could lead to a higher fidelity for small Δ. Whereas, for larger Δs, we need to have cooperativity which is comparable to Δ. Similarly the success probability also increases sharply for smaller values of cooperativity for smaller Δ. We should also note that once the heralded fidelity and success probability reach their maxima, they do not decrease. This could be explained by looking at the values of Δ_1 and ω_d where these maxima are reached. For $\Delta = 20\gamma$ the values of Δ_1 and ω_d corresponding to the optimum point are summarised in the table 4.1.

C	ω_d/γ	Δ_1/γ	Heralded fidelity	Success Probability
2	6.0	-4.5	0.9895	0.8896
4	4.5	0.0	0.9988	0.9179
6	30.0	-19.5	0.9994	0.9180
8	45.0	-31.5	0.9994	0.9177
10	57.0	-42.0	0.9994	0.9181
20	96.0	-75.0	0.9992	0.9183
30	123.0	-97.5	0.9991	0.9183
40	142.5	-112.5	0.9993	0.9181
50	162.0	-129.0	0.9992	0.9182
60	180.0	-144.0	0.9993	0.9181
70	193.5	-154.5	0.9994	0.9181
80	211.5	-171.0	0.9992	0.9183
90	222.0	-178.5	0.9993	0.9182
100	237.0	-192.0	0.9992	0.9183

Table 4.1: Values of Δ_1 and ω_d for different C with the maximum heralded fidelity and success probability, for $\Delta/\gamma = 20$ and $\kappa/\gamma = 100$

It can be observed that the errors in success probability and heralded fidelity are small and most of the values have errors the order of 10^{-4}. A surprising observation that can be made here is that increasing cooperativity does not help, as one might intuitively think. We can observe that as the cooperativity becomes large compared to Δ, the values of detunings, Δ_1 and ω_d, needed for optimal entanglement also become large. Therefore, for maximum performance and smaller detunings Δ_1 and ω_d, we should have a cooperativity which is close to the value of Δ/γ so that the required values of detunings Δ_1 and ω_d are not large.

Finally, we optimize the entanglement fidelity over the values of Δ_1/γ, ω_d/γ and cooperativity for a range of values of Δ/γ. As described earlier we keep the values of κ and κ_a fixed at 100γ. The plot for maximum heralded infidelity is shown in figure 4.8a and the plot for success probability is shown in fig. 4.8b.

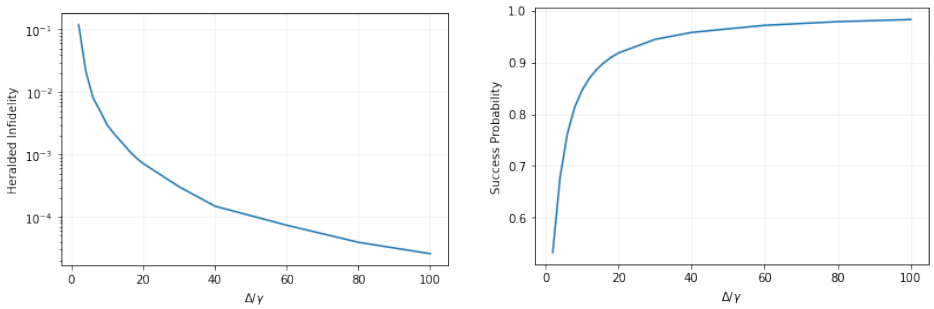

(a) Heralded infidelity vs Δ/γ

(b) Success probability vs Δ/γ

Figure 4.4: Performance of the Gate for different values of Δ/γ for, $\kappa = 100\gamma$

It can be inferred from the plots that we need to have a large splitting between the excited states to have a good performance of the system. For a value of $\Delta/\gamma = 20$ we can get a probability of success greater than 0.9 and an heralded infidelity less that 0.001. The value of splitting between the excited states, Δ, is varied from 2γ to 100γ and the value of cavity decay rate is kept constant at 100γ. If the value of κ/γ is changed from 100, it would not have any effect on the performance because of the contribution of κ in the reflection coefficients. κ contributes to the reflection coefficients at two places, κ_a/κ and ω_d/κ. Since we assumed that there are no losses in the cavity, so the first term

assumes a value of one. Let us now look at the contribution of κ in the reflection coefficients at the other place.

$$r_0 = \left[1 - \frac{1}{\frac{-i\omega_d}{\kappa} + \frac{1}{2} + \frac{C_0 \hat{P}_0}{\frac{-i}{\gamma_0}(\omega_d + \Delta_0) + \frac{1}{2}}} \right] \tag{4.13}$$

To study the effects of changing the value of κ, let us assume that we have the optimal values of ω_d and Δ_1 for a given value of γ, C, Δ and κ. Changing the value of κ would change the ratio of ω_d/κ. Therefore, we would not be at the optimal point for this new value of κ. In order to move to the optimal point, we can change the value of ω_d such that the ratio ω_d/κ is same as before. We would then also have to change the value of Δ_1 to go to the optimal point. Thus, it would only change the range of Δ_1 and ω_d over which we can get maximum performance. We summarize the values of Δ_1 and ω_d which optimize the Gate performance for $\kappa = 50\gamma$ in the following table for $\Delta = 20$ and for various values of C.

C	ω_d/γ	Δ_1/γ	Heralded fidelity	Success Probability
2	3.0	-1.55	0.9901	0.8892
4	2.0	2.65	0.9989	0.9181
6	16.0	-5.75	0.9993	0.9182
8	23.0	-9.95	0.9993	0.9181
10	29.0	-14.15	0.9992	0.9182
20	48.0	-26.75	0.9993	0.9182
30	61.0	-35.15	0.9992	0.9182
40	72.0	-42.5	0.9992	0.9182
50	81.0	-47.75	0.9994	0.9181
60	90.0	-54.05	0.9993	0.9182
70	97.0	-58.25	0.9993	0.9182
80	106.0	-65.6	0.9992	0.9183
90	112.0	-68.75	0.9992	0.9182
100	119.0	-74.0	0.9992	0.9183

Table 4.2: Values of ω_d/γ and Δ_1/γ corresponding to maximum performance, and the values of heralded fidelity and success probability for varying C. Δ is kept constant at 20γ and κ is 50γ

We can observe that for the same value of $\Delta = 20\gamma$, changing the value of κ from $\kappa = 100\gamma$ to $\kappa = 50\gamma$ does not change the heralded fidelity or the success probability. It just affects the values of Δ_1 and ω_d which result in maximum performance.

To summarize, we optimized the performance of the entanglement operation of the Gate. We found the maximum heralded fidelity and success probability for a range of values of the splitting between the excited states. Although, we did not consider the presence of losses in the cavity ($\kappa_a = \kappa$), it is easy to extend this analysis to include cavity losses in the Gate.

In the next section, we will introduce the protocol for generating tree-cluster states.

4.2. Tree generation protocol

So far, we have introduced the protocol for entangling time-bin photons with a spin, and modeled the Emitter and the Gate. In the previous section, we evaluated the performance of the Gate for different values of its parameters. In this section, we introduce the protocol for generating the tree-cluster state.

Our approach can generate a tree-cluster state with three levels for an arbitrary branching vector $\bar{B} = [b_0, b_1, b_2]$. The protocol requires one spin (for our system, it will be the spin of the Gate) and

two memory spins that can be entangled with the spin similar to the protocol in [21]. One memory spin serves as the zeroth level node, and the other serves as the first level node of the tree. For photon-spin entanglement, the Emitter generates time-bin photons which scatter off the Gate and entangle with the Gate spin.

We start by preparing the spin, and the memory spins in $|+\rangle$ state. Then the memory spins (the dark blue and light blue spins in fig. 4.5) are entangled with each other, and the level one memory spin (light blue spin) is entangled with the spin (the black spin in fig. 4.5). After the entanglement between the spin and memory spins, b_2 number of photons are generated in the Emitter in $|-i\rangle$ state and entangled to the spin (recall that the entangling protocol requires the photon in the $|-i\rangle$ state and not the $|+\rangle$ state) ((b) in fig. 4.5). Then the state of the spin is swapped to a photon using the teleportation circuit shown in fig. 4.6 to get (c) in fig. 4.5. Swapping the state detaches the spin from the system, therefore, we re-entangle it with the first level memory spin. This process is repeated $b_1 - 1$ more times to make the remaining branches, (d) in fig. 4.5. The state of the first level memory spin is swapped to the spin and later to a photon. As shown in (e) in fig. 4.5, this generates one of the tree branches. The memory spins are re-entangled with each other, and this whole process is repeated $b_0 - 1$ more times to generate the remaining branches of the tree. Finally, the state of the zeroth level memory spin is swapped with the spin and subsequently swapped with the photon to generate an all-photonic tree-cluster state.

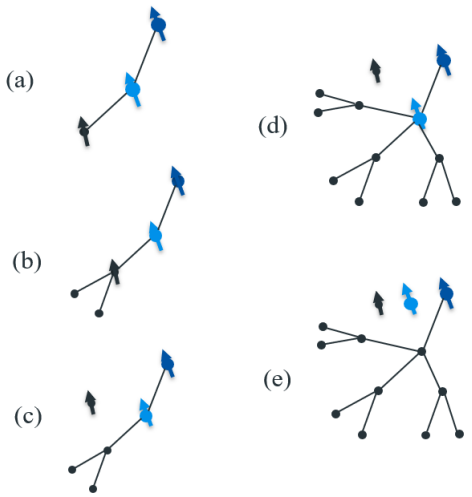

Figure 4.5: For a $\bar{B} = [2,3,2]$ tree, we entangle the memory spins and Gate the spin as shown in (a). We emit two photons from the Emitter and entangle them with the Gate spin, shown in (b). The third step (c) is swapping the state of spin with another photon using teleportation circuit. We repeat the previous three steps 3 times to generate level three and level two photons of the tree (d). Swapping the state of the memory spin with a photon gives (e). This generates one branch of the tree. Repeating the whole process once again will give us the second branch of the tree. Then we swap the state of memory spin with a photon to get a $\bar{B} = [2,3,2]$ tree.

We use the circuit shown in fig. 4.6 to swap the state of the spin to a photon. The circuit maps an arbitrary state of the spin to the photon generated in the $|-i\rangle$ state. The circuit requires a Hadamard gate on the time-bin qubits, and it could be implemented using the scheme in [46].

This protocol requires the entanglement of the spin with memory spins to generate a tree-cluster state. Therefore, we require systems with access to nearby quantum memories for the experimental implementation of tree-cluster generation. SiV centers have access to nearby ^{13}C nuclear spins, and the entanglement between them has been demonstrated [47]. Moreover, ^{29}SiV centers could also be used because of the presence of nuclear spin and electronic spin in the same defect center [48].

The states of memory spins can be swapped with the state of electron spin by using two CZ gates [21]. However, we will use a circuit similar to the one in fig. 4.6 to swap the states of memory spins with the spin. SiV centers coupled to diamond nanocavities provide an effective spin-photon interface, and an accessible quantum memory [32, 48, 47]. These qualities make SiV centers an attractive candidate for the experimental generation of tree-cluster states.

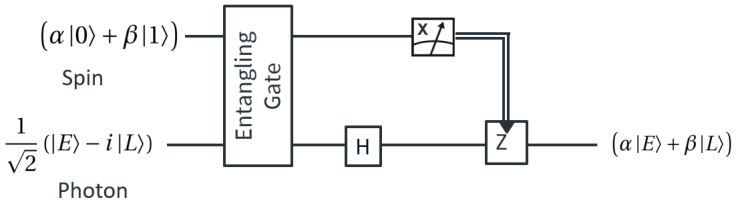

Figure 4.6: Circuit for swapping the state of spin with photon. The "Entangling Gate" in the circuit is the entanglement operation between a photon and the Gate spin using the protocol illustrated in 3.1. It involves first entangling the spin with a photon. Then a Hadamard gate is applied to the photon. The spin is measured in X basis and the measurement result is used to correct the state of the photon to swap the state of spin to the photon.

We can use the tree-cluster generation protocol to generate trees with three levels and for an arbitrary branching vector. We will show in the next section how we estimate the fidelity of the generated tree-cluster state.

4.3. Fidelity estimation of the tree

In the previous section, we introduced the protocol for tree-cluster generation. The protocol can generate a tree-cluster state of three levels, using two memory spins and one spin for scattering and entangling the photons, given the branching parameters of the tree. This section characterizes and estimates the fidelity of the generated tree-cluster states. Tree-cluster states can suffer from correlated errors on the photons due to errors during generation. By now, we have a model for entangling spins and photons and the protocol for generating the tree-cluster states already. We first introduce the method for estimating the fidelity of the generated tree-cluster states, and then we simulate the tree-cluster generation and use the measure to assess the performance of tree-cluster states.

4.3.1. Estimation of tree-cluster fidelity

Tree cluster states are part of a larger class of multipartite entangled states, and characterizing the entanglement of multipartite entangled states is a difficult task [49]. As the size of the multiqubit state increases, the resources required to detect and measure the quality of entanglement increase exponentially. There exist methods for estimating the lower bound fidelity of cluster states [49, 50, 51]. Tiurev et al. [50] used the stabilizer description of cluster states to estimate their fidelity. We know that a complete set of stabilizer operators can define a tree-cluster state. Therefore, measuring different combinations of these stabilizers can help us estimate the fidelity. The stabilizer s_i associated with each vertex i of the state is defined as

$$s_i = \sigma_i^x \bigotimes_{j \in N(i)} \sigma_j^z \tag{4.14}$$

where $N(i)$ is the set of vertices which are neighbors to the vertex i. The tree cluster state, $|\Psi\rangle$, is the eigenstate of the stabilizer operators with eigenvalue 1

$$s_i |\Psi\rangle = |\Psi\rangle \tag{4.15}$$

Furthermore, the stabilizers can be used to describe the ideal state $|\Psi\rangle$ [50],

$$|\Psi\rangle\langle\Psi| = \prod_{i=1}^{N} \frac{1+s_i}{2} = \prod_{i=1}^{N} S_i \tag{4.16}$$

For an arbitrary cluster state ρ, the fidelity is defined as $F = Tr(\rho|\Psi\rangle\langle\Psi|)$. The fidelity of a state can be estimated by measuring a combination of the stabilizers s_i, as shown in [50]. Similar to the authors in [50], we define two combinations of stabilizers that can help us estimate fidelity of the tree. We define the two combinations in terms of the levels of the tree. The first combination is product of S_i corresponding to all the vertices on odd levels, S_o, and the second combination is product of stabilizers of vertices on even levels (including zero), referred to as S_e.

$$|\Psi\rangle\langle\Psi| = \prod_{i=1}^{N} \frac{1+s_i}{2} = \prod_{i=1}^{N} S_i = S_o S_e = S_o + S_e - 1 + (1-S_o)(1-S_e) \tag{4.17}$$

where S_o and S_e are defined as

$$S_o = \prod_{\text{level(i)}\in\text{odd}} S_i \qquad S_e = \prod_{\text{level(j)}\in\text{even}} S_j \tag{4.18}$$

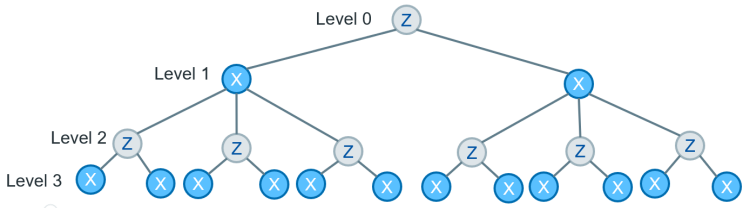

(a) S_o operator with stabilizers on the odd levels.

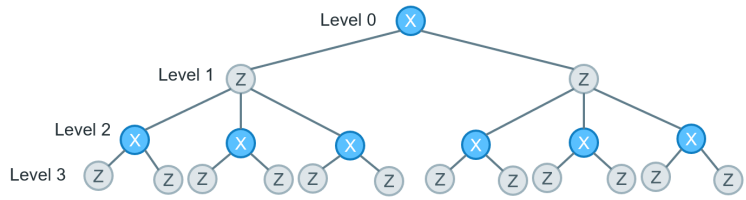

(b) S_e operator with even-level stabilizers

Figure 4.7: Operators S_o and S_e used for lower-bound fidelity estimations. S_o (S_e) would require X-measurement on the photons on odd (even) levels and Z-measurement on photons on even (odd) levels. Since only one measurement has to be done on a photon in each of S_o and S_e, we can measure each stabilizer in just one measurement setting.

To find a lower bound of the fidelity we ignore the non-negative term $(1-S_o)(1-S_e)$ in 4.17 [50]. The lower bound fidelity can be written in terms of $\hat{P}$ operator defined as

$$\hat{P} = S_o + S_e - 1 \leq |\Psi\rangle\langle\Psi| \tag{4.19}$$

The relation between fidelity and expectation value of this operator is,

$$F = Tr(\rho|\Psi\rangle\langle\Psi|) \geq Tr(\rho\hat{P}) \tag{4.20}$$

Therefore, if we find the expectation value of $\hat{P}$ operator, we can find a lower bound on the fidelity of the generated tree-cluster state. In the next part of this section, we will discuss the method used to measure the stabilizers to find the expectation value of $\hat{P}$.

4.3.2. Estimation of fidelity

In the previous section, we found the expression for the lower bound fidelity of a tree-cluster state. For making the estimation, we are required to measure a combination of stabilizers. More specifically, we need to find the expectation value of the $\hat{P}$ operator. In this section, we describe how we find the expectation value of $\hat{P}$ by simulating the tree generation process to estimate the fidelity.

Generating a tree-cluster state requires us to entangle multiple photons to the spin. To estimate the fidelity, we need to measure the tree photons in a certain basis (depending on the stabilizer) for each photon. A tree-cluster state with a large number of photons has an exponentially large number of real numbers in the density matrix of the state. Consequently in our simulations, we cannot generate the complete tree cluster and then measure the stabilizers. To rid ourselves of large density matrices, we measure the photon as soon as it is entangled with the spin and save the measurement result for later analysis. This way, we only have to deal with states of two memory spins, the Gate spin, and a photon. As a result, the amount of variables we need to deal with reduces tremendously. Hence, the computational power required reduces as well. In simpler words, we measure a photon before another photon entangles with spin rather than entangling photons first and then measuring. The order of these two operations does not affect the generation of the tree-cluster state because the emitted photons do not interact with the spin or the photons. This way, we go through the tree generation and measurement in one go, and we have the measurement results of each photon at the end of the run. From the measurement results, we can find the value of the stabilizer for the run. We have to repeat this process multiple times for each stabilizer S_o and S_e.

For estimation of tree fidelity, we first fix the heralded entanglement fidelity between spin and a photon to a particular value and repeat the process of tree generation and measurement several times. For each value of the heralded entanglement fidelity, we input the reflection coefficients which correspond to it and entangle the spin with a photon using the photon-spin entangling protocol from section 3.1. Heralded entanglement fidelity means that we do not lose the photon to Gate errors and all the photons come out after interaction with the Gate. Moreover, we assume that the single-qubit operations on the spin and memory qubits are perfect during this whole process. Furthermore, we assume that the entanglement between the memory qubits and between the memory qubit and the spin is perfect. We will also assume that any qubit (spin or time-bin) measurement does not introduce any errors to the system. Therefore, the only source of error during the tree generation is the imperfect photon-spin entangling operation.

We generate a tree with branching vector $\vec{B} = [2,3,2]$ in the simulation. The estimate of the tree-cluster fidelity gets better as we increase the number of tries. For an uncorrelated state with 21 qubits, finding the expectation value of an operator might require a huge number of tries. However, the correlations between different photon states in the tree can help us estimate the fidelity for a relatively lower number of tries. To see if we can find a good estimate, we first plot the tree-cluster fidelity against the number of tries for two values of heralded entanglement fidelity. As we increase the number of tries, we want the fidelity to approach a certain value as the number of tries increases.

From the figures, we can observe that as the number of tries increases, the difference between consecutive values of fidelity decreases, and it seems that the fidelity approaches a certain value. We can find the mean and the variance of the values of tree-cluster fidelity for the two given heralded entanglement fidelities. For heralded entanglement fidelity of0.9849 the mean tree-cluster fidelity is 0.39184 and the variance is 0.00017, while for 0.9958 heralded entanglement fidelity the mean and variance are 0.8093 and 0.00009 respectively. The tree-cluster fidelity increases as the heralded entanglement fidelity increases, and the variance over all the number of tries decreases. The reason for this could be the correlations in the tree-cluster state. As heralded entanglement fidelity increases, the tree-cluster state comes closer to the ideal state, and thus the variance decreases, and the mean fidelity comes closer to one.

To assess the effect of heralded entanglement fidelity on the tree-cluster fidelity, we vary the

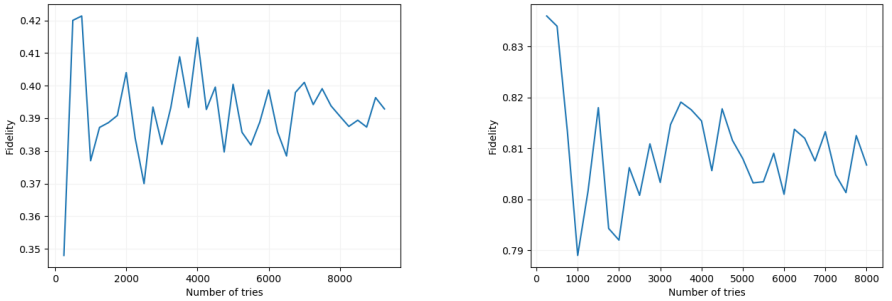

(a) Heralded entanglement fidelity = 0.9849 (b) Heralded entanglement fidelity = 0.9958

Figure 4.8: Fidelity vs Number of tries for fixed heralded entanglement fidelity

heralded entanglement fidelity of the photon-spin interaction and simulate $n = 5000$ tries. The plot of the tree cluster fidelity estimate after varying the heralded entanglement fidelity is shown in fig. 4.9.

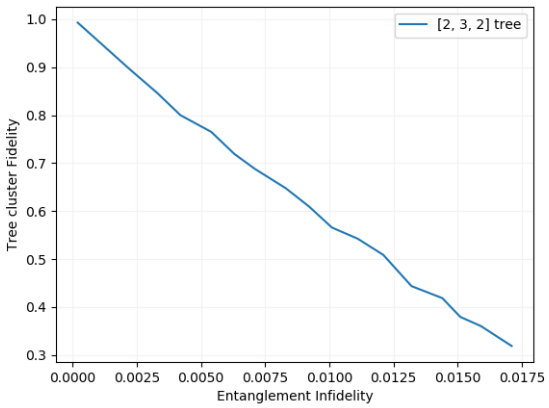

Figure 4.9: Fidelity of tree-cluster state for different values of heralded entanglement infidelity

We can observe that the tree cluster fidelity approaches unity as the infidelity approaches zero, as it should for perfect entanglement. The tree cluster fidelity decreases linearly with increasing heralded entanglement infidelity, but the values of infidelity may be so small that we can only find the linear approximation of their actual relation. It is also possible that the relation between tree-cluster fidelity and heralded entanglement fidelity is not linear even for these values of heralded fidelity. We cannot comment because we only calculate the lower bound fidelity of the tree.

To relate the effect of correlated errors, caused by imperfect entanglement, to non-correlated errors, we introduced single-qubit depolarising errors on individual photons of the tree-cluster state, similar to [21]. The errors on each photon are thus independent of errors on other photons. A depolarising channel on the i'th photon is given by eq. 4.21.

$$\Lambda_i(\hat{\rho}) = (1-\epsilon)\hat{\rho} + \frac{\epsilon}{3}(\sigma_i^x \hat{\rho} \sigma_i^x + \sigma_i^z \hat{\rho} \sigma_i^x + \sigma_i^y \hat{\rho} \sigma_i^y) \tag{4.21}$$

Where σ_i^x is the Pauli-X operator on the i'th photon and ϵ is the error.

For this simulation, we first generate perfect entanglement between spin and photon. To calculate the tree fidelity, we run Monte-Carlo simulations such that a Pauli operator can act on the photon with a probability $\epsilon/3$. The value of ϵ is chosen such that the fidelity of the tree state after applying the depolarising errors is in the same range as the fidelity of tree state after imperfect

entanglement. The method of fidelity estimation is same as before. We measure the photon after it is entangled with the spin and depolarising errors are applied to it. The simulation was run for $n = 5000$ tries, same as before. The plot the tree fidelity for depolarising errors juxtaposed with correlated errors as shown in fig. 4.10. It can be observed from the plot that for the same depolarising

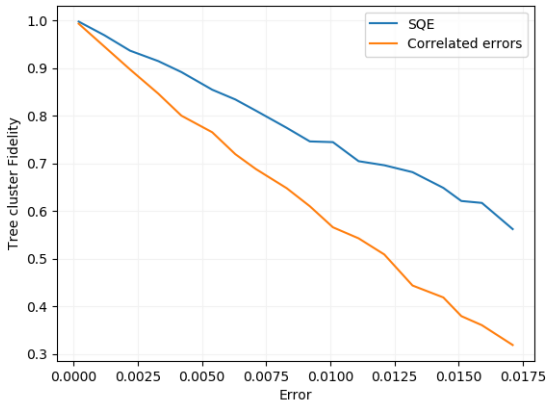

Figure 4.10: Comparison between single-qubit depolarising errors (SQE) and correlated errors for [2, 3, 2] tree

error and entanglement infidelity, the fidelity of the tree in case of depolarising errors is better than it is for imperfect entanglement. This is because depolarising errors on the photons are independent of each other. A depolarising error on one photon does not affect the other photons. On the other hand, an imperfect entanglement between photon and a spin affects the spin state and thus could lead to errors during the entanglement of other photons to the spin. Therefore, entanglement infidelity has a more severe effect on tree fidelity than depolarizing errors.

To compare the relative effect of errors, we find the slope of the two plots. The slope of the two plots can be used to find how much an error during the spin-photon entanglement affects the tree fidelity. To find the slope, we used the NumPy function `numpy.polyfit` to fit the two curves with a straight line. The plot of the fit with the curves is shown in fig. 4.11. The respective values of slopes for correlated errors and single-qubit errors are -39.564 and -24.580. The slopes are negative because the x-axis is infidelity or the error. It can be seen that the slope of the two fits can be related to the number of photons in the [2, 3, 2] tree-cluster state, which is 21. The slope for single-qubit errors is close to the number of photons, while the slope of fit for entanglement infidelity is close to twice the number of photons.

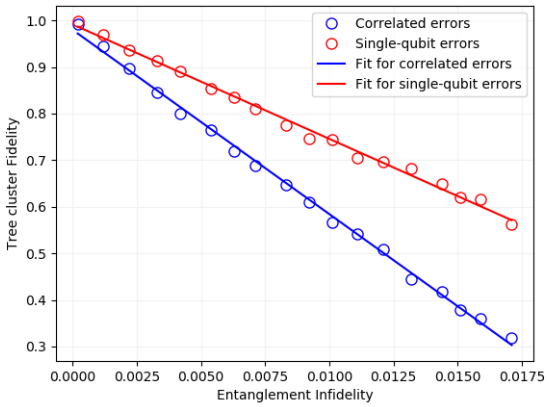

Figure 4.11: Linear fits for entanglement infidelity and single-qubit errors

So far, we have varied the entanglement infidelity for just the $[2,3,2]$ tree. Now, we would like to investigate the tree fidelity for different types of tree-clusters with different number of photons. For that, we run the simulations for a tree with branching vector $\bar{B} = [1,1,x]$, shown in fig. 4.12. Here x can take integer values greater than 1. We chose such a branching vector because it allows us to vary the photon number uniformly. Another advantage of generating a relatively small tree is that the simulation does not take a long time, thus allowing us to generate more data. We simulated from $x = 2$ to $x = 6$ to find the tree fidelity for various entanglement infidelities and for $n = 4000$ tries, as shown in fig. 4.13. Moreover, we fit the resulting plot to a line, using the function `numpy.polyfit` to get the slopes. The fit and the curves are plotted in fig. 4.13.

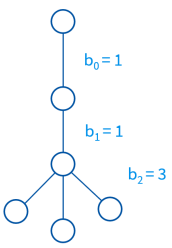

Figure 4.12: $\bar{B} = [1,1,x]$ for $x = 3$. Total number of photons in such a tree are x+3.

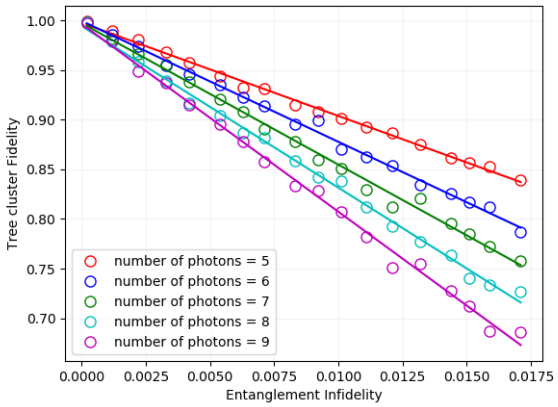

Figure 4.13: Tree-cluster fidelity vs heralded entanglement infidelity for [1, 1, x] tree. The solid lines in the plot depict the linear fits of the fidelity.

The values of the slopes are summarized in the table 4.3. We have also included the slope from the fitting of the [2, 3, 2] tree.

Total number of photons	Slope of linear fit
5	-9.385
6	-12.188
7	-14.262
8	-16.293
9	-18.929
21	-39.564

Table 4.3: Table summarizing the slopes

From these values, it can be concluded that the relation between tree-cluster fidelity F and the entanglement infidelity ϵ can be roughly written in terms of the total number of photons N in a tree. It can be observed that the slope of the curves depends nearly on twice the number of photons ($2N$). The relationship between F and ϵ can be expressed as

$$F(n,\epsilon) = 1 - 2n\epsilon \tag{4.22}$$

However, our confidence in this relation is low. This is because of two reasons, firstly, the values of x ($x \in \{2,3,4,5,6\}$) were too small in this analysis, secondly, the number of tries ($n = 4000$) was too small, which led to errors during fidelity estimation. We could not conclusively find the parameter the tree-fidelity depends on and the answer to that question is still unknown. One could use the method we have developed to find a more accurate relation between tree fidelity and heralded entanglement infidelity.

We think that the connectivity of a tree-state could be the reason for slope dependence on $2N$, where N is the total number of photons in a tree-state. The depolarising errors do not result in correlated errors because all the errors are independent of each other. However, in presence of entanglement infidelity, imperfect entanglement in one edge of the tree state could affect other edges of the tree state. Moreover, we believe that for a more connected graph state, the heralded entanglement infidelity could lead to more errors in the fidelity of the graph state than its effect on tree-cluster fidelity. It is important to find a metric that could be used to characterize the effect of imperfect entanglement on the generated tree-cluster state, and graph theory could help us find this metric.

From graph theory, one metric that denotes the connectivity of a graph is the sum of all the degrees (D) of a graph. For a tree graph, it is related to the number of vertices, N, as $D = 2(N-1)$. If the fidelity of the tree-cluster state depends on the metric D, then it could depend on the heralded entanglement infidelity as,

$$\begin{aligned} F_{tree} &= 1 - D\epsilon \\ &= 1 - 2(n-1)\epsilon \end{aligned} \tag{4.23}$$

This relation is really close to the relation we had before in eq. 4.22. From our analysis we cannot say which of the relations is correct. To investigate if the relationship between fidelity of a graph and heralded entanglement infidelity does depend on the sum of all degrees, one could generate different graphs and find an estimate of the fidelity for varying heralded entanglement infidelity.

In this section, we developed a method for estimating the fidelity of tree-cluster states. Moreover, we used this metric and the error model of the Gate to compare errors caused by imperfect entanglement to single-qubit depolarising errors, which were used as the error model for trees [21]. This error model is a model that is motivated by physical parameters in a spin-cavity system (the Gate) and it can be used to model correlated errors in tree-cluster state more accurately.

To summarize, in this chapter, we optimized the parameters of the Gate in order to get maximum fidelity. We then introduced the protocol for generating tree-cluster states. We also introduced a method to estimate the lower bound fidelity of tree-cluster states. We implemented the protocol to generate tree-cluster states and used the method to find a relation between lower bound tree-cluster fidelity and heralded entanglement infidelity. Moreover, we compared the tree-fidelity of imperfect entangling operations with single-qubit errors on the photons (independent errors on each photon) using the same approach. However, we could not conclude the exact dependence of tree-cluster fidelity on heralded entanglement infidelity.

5

Conclusions and outlook

5.1. Conclusions

In the thesis, we have introduced a system for generating tree-cluster states. We introduced a scheme for entangling spin and photon by scattering them off a cavity. The schemes that have been introduced in literature earlier use an emitter for generating and entangling photons to the spin. This emission based entanglement generation suffers from multiple excitations during the generation of a single photon. Our system mitigates the problem of multiple excitations during photon generation by separating the generation and entanglement of photon. Our scheme has two spin-cavity systems, one of which generates single-photons in time-bin qubits and the other entangles with them. The photons are generated by a cavity-assisted Raman scheme, which inherently prevents emission of multiple photons.

In chapter 3, we introduced the protocol and the operations required to entangle a time-bin photon with a spin (sec. 3.1). The underlying idea for generating entanglement is using a combination of single-qubit gates on the spin before and after a time-bins reflect off the cavity. The time-bins reflect off the cavity with reflection coefficients depending on the spin state. We then modeled the system responsible for generating time-bin photons and found the analytical expression of time-bin qubit states (sec. 3.2). Furthermore, we modeled the errors in the Emitter and found the probability of emitting a photon after multiple spontaneous decays (sec. 3.3). We observed that the probability of generating a photon after several spontaneous decays followed by excitations decreases by $1/(1+4C)$ with each consecutive decay (3.3.1), where C is the cooperativity of the spin-cavity. Thus, increasing the efficiency of the spin-cavity coupling (C), reduces the probability of emitting photon after multiple excitations. Later in the chapter, we modeled the system (referred to as the Gate) responsible for reflecting and entangling with the generated time-bin photons (sec. 3.4). We then modeled the different errors that could occur during any photon-spin interaction and found the output density matrix after the interaction (sec. 3.5).

Chapter 4 discussed the performance of the system. We began by optimizing the parameters of the Gate in order to maximize the entanglement fidelity (sec. 4.1). We introduced the splitting between the excited states (Δ) and ran a numerical simulation to find the maximum fidelity depending on the splitting (Δ), the cavity decay rate (κ) and the spontaneous decay rate (γ). We found that, in order to maximize the heralded fidelity and the success probability of entanglement, we need to maximize the splitting between the excited states and have a cooperativity that is close to the value of the splitting. Following that, we introduced the protocol for generating tree-cluster states (sec. 4.2). The protocol is based on a previously introduced protocol [21] that requires two memory qubits and one spin for generating trees with three levels. After that, we introduced the methodology for the estimation of fidelity of generated tree-cluster states (sec. 4.3.1). We simulated

the generation of the tree using the protocol in sec. 4.2 and used the procedure for fidelity measurement (sec. 4.3.1) to estimate the effect of heralded entanglement infidelity on tree-cluster fidelity (sec. 4.3).

Moreover, we compared the effect of heralded entanglement infidelity and single-qubit depolarising errors on the tree-cluster fidelity (fig. 4.10). We found that the tree-cluster fidelity depends linearly on both errors for small values of the errors. Furthermore, we found that the slope of the linear relation between the tree-cluster fidelity and single-qubit depolarising error probability depends nearly on the number of photons in the tree-cluster. While, for the case of entanglement infidelity, the slope depends on nearly twice the number of photons (as summarized in table 4.3). Unfortunately, from our study, we could not conclude the exact relation between the slope and the number of photons for imperfect entanglement.

5.2. Future Outlook

In this thesis, we modeled a system capable of generating a tree-cluster state, and we used the model to simulate tree-cluster generation. We also found the impact of correlated errors caused by imperfect entanglement on tree-cluster fidelity and compared them to the effect of single-qubit depolarising errors.

In this study, we assumed that the only source of errors during tree-cluster generation is imperfect entanglement, and all the other operations to be perfect. Moreover, we assumed that no photon was lost during photon-spin interaction at the Gate. One could also extend the analysis that we have done to include those errors and find their effect on the tree-cluster state. Moreover, the measure of tree-fidelity that we have used (from sec. 4.3.1) gives us the lower bound fidelity. A more accurate measure could be used to find tree-cluster fidelity instead of using the pessimistic approach of the lower bound measure.

The comparison between single-qubit depolarising errors and imperfect entanglement showed us that imperfect entanglement has a more drastic effect on the tree-cluster fidelity. We suspect it might be related to the connectivity of the tree. For a more connected graph state, the effect of entanglement infidelity on tree-cluster fidelity might be more drastic than it is for a tree state. The slope of the linear approximation of the curve for such a graph might be steeper than what we have for tree-cluster fidelity for the same values of entanglement infidelity. The relation between the dependence of fidelity of a graph state on the entanglement infidelity can be found. Moreover, the dependence could be related to the connectivity metrics of a graph.

The property of tree-cluster states that make them ideal for one-way quantum communication is their loss tolerance [21, 13]. In case of loss of some photons from the tree-cluster state, it might be possible to extract the information from the remaining vertices of the tree state. This is done by "indirect measurement" [13]. An indirect Z measurement can be done by measuring a vertex in X basis and measuring all but one neighbour of it in the Z basis. In the presence of correlated errors, one could potentially use majority voting to predict or correct the outcome of an indirect measurement. Furthermore, an analysis of the effect of imperfect entanglement on the coding and decoding procedure of a tree could also be done. The error model developed in this thesis could also be used to analyse the performance of one-way quantum repeaters in presence of imperfect entanglement.

On that note, we hope that this thesis will help us take another step towards fault-tolerant tree-cluster generation. We hope that the simulation framework that we have built for estimation of tree-cluster fidelity could be used to build a better estimate of fidelity of graph states.

A

Solving the differential equations

In this chapter, the differential equations of the dash system are solved in detail.

While solving these equations, we will keep in mind that the driving is weak compared to the detuning $\Omega \ll \Delta$ and that we are in the Purcell regime, $\gamma \ll g \ll \kappa$.

The equations of motion are as follows:

$$\begin{aligned}
\frac{d}{dt}|g'\rangle\langle g'| &= i(\Omega|e'\rangle\langle g'| - \Omega^*|g'\rangle\langle e'|) + \gamma_g|e\rangle\langle e| \\
\frac{d}{dt}|f'1\rangle\langle f'1| &= i(g|e'\rangle\langle f'1| - g^*|f'1\rangle\langle e'|) - \kappa|f'1\rangle\langle f'1| \\
\frac{d}{dt}|e'\rangle\langle e'| &= -i(\Omega|e'\rangle\langle g'| - \Omega^*|g'\rangle\langle e'|) - i(g|e'\rangle\langle f'1| - g^*|f'1\rangle\langle e'|) - \gamma|e'\rangle\langle e'| \\
\frac{d}{dt}|g'\rangle\langle f'1| &= i(\Omega|e'\rangle\langle f'1| - g^*|g'\rangle\langle e'|) - \frac{\kappa}{2}|g'\rangle\langle f'1| \\
\frac{d}{dt}|e'\rangle\langle g'| &= i(\Delta|e'\rangle\langle g'| + g^*|f'1\rangle\langle g'| + \Omega^*|g'\rangle\langle g'| - \Omega^*|e'\rangle\langle e'|) - \frac{\gamma}{2}|e'\rangle\langle g'| \\
\frac{d}{dt}|e'\rangle\langle f'1| &= i(\Delta|e'\rangle\langle f'1| + g^*|f'1\rangle\langle f'1| + \Omega^*|g'\rangle\langle f'1| - g^*|e'\rangle\langle e'|) - \frac{1}{2}(\gamma+\kappa)|e'\rangle\langle f'1|
\end{aligned} \tag{A.1}$$

We start by adiabatically eliminating the third last equation. It give us,

$$\begin{aligned}
\frac{d}{dt}|g'\rangle\langle f'1| &= i(\Omega|e'\rangle\langle f'1| - g^*|g'\rangle\langle e'|) - \frac{\kappa}{2}|g'\rangle\langle f'1| \approx 0 \\
|g'\rangle\langle f'1| &= \frac{2i}{\kappa}(\Omega|e'\rangle\langle f'1| - g^*|g'\rangle\langle e'|)
\end{aligned} \tag{A.2}$$

adiabatically eliminating and substituting the value of $|f'1\rangle\langle g'|$ and solving for $|e'\rangle\langle g'|$ in the fifth equation gives

$$\begin{aligned}
\frac{d}{dt}|e'\rangle\langle g'| &= i(\Delta|e'\rangle\langle g'| + g^*|f'1\rangle\langle g'| + \Omega^*|g'\rangle\langle g'| - \Omega^*|e'\rangle\langle e'|) - \frac{\gamma}{2}|e'\rangle\langle g'| \approx 0 \\
0 &\approx (\Delta + \frac{i\gamma}{2})|e'\rangle\langle g'| + (\Omega|e'\rangle\langle f'1| - g^*|g'\rangle\langle e'|) - \frac{2ig^*}{\kappa}(\Omega^*|f'1\rangle\langle e'| - g|e'\rangle\langle g'|) \\
|e'\rangle\langle g'| &\approx \frac{1}{(\Delta + \frac{i\gamma}{2}(1+4C))}\left[-(\Omega|e'\rangle\langle f'1| - g^*|g'\rangle\langle e'|) + \frac{2ig^*\Omega^*}{\kappa}|f'1\rangle\langle e'|\right]
\end{aligned} \tag{A.3}$$

$$\begin{aligned}\frac{d}{dt}|e'\rangle\langle f'1| &= i(\Delta|e'\rangle\langle f'1| + g^*|f'1\rangle\langle f'1| + \Omega^*|g'\rangle\langle f'1| - g^*|e'\rangle\langle e'|) \\ &\quad -\frac{1}{2}(\gamma+\kappa)|e'\rangle\langle f'1| \approx 0 \\ \left(\Delta + \frac{i(\gamma+\kappa)}{2} + \frac{2i|\Omega|^2}{\kappa}\right)|e'\rangle\langle f'1| &\approx -g^*(|f'1\rangle\langle f'1| + |e'\rangle\langle e'|) + \frac{2ig^*\Omega^*}{\kappa}|g'\rangle\langle e'|\end{aligned} \tag{A.4}$$

We are in the weak driving regime $\Omega \ll \Delta$, so we can approximate the $\Delta + \frac{2i|\Omega|^2}{\kappa}$ as Δ. Furthermore, we are in the Purcell regime, $\kappa \gg g \gg \gamma$, so we can assume, $\kappa + \gamma \approx \kappa$. The simplified expression is,

$$|e'\rangle\langle f'1| = \frac{-g^*}{\Delta + i\kappa}(|f'1\rangle\langle f'1| - |e'\rangle\langle e'|) + \frac{2ig^*\Omega^*}{\kappa(\Delta+i\kappa)}|g'\rangle\langle e'| \tag{A.5}$$

Substituting the expression for $|e'\rangle\langle f'1|$ into the expression for $|g'\rangle\langle e'|$, gives

$$\begin{aligned}|g'\rangle\langle e'| = &-\frac{\Omega}{\Delta - \frac{i\gamma}{2}(1+4C)}\left(|g'\rangle\langle g'| - |e'\rangle\langle e'|\right) \\ &+\frac{2i\Omega|g|^2}{\kappa(\Delta - \frac{i\gamma}{2}(1+4C))(\Delta+i\kappa)}\left(|f'1\rangle\langle f'1| - |e'\rangle\langle e'|\right) \\ &+\frac{4|\Omega|^2|g|^2}{\kappa^2(\Delta - \frac{i\gamma}{2}(1+4C))(\Delta+i\kappa)}|g'\rangle\langle e'|\end{aligned} \tag{A.6}$$

again, being in the weak driving regime and in the Purcell regime, we can assume that the contribution of the second and third term on the R.H.S. of the equation is negligible. This simplifies the final expression,

$$|g'\rangle\langle e'| = -\frac{\Omega}{\Delta - \frac{i\gamma}{2}(1+4C)}\left(|g'\rangle\langle g'| - |e'\rangle\langle e'|\right) \tag{A.7}$$

similarly for $|e\rangle\langle f'1|$ we will neglect the terms with g/κ. Thus, simplifying the expression to the following,

$$|e'\rangle\langle f'1| = -\frac{g^*}{\Delta+i\kappa}(|f'1\rangle\langle f'1| - |e'\rangle\langle e'|) \tag{A.8}$$

If we now substitute the expression for $|e'\rangle\langle f'1|$ into the differential equation for $|f'1\rangle\langle f'1|$, we get

$$\begin{aligned}\frac{d}{dt}|f'1\rangle\langle f'1| &= i(g|e'\rangle\langle f'1| - g^*|f'1\rangle\langle e'|) - \kappa|f'1\rangle\langle f'1| \\ &= -\frac{|g|^2\kappa}{\Delta^2 + \frac{\kappa^2}{4}}(|f'1\rangle\langle f1| - |e'\rangle\langle e'|) - \kappa|f'1\rangle\langle f1| \approx 0\end{aligned} \tag{A.9}$$

this gives a relation between $|f'1\rangle\langle f'1|$ and $|e'\rangle\langle e'|$.

$$\begin{aligned}|f'1\rangle\langle f'1| &= \left(\frac{\frac{|g|^2}{\Delta^2+\frac{\kappa^2}{4}}}{\frac{|g|^2}{\Delta^2+\frac{\kappa^2}{4}}+1}\right)|e'\rangle\langle e'| \\ |f'1\rangle\langle f'1| &\approx \left(\frac{|g|^2}{\Delta^2+\frac{\kappa^2}{4}}\right)|e'\rangle\langle e'|\end{aligned} \tag{A.10}$$

we can make this approximation because we are in the Purcell regime. Making substitutions for $|e'\rangle\langle f'1|$ and $|g'\rangle\langle e'|$ in the differential equation for $|e'\rangle\langle e'|$ would give us

$$\begin{aligned}\frac{d}{dt}|e'\rangle\langle e'| =& -i(\Omega|e'\rangle\langle g'| - \Omega^*|g'\rangle\langle e'|) - i(g|e'\rangle\langle f'1| - g^*|f'1\rangle\langle e'|) - \gamma|e'\rangle\langle e'| \\ =& \frac{|g|^2\kappa}{\Delta^2+\frac{\kappa^2}{4}}(|f'1\rangle\langle f'1| - |e'\rangle\langle e'|) \\ &+ \frac{|\Omega|^2\gamma(1+4C)}{\Delta^2+\frac{\gamma^2}{4}(1+4C)^2}(|g'\rangle\langle g'| - |e'\rangle\langle e'|) \\ &- \gamma|e'\rangle\langle e'|\end{aligned} \tag{A.11}$$

Substituting $|f'1\rangle\langle f'1|$ in the equation and neglecting terms which are of second order in $|g|^2/\kappa^2$

$$\begin{aligned}\frac{d}{dt}|e'\rangle\langle e'| = -\left(\frac{|g|^2\kappa}{\Delta^2+\frac{\kappa^2}{4}} + \frac{|\Omega|^2\gamma(1+4C)}{\Delta^2+\frac{\gamma^2}{4}(1+4C)^2} + \gamma\right)|e'\rangle\langle e'| \\ + \frac{|\Omega|^2\gamma(1+4C)}{\Delta^2+\frac{\gamma^2}{4}(1+4C)^2}|g'\rangle\langle g'| \approx 0\end{aligned} \tag{A.12}$$

At this point we will make an assumptions. We will assume the following:

$$\frac{|g|^2\kappa}{\Delta^2+\frac{\kappa^2}{4}} >> \frac{|\Omega|^2\gamma(1+4C)}{\Delta^2+\frac{\gamma^2}{4}(1+4C)^2} \tag{A.13}$$

if we further assume, that the rate of photon emission is huge compared to the detuning, that is $\kappa >> \Delta$, then we can simplify the above relation to the following,

$$\frac{4|g|^2}{\kappa} >> \frac{|\Omega|^2\gamma(1+4C)}{\Delta^2+\frac{\gamma^2}{4}(1+4C)^2} \tag{A.14}$$

dividing both sides by $\gamma(1+4C)$,

$$\frac{4C}{1+4C} >> \frac{|\Omega|^2}{\Delta^2+\frac{\gamma^2}{4}(1+4C)^2} \tag{A.15}$$

This is not a new assumption. It is one of the consequences of having a really weak driving. Now, neglecting the term in the differential equation for $|e'\rangle\langle e'|$ will give us a relation between $|g'\rangle\langle g'|$ and $|e'\rangle\langle e'|$.

$$\begin{aligned}\left(\frac{|g|^2\kappa}{\Delta^2+\frac{\kappa^2}{4}} + \gamma\right)|e'\rangle\langle e'| &= \frac{|\Omega|^2\gamma(1+4C)}{\Delta^2+\frac{\gamma^2}{4}(1+4C)^2}|g'\rangle\langle g'| \\ \frac{\frac{\kappa^2\gamma}{4}(1+4C+\frac{\Delta^2}{\kappa^2})}{\Delta^2+\frac{\kappa^2}{4}}|e'\rangle\langle e'| &= \frac{|\Omega|^2\gamma(1+4C)}{\Delta^2+\frac{\gamma^2}{4}(1+4C)^2}|g'\rangle\langle g'|\end{aligned} \tag{A.16}$$

we neglect terms with Δ^2/κ^2, to get a final relation as,

$$|e'\rangle\langle e'| = \frac{|\Omega|^2}{\Delta^2+\frac{\gamma^2}{4}(1+4C)^2}|g'\rangle\langle g'| \tag{A.17}$$

Finally, we will use the relations we have found so far to first simplify the differential equation for $|g'\rangle\langle g'|$

$$\begin{aligned}\frac{d}{dt}|g'\rangle\langle g'| =& i(\Omega|e'\rangle\langle g'| - \Omega^*|g'\rangle\langle e'|) + \gamma_g|e\rangle\langle e| \\ =& -\frac{|\Omega|^2\gamma(1+4C)}{\Delta^2+\frac{\gamma^2}{4}(1+4C)^2}(|g'\rangle\langle g'| - |e'\rangle\langle e'|) + \gamma_g|e\rangle\langle e|\end{aligned} \tag{A.18}$$

Substituting $|e'\rangle\langle e'|$ would give us,

$$\begin{aligned}\frac{d}{dt}|g'\rangle\langle g'| &= i(\Omega|e'\rangle\langle g'| - \Omega^*|g'\rangle\langle e'|) + \gamma_g|e\rangle\langle e| \\ &= -\frac{|\Omega|^2\gamma(1+4C)}{\Delta^2+\frac{\gamma^2}{4}(1+4C)^2}\left(1-\frac{|\Omega|^2}{\Delta^2+\frac{\gamma^2}{4}(1+4C)^2}\right)|g'\rangle\langle g'| + \gamma_g|e\rangle\langle e|\end{aligned} \tag{A.19}$$

neglecting $|\Omega|^2/\Delta^2$ compared to 1 would give us,

$$\frac{d}{dt}|g'\rangle\langle g'| = -\frac{|\Omega|^2\gamma(1+4C)}{\Delta^2+\frac{\gamma^2}{4}(1+4C)^2}|g'\rangle\langle g'| + \gamma_g|e\rangle\langle e| \tag{A.20}$$

We know the time dependence of $|e\rangle$ state from our analysis of the decay-less system in the previous section. The state $|e\rangle\langle e|$ as a function of time is

$$|e\rangle\langle e|(t) = \frac{|\Omega|^2}{\Delta^2+\frac{\gamma^2}{4}(1+4C)^2}e^{-\frac{|\Omega|^2\gamma(1+4C)}{\Delta^2+\frac{\gamma^2}{4}(1+4C)^2}} \tag{A.21}$$

to simplify the representations, we define a new parameter Q as

$$Q = \frac{|\Omega|^2}{\Delta^2+\frac{\gamma^2}{4}(1+4C)^2} \tag{A.22}$$

Therefore, the differential equation now becomes,

$$\frac{d}{dt}|g'\rangle\langle g'| = -Q\gamma(1+4C)|g'\rangle\langle g'| + \left(\gamma_g Q e^{-Q\gamma(1+4C)t}\right) \tag{A.23}$$

Solving this differential equation gives us

$$|g'\rangle\langle g'|(t) = \gamma_g Q t e^{-Q\gamma(1+4C)t} \tag{A.24}$$

From the relations between $|g'\rangle\langle g'|$ and $|e'\rangle\langle e'|$, and $|e'\rangle\langle e'|$ and $|f'1\rangle\langle f'1|$, we can find $|f'1\rangle\langle f'1|(t)$ and therefore the probability of emitting a photon.

Bibliography

[1] T. D. Ladd et al. “Quantum computers”. In: Nature 464.7285 (Mar. 2010), pp. 45–53. ISSN: 1476-4687. DOI: 10.1038/nature08812. URL: https://doi.org/10.1038/nature08812.

[2] Frank Arute et al. “Quantum supremacy using a programmable superconducting processor”. In: Nature 574.7779 (Oct. 2019), pp. 505–510. ISSN: 1476-4687. DOI: 10.1038/s41586-019-1666-5. URL: https://doi.org/10.1038/s41586-019-1666-5.

[3] Nicolas Gisin et al. “Quantum cryptography”. In: Rev. Mod. Phys. 74 (1 Mar. 2002), pp. 145–195. DOI: 10.1103/RevModPhys.74.145. URL: https://link.aps.org/doi/10.1103/RevModPhys.74.145.

[4] Valerio Scarani et al. “The security of practical quantum key distribution”. In: Reviews of Modern Physics 81.3 (Sept. 2009), pp. 1301–1350. ISSN: 1539-0756. DOI: 10.1103/revmodphys.81.1301. URL: http://dx.doi.org/10.1103/RevModPhys.81.1301.

[5] H. J. Kimble. “The quantum internet”. In: Nature 453.7198 (June 2008), pp. 1023–1030. ISSN: 1476-4687. DOI: 10.1038/nature07127. URL: https://doi.org/10.1038/nature07127.

[6] Stephanie Wehner, David Elkouss, and Ronald Hanson. “Quantum internet: A vision for the road ahead”. In: Science 362.6412 (2018), eaam9288. DOI: 10.1126/science.aam9288. eprint: https://www.science.org/doi/pdf/10.1126/science.aam9288. URL: https://www.science.org/doi/abs/10.1126/science.aam9288.

[7] H. -J. Briegel et al. Quantum repeaters for communication. 1998. arXiv: quant-ph/9803056 [quant-ph].

[8] William J. Munro et al. “Inside Quantum Repeaters”. In: IEEE Journal of Selected Topics in Quantum Electronics 21.3 (2015), pp. 78–90. DOI: 10.1109/JSTQE.2015.2392076.

[9] Sreraman Muralidharan et al. “Optimal architectures for long distance quantum communication”. In: Scientific Reports 6.1 (Feb. 2016). ISSN: 2045-2322. DOI: 10.1038/srep20463. URL: http://dx.doi.org/10.1038/srep20463.

[10] Koji Azuma, Kiyoshi Tamaki, and Hoi-Kwong Lo. “All-photonic quantum repeaters”. In: Nature Communications 6.1 (Apr. 2015). ISSN: 2041-1723. DOI: 10.1038/ncomms7787. URL: http://dx.doi.org/10.1038/ncomms7787.

[11] Austin G. Fowler et al. “Surface Code Quantum Communication”. In: Phys. Rev. Lett. 104 (18 May 2010), p. 180503. DOI: 10.1103/PhysRevLett.104.180503. URL: https://link.aps.org/doi/10.1103/PhysRevLett.104.180503.

[12] Fabian Ewert and Peter van Loock. “Ultrafast fault-tolerant long-distance quantum communication with static linear optics”. In: Phys. Rev. A 95 (1 Jan. 2017), p. 012327. DOI: 10.1103/PhysRevA.95.012327. URL: https://link.aps.org/doi/10.1103/PhysRevA.95.012327.

[13] Michael Varnava, Daniel E. Browne, and Terry Rudolph. “Loss Tolerance in One-Way Quantum Computation via Counterfactual Error Correction”. In: Phys. Rev. Lett. 97 (12 Sept. 2006), p. 120501. DOI: 10.1103/PhysRevLett.97.120501. URL: https://link.aps.org/doi/10.1103/PhysRevLett.97.120501.

[14] Sergei Slussarenko and Geoff J. Pryde. “Photonic quantum information processing: A concise review”. In: Applied Physics Reviews 6.4 (2019), p. 041303. DOI: 10.1063/1.5115814. eprint: https://doi.org/10.1063/1.5115814. URL: https://doi.org/10.1063/1.5115814.

[15] Michael A. Nielsen. “Optical Quantum Computation Using Cluster States”. In: Phys. Rev. Lett. 93 (4 July 2004), p. 040503. DOI: 10.1103/PhysRevLett.93.040503. URL: https://link.aps.org/doi/10.1103/PhysRevLett.93.040503.

[16] Xiao-song Ma et al. “Quantum simulation of the wavefunction to probe frustrated Heisenberg spin systems”. In: Nature Physics 7.5 (Feb. 2011), pp. 399–405. ISSN: 1745-2481. DOI: 10.1038/nphys1919. URL: http://dx.doi.org/10.1038/nphys1919.

[17] Darrick E. Chang, Vladan Vuletić, and Mikhail D. Lukin. “Quantum nonlinear optics — photon by photon”. In: Nature Photonics 8.9 (Sept. 2014), pp. 685–694. ISSN: 1749-4893. DOI: 10.1038/nphoton.2014.192. URL: https://doi.org/10.1038/nphoton.2014.192.

[18] Daniel E. Browne and Terry Rudolph. “Resource-Efficient Linear Optical Quantum Computation”. In: Phys. Rev. Lett. 95 (1 June 2005), p. 010501. DOI: 10.1103/PhysRevLett.95.010501. URL: https://link.aps.org/doi/10.1103/PhysRevLett.95.010501.

[19] Donovan Buterakos, Edwin Barnes, and Sophia E. Economou. “Deterministic Generation of All-Photonic Quantum Repeaters from Solid-State Emitters”. In: Phys. Rev. X 7 (4 Oct. 2017), p. 041023. DOI: 10.1103/PhysRevX.7.041023. URL: https://link.aps.org/doi/10.1103/PhysRevX.7.041023.

[20] Konstantin Tiurev et al. High-fidelity multi-photon-entangled cluster state with solid-state quantum emitters in photonic nanostructures. 2021. arXiv: 2007.09295 [quant-ph].

[21] Johannes Borregaard et al. “One-Way Quantum Repeater Based on Near-Deterministic Photon-Emitter Interfaces”. In: Phys. Rev. X 10 (2 June 2020), p. 021071. DOI: 10.1103/PhysRevX.10.021071. URL: https://link.aps.org/doi/10.1103/PhysRevX.10.021071.

[22] Yuan Zhan and Shuo Sun. “Deterministic Generation of Loss-Tolerant Photonic Cluster States with a Single Quantum Emitter”. In: Phys. Rev. Lett. 125 (22 Nov. 2020), p. 223601. DOI: 10.1103/PhysRevLett.125.223601. URL: https://link.aps.org/doi/10.1103/PhysRevLett.125.223601.

[23] J. Brendel et al. “Pulsed Energy-Time Entangled Twin-Photon Source for Quantum Communication”. In: Phys. Rev. Lett. 82 (12 Mar. 1999), pp. 2594–2597. DOI: 10.1103/PhysRevLett.82.2594. URL: https://link.aps.org/doi/10.1103/PhysRevLett.82.2594.

[24] E.T. Jaynes and F.W. Cummings. “Comparison of quantum and semiclassical radiation theories with application to the beam maser”. In: Proceedings of the IEEE 51.1 (1963), pp. 89–109. DOI: 10.1109/PROC.1963.1664.

[25] Ying Wu. “Effective Raman theory for a three-level atom in the Λ configuration”. In: Phys. Rev. A 54 (2 Aug. 1996), pp. 1586–1592. DOI: 10.1103/PhysRevA.54.1586. URL: https://link.aps.org/doi/10.1103/PhysRevA.54.1586.

[26] Leonard Mandel and Emil Wolf. Optical Coherence and Quantum Optics. Cambridge University Press, 1995. DOI: 10.1017/CBO9781139644105.

[27] Mikhail Lukin. Notes of Modern Atomic and Optical Physics 2. Harvard University, 2016.

[28] Anders S. Sørensen and Klaus Mølmer. “Measurement Induced Entanglement and Quantum Computation with Atoms in Optical Cavities”. In: Physical Review Letters 91.9 (Aug. 2003). ISSN: 1079-7114. DOI: 10.1103/physrevlett.91.097905. URL: http://dx.doi.org/10.1103/PhysRevLett.91.097905.

[29] Christian Hepp et al. “Electronic Structure of the Silicon Vacancy Color Center in Diamond”. In: Physical Review Letters 112.3 (Jan. 2014). ISSN: 1079-7114. DOI: 10.1103/physrevlett.112.036405. URL: http://dx.doi.org/10.1103/PhysRevLett.112.036405.

[30] D. D. Sukachev et al. “Silicon-Vacancy Spin Qubit in Diamond: A Quantum Memory Exceeding 10 ms with Single-Shot State Readout”. In: Phys. Rev. Lett. 119 (22 Nov. 2017), p. 223602. DOI: 10.1103/PhysRevLett.119.223602. URL: https://link.aps.org/doi/10.1103/PhysRevLett.119.223602.

[31] Lachlan J. Rogers et al. “All-Optical Initialization, Readout, and Coherent Preparation of Single Silicon-Vacancy Spins in Diamond”. In: Phys. Rev. Lett. 113 (26 Dec. 2014), p. 263602. DOI: 10.1103/PhysRevLett.113.263602. URL: https://link.aps.org/doi/10.1103/PhysRevLett.113.263602.

[32] R. E. Evans et al. “Photon-mediated interactions between quantum emitters in a diamond nanocavity”. In: Science 362.6415 (2018), pp. 662–665. DOI: 10.1126/science.aau4691. eprint: https://www.science.org/doi/pdf/10.1126/science.aau4691. URL: https://www.science.org/doi/abs/10.1126/science.aau4691.

[33] Erik N. Knall et al. Efficient Source of Shaped Single Photons Based on an Integrated Diamond Nanophotonic System. 2022. DOI: 10.48550/ARXIV.2201.02731. URL: https://arxiv.org/abs/2201.02731.

[34] Daniel Manzano. “A short introduction to the Lindblad master equation”. In: AIP Advances 10.2 (2020), p. 025106. DOI: 10.1063/1.5115323. eprint: https://doi.org/10.1063/1.5115323. URL: https://doi.org/10.1063/1.5115323.

[35] Jean Dalibard, Yvan Castin, and Klaus Mølmer. “Wave-function approach to dissipative processes in quantum optics”. In: Phys. Rev. Lett. 68 (5 Feb. 1992), pp. 580–583. DOI: 10.1103/PhysRevLett.68.580. URL: https://link.aps.org/doi/10.1103/PhysRevLett.68.580.

[36] H. J. Carmichael. “Quantum trajectory theory for cascaded open systems”. In: Phys. Rev. Lett. 70 (15 Apr. 1993), pp. 2273–2276. DOI: 10.1103/PhysRevLett.70.2273. URL: https://link.aps.org/doi/10.1103/PhysRevLett.70.2273.

[37] Hans J. Briegel and Robert Raussendorf. “Persistent Entanglement in Arrays of Interacting Particles”. In: Phys. Rev. Lett. 86 (5 Jan. 2001), pp. 910–913. DOI: 10.1103/PhysRevLett.86.910. URL: https://link.aps.org/doi/10.1103/PhysRevLett.86.910.

[38] Marc Hein et al. “Entanglement in graph states and its applications”. In: arXiv preprint quant-ph/0602096 (2006).

[39] M. Hein, J. Eisert, and H. J. Briegel. “Multiparty entanglement in graph states”. In: Phys. Rev. A 69 (6 June 2004), p. 062311. DOI: 10.1103/PhysRevA.69.062311. URL: https://link.aps.org/doi/10.1103/PhysRevA.69.062311.

[40] M. Ruiz. Towards a fault-tolerant one-way quantum repeater. Delft University of Technology, 2021.

[41] C. W. Gardiner and M. J. Collett. “Input and output in damped quantum systems: Quantum stochastic differential equations and the master equation”. In: Phys. Rev. A 31 (6 June 1985), pp. 3761–3774. DOI: 10.1103/PhysRevA.31.3761. URL: https://link.aps.org/doi/10.1103/PhysRevA.31.3761.

[42] Peter Zoller and C. W. Gardiner. Quantum Noise in Quantum Optics: the Stochastic Schrödinger Equation. 1997. DOI: 10.48550/ARXIV.QUANT-PH/9702030. URL: https://arxiv.org/abs/quant-ph/9702030.

[43] Konstantin Tiurev et al. “Fidelity of time-bin-entangled multiphoton states from a quantum emitter”. In: Physical Review A 104.5 (Nov. 2021). ISSN: 2469-9934. DOI: 10.1103/physreva.104.052604. URL: http://dx.doi.org/10.1103/PhysRevA.104.052604.

[44] Alexander Holm Kiilerich and Klaus Mølmer. “Quantum interactions with pulses of radiation”. In: Physical Review A 102.2 (Aug. 2020). ISSN: 2469-9934. DOI: 10.1103/physreva.102.023717. URL: http://dx.doi.org/10.1103/PhysRevA.102.023717.

[45] Anders S. Sørensen and Klaus Mølmer. “Probabilistic Generation of Entanglement in Optical Cavities”. In: Phys. Rev. Lett. 90 (12 Mar. 2003), p. 127903. DOI: 10.1103/PhysRevLett.90.127903. URL: https://link.aps.org/doi/10.1103/PhysRevLett.90.127903.

[46] Yasaman Soudagar et al. “Cluster-state quantum computing in optical fibers”. In: Journal of the Optical Society of America B 24.2 (Jan. 2007), p. 226. DOI: 10.1364/josab.24.000226. URL: https://doi.org/10.1364%2Fjosab.24.000226.

[47] C. T. Nguyen et al. “An integrated nanophotonic quantum register based on silicon-vacancy spins in diamond”. In: Physical Review B 100.16 (Oct. 2019). ISSN: 2469-9969. DOI: 10.1103/physrevb.100.165428. URL: http://dx.doi.org/10.1103/PhysRevB.100.165428.

[48] C. T. Nguyen et al. “Quantum Network Nodes Based on Diamond Qubits with an Efficient Nanophotonic Interface”. In: Physical Review Letters 123.18 (Oct. 2019). ISSN: 1079-7114. DOI: 10.1103/physrevlett.123.183602. URL: http://dx.doi.org/10.1103/PhysRevLett.123.183602.

[49] Otfried Gühne and Géza Tóth. “Entanglement detection”. In: Physics Reports 474.1–6 (Apr. 2009), pp. 1–75. ISSN: 0370-1573. DOI: 10.1016/j.physrep.2009.02.004. URL: http://dx.doi.org/10.1016/j.physrep.2009.02.004.

[50] Konstantin Tiurev and Anders S. Sørensen. Fidelity measurement of a multiqubit cluster state with minimal effort. 2021. arXiv: 2107.10386 [quant-ph].

[51] Lukas Knips et al. “Multipartite Entanglement Detection with Minimal Effort”. In: Phys. Rev. Lett. 117 (21 Nov. 2016), p. 210504. DOI: 10.1103/PhysRevLett.117.210504. URL: https://link.aps.org/doi/10.1103/PhysRevLett.117.210504.